ACS APPLIED MATERIALS & INTERFACES

Review

www.acsami.org

Flexible Graphene-Based Wearable Gas and Chemical Sensors

Eric Singh,[†] M. Meyyappan,*[,‡] and Hari Singh Nalwa*[,§]

[†]Department of Computer Science, Stanford University, Stanford, California 94305, United States

[‡]Center for Nanotechnology, NASA Ames Research Center, Moffett Field, California 94035, United States

[§]Advanced Technology Research, 26650 The Old Road, Valencia, California 91381, United States

ABSTRACT: Wearable electronics is expected to be one of the most active research areas in the next decade; therefore, nanomaterials possessing high carrier mobility, optical transparency, mechanical robustness and flexibility, lightweight, and environmental stability will be in immense demand. Graphene is one of the nanomaterials that fulfill all these requirements, along with other inherently unique properties and convenience to fabricate into different morphological nanostructures, from atomically thin single layers to nanoribbons. Graphene-based materials have also been investigated in sensor technologies, from chemical sensing to detection of cancer biomarkers. The progress of graphene-based flexible gas and chemical sensors in terms of material preparation, sensor fabrication, and their performance are reviewed here. The article provides a brief introduction to graphene-based materials and their potential applications in flexible and stretchable wearable electronic devices. The role of graphene in fabricating flexible gas sensors for the detection of various hazardous gases, including nitrogen dioxide (NO_2), ammonia (NH_3), hydrogen (H_2), hydrogen sulfide (H_2S), carbon dioxide (CO_2), sulfur dioxide (SO_2), and humidity in wearable technology, is discussed. In addition, applications of graphene-based materials are also summarized in detecting toxic heavy metal ions (Cd, Hg, Pb, Cr, Fe, Ni, Co, Cu, Ag), and volatile organic compounds (VOCs) including nitrobenzene, toluene, acetone, formaldehyde, amines, phenols, bisphenol A (BPA), explosives, chemical warfare agents, and environmental pollutants. The sensitivity, selectivity and strategies for excluding interferents are also discussed for graphene-based gas and chemical sensors. The challenges for developing future generation of flexible and stretchable sensors for wearable technology that would be usable for the Internet of Things (IoT) are also highlighted.

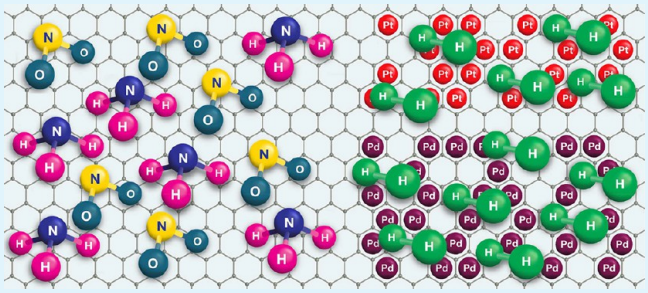

KEYWORDS: *graphene, graphene oxide, gas sensors, chemical sensors, flexible sensors, selectivity, wearable electronics, Internet of Things*

1. INTRODUCTION

Graphene is a two-dimensional atomic sheet of sp^2-hybridized carbon atoms that displays outstanding physical properties including high carrier mobility up to 350 000 $cm^2/(V\,s)$,[1−3] high optical transparency up to 97.7% for single-layer graphene,[4] high mechanical strength with Young's modulus of 1 TPa and fracture strength of 130 GPa,[5] and thermal stability.[2] Graphene can be easily processed into different morphological nanostructures, including ultrathin films,[6,7] nanosheets,[8−10] paper,[11] nanoribbons,[12,13] and foams.[14,15] Graphene-based materials have shown a great potential for application in supercapacitors,[16−18] energy storage,[19,20] solar cells,[21−23] sensors,[24−27] light-emitting diodes,[28−30] touch screen-panel devices,[31,32] field emission devices,[33−35] aerospace,[36,37] medicine,[38,39] and others.[40] The simplest route to prepare graphene is by the reduction of graphene oxide (GO) sheets. The pristine graphene nanosheet obtained after removing all oxygenated functional groups is hydrophobic in nature. Different types of graphene-based materials described as graphene, GO, reduced graphene oxide (rGO), graphene analogs, hybrids, and nanocomposites have been discussed in the literature. The graphene-nanosheet was first isolated by mechanical exfoliation using a simple adhesive tape.[1] Thereafter, a variety of synthetic routes have been employed for preparing graphene layers and thin films, including chemical vapor deposition (CVD),[40,41] liquid-phase mechanical exfoliation of graphite,[42] graphite intercalation compounds,[43,44] graphite fluoride,[45,46] chemical exfoliation from GO,[47−49] epitaxial growth[50,51] and atomic layer deposition.[52] All these different methods have been summarized in the literature.[53−58]

One of the most common methods for preparing flexible monolayer and multilayers of graphene is the CVD technique. The large-area ultrathin films of graphene are deposited on Ni or Cu foils by CVD, and then these films are transferred onto flexible substrates including poly(dimethylsiloxane) (PDMS), poly(methyl methacrylate) (PMMA), poly(ethylene terephthalate) (PET), poly(ethylene naphthalate) (PEN), polyimide (PI), and Ecoflex for developing flexible and stretchable electronic devices. The sheet resistance of 980 Ω/sq and optical transmittance of 97.6% has been reported for the CVD-grown monolayer graphene film transferred onto a glass substrate.[59]

Received: May 18, 2017
Accepted: September 6, 2017
Published: September 6, 2017

DOI: 10.1021/acsami.7b07063
ACS Appl. Mater. Interfaces 2017, 9, 34544−34586

An interesting study was conducted by Reina et al.[60] where large-area monolayer and few-layer graphene films were grown by CVD at 900−1000 °C on Ni films and then transferred to different substrates. Raman spectroscopy of these graphene layers showed D-band at ∼1350 cm^{-1}, G-band at ∼1580 cm^{-1}, and 2D-band at 2700 cm^{-1}. Graphene film also exhibited 90% transparency in the 500−1000 nm wavelength region and the sheet resistance of 770−1000 Ω/sq. In another study, large area flexible graphene film was CVD-grown on Cu foil and transferred onto a flexible PET substrate, which exhibited 88.8% transparency and a sheet resistance of 1.1742 kΩ/sq.[61] The roll-to-roll transfer of CVD-grown graphene film from Cu to flexible plastic substrates has also been achieved.[62] The production of 30 in. flexible graphene films with a roll-to-roll transfer technique was accomplished by CVD process on a flexible Cu substrate that showed 97.4% optical transparency at 550 nm and a sheet resistance of 125 Ω/sq.[63] A 100 m-long transparent graphene film on flexible PET substrate by roll-to-roll CVD has also been reported.[64] Besides graphene thin films, large-area flexible graphene paper has been developed.[65−69] In an interesting study, Yang et al.[70] directly developed large-area graphene films on various substrates such as quartz, GaN, SiO_2/Si, and textured Si substrates without using a transfer process. The bottom-up and transfer-free growth of multilayer graphene was achieved by a self-assembled monolayer where trimethoxy(phenyl)silane was used as the carbon source. Raman spectra of graphene films developed on textured Si, GaN, and quartz substrates, optical transmittance and an HR-TEM image of multilayer graphene grown on quartz were compared. Raman spectroscopy of the transfer-free multilayer graphene grown on a SiO_2/Si substrate showed a D-band at ∼1360 cm^{-1}, G-band at ∼1595 cm^{-1}, and 2D-band at 2700 cm^{-1}. The quality of graphene films grown on GaN and textured Si substrates were not found to be as high as films grown on the SiO_2/Si and quartz substrates. Graphene films grown on quartz substrate showed 84.3% optical transmittance at 550 nm and the sheet resistance of 3500 Ω/sq.

The sheet resistance and optical transmittance of graphene depends upon the number of graphene layers and also on different flexible substrates. Martins et al.[71] transferred CVD-grown graphene onto different types of flexible substrates which showed sheet resistance of 1890 ± 309, 1440 ± 151, 301 ± 10, 2920 ± 191, 1210 ± 187, 812 ± 97, 35 000 ± 10 500 and 172 ± 18 Ω/sq for polycarbonate (PC), poly(vinyl chloride) (PVC), paper with PMMA coating, paraffin, poly(ethylene terephthalate) with PMMA coating, cloth with PMMA coating, poly(tetrafluoroethylene) (PTFE) filter membranes, and cellulose nitrate/cellulose acetate (CN/CA) filter membrane with PMMA coating, repectively. The significantly large variations in the sheet resistance arise due to the different hydrophobicity of flexible substrates and substrate induced molecular interactions with CVD-graphene films. The optical transmittance of CVD-grown graphene layers on different flexible and rigid transparent substrates were studied by Gabriel et al.[72] The optical transmittance of 85% for graphene (4-layer)/PET, 85.24% for graphene (monolayer)/PEN, and 88.7% for graphene (monolayer)/quartz were measured at 550 nm which corresponded to 96.7%, 97.98%, and 97.35% optical transmittance for graphene, respectively. In comparison to indium tin oxide (ITO), graphene showed higher transmittance and equivalent or higher electrical conductivity than ITO. These studies demonstrated that the sheet resistance and optical transmittance of graphene vary on different flexible substrates and graphene films can be used in developing transparent and flexible electronic devices.

Graphene can be easily oxidized to GO sheet containing oxygenated functional groups such as carboxyl (−COOH), hydroxyl (−OH), epoxy (C—O—C), carbonyl (−C—OH), ketone (−C═O), and 5- and 6-membered ring lactols (O—C—O);[73,74] therefore, GO imparts quite different physical and chemical properties than that of graphene and makes it interesting for gas and chemical sensing applications. Contrary to graphene, the presence of oxygenated functional groups on the GO sheets give rise to their hydrophilic nature which inherently makes GO highly sensitive to water molecules and therefore usable as a humidity sensor. The oxygenated functional groups on GO sheets also offer tremendous possibilities for the surface functionalization. In order to enhance sensitivity and selectivity to particular analytes and induce flexibility and stretchability, graphene, GO and rGO can be hybridized with metallic nanoparticles, organic polymers, semiconductor nanostructures, carbon nanomaterials, and transformed into different morphological structures including hydrogels and porous networks.

Flexible materials are gaining a lot of attention in order to develop future generation wearable and bendable electronic devices for healthcare, prosthetics, wearable watches, displays, smart phones, light-emitting diodes, solar panels, robotics, artificial intelligence, aerospace, military, space exploration and to connect billions of electronic devices to the worldwide population via the Internet/cloud. For example, wearable sensors those can be directly attached to human body or embedded in body-worn textile and other consumer products are expected to play a major role not only in the field of healthcare for monitoring vital signs but also in all those sectors related to the Internet of Things (IoT). Different types of flexible wearable sensors will be required to fulfill the growing demands in IoT sector. Finding right materials for fabricating wearable electronic devices has been quite challenging because conventional semiconducting inorganic materials such as ITO, silicon (Si), germanium (Ge), gallium arsenide (GaAs), gallium arsenide phosphide (GaAsP), cadmium sulfide (CdS), etc., used for electronics and communication devices, are rigid and brittle in nature. However, graphene being optically transparent, thermally stable, mechanically strong, lightweight, flexible, stretchable, and biocompatible is a unique material that fits well to the criteria's required for fabricating large-area wearable electronic devices including flexible sensors for monitoring and detecting toxic gases and chemicals hazardous to human health. The literature on graphene-based wearable gas and chemical sensors remains scattered; therefore, author's aim is to summarize all available data in this review article.

Though several reviews have been published on graphene-based gas, chemical and biosensors,[24−27] however, a comprehensive review mainly focused on the recent developments in graphene-based flexible gas and chemical sensors usable for wearable technology has not yet been reported. This review may further spur research interest for the use of graphene-based materials in the emerging field of wearable electronics. In this review, a brief introduction is provided to the graphene and graphene-based materials those have been integrated into flexible wearable electronic devices. The graphene-based flexible gas and chemical sensors to detect nitrogen dioxide (NO_2), ammonia (NH_3), hydrogen (H_2), hydrogen sulfide (H_2S), carbon dioxide (CO_2), sulfur dioxide (SO_2), and a number of volatile organic chemicals (VOCs) are summarized. Furthermore, the applications of graphene-based materials in detecting toxic heavy metal ions (Cd, Hg, Pb, Cr, Fe, Ni, Co, Cu, Ag), bisphenol A (BPA), nitrobenzene, toluene, acetone, formaldehyde, amines, phenols,

DOI: 10.1021/acsami.7b07063
ACS Appl. Mater. Interfaces 2017, 9, 34544−34586

explosives, chemical warfare agents, and environmental pollutants are discussed. The sensitivity, selectivity and strategies to exclude effects of interfering analytes for graphene-based sensors for different chemical analytes and plausible sensing mechanisms are evaluated. The role of graphene-based materials in developing future generation of flexible sensors for wearable technology usable for the Internet of Things (IoT) is also highlighted.

2. GRAPHENE FOR FLEXIBLE ELECTRONICS

Metal oxides such as tin (Sn)-doped indium oxide (In_2O_3) referred to as (ITO) transparent electrodes are most commonly used in the field of electronics and optoelectronics. However, ITO transparent conductive electrodes (TCEs) are not mechanically strong and their brittleness leads to cracks when subjected to mechanical strains; in addition, ITO exhibits degradation against illumination and chemicals.[75] These shortcomings preclude the use of ITO transparent electrodes for developing flexible and stretchable electronic devices. Furthermore, indium sources are limited. Therefore, there is a growing demand to replace ITO and find alternate transparent conductive materials for ITO-free electronic devices.[76−79] Two-dimensional nanomaterials such as graphene and transition metal dichalcogenides (TMDs) are gaining the attention of the scientific community due to their unique properties.[80−84] In particular, graphene is attractive due to its high carrier mobility, high optical transparency, high mechanical strength and abundant availability in nature in forms of graphite. Today, flexible and stretchable sensing devices are in great demand due to their promising applications in wearable electronics, especially for healthcare industries. Graphene monolayer and multilayers can be transferred to different flexible substrates without any cracks or defects for fabricating flexible, stretchable, and foldable electronic devices. Compared to rigid silicon and metal oxide semiconductor-based electrodes, flexible graphene electrodes are easy to deposit in desirable patterns on large-area highly flexible substrates, which can be twisted and folded.

Graphene-based materials in the form of thin films, nanosheets, papers, and woven-fabric have been studied as flexible transparent conductive electrodes for nonvolatile memory,[85] charge-trap memory,[86] field-effect transistors (FETs),[87−89] light-emitting diodes (LEDs),[90−93] displays,[94,95] supercapacitors,[96−99] solar cells,[100−103] and other flexible electronic devices.[104,105] Ryu et al.[106] prepared graphene films of 400 × 300 mm area by hydrogen-free rapid thermal CVD process having a sheet resistance of 249 ± 17 Ω/sq. The rapid thermal-CVD graphene films were install as capacitive touch-screen for mobile phones. Liang et al.[107] developed transparent conductive electrodes using GO soldered silver nanowire (AgNW) for flexible and stretchable electronics. Figure 1a−c shows photographs of a flexible GO-AgNW/PET sheet, bending performed at 4 mm radius and relative resistance change ($\Delta R/R_0$) of TCE during repeated bending cycles. The GO-soldered AgNW composite network on PET substrate showed a sheet resistance of 14 Ω/sq and 88% optical transmittance at 550 nm. The sheet resistance increased by 2−3% after repeated 12 000 bending cycles at a bending radius of 4 mm showing a great flexibility of GO-AgNW composite TCE. GO solder was also used to introduce stretchability into the AgNW network. The GO-AgNW composite TCE fabricated on poly(urethane acrylate) showed stretchability over 100% linear strains without any change in electrical conductivity. The stretchable white LEDs were fabricated using stretchable TCE, which showed stability up to 100 stretching cycles between

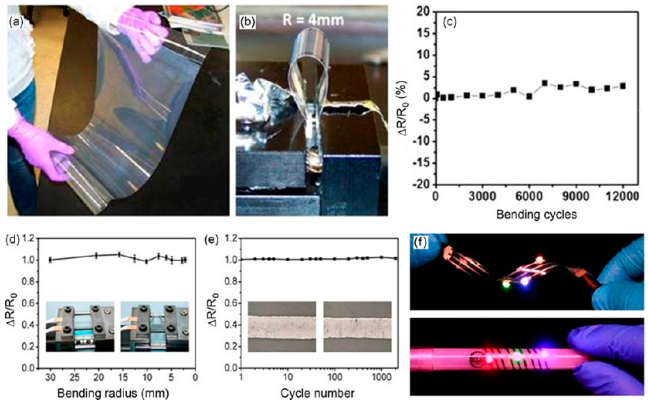

Figure 1. (a) Photograph of flexible graphene oxide−silver nanowire/poly(ethylene terephthalate) (GO-AgNW/PET) sheet (coating area = 20 × 40 cm). (b) Photograph of a flexible GO-AgNW/PET film bent to 4 mm radius. (c) Relative resistance change ($\Delta R/R_0$) of the flexible GO-AgNW/PET electrode during repeated bending cycles at a bending radius of 4 mm. [Reprinted with permission from ref 107. Copyright American Chemical Society.] (d) Relative resistance change ($\Delta R/R_0$) of the flexible reduced graphene oxide (rGO)/PDMS sheet-based circuit as a function of the bending radius varying from 2 mm to 30 mm during the bending test. (e) Relative resistance change ($\Delta R/R_0$) of the rGO sheet-based circuit at 5 mm bending radius up to 1000 bending cycles. Insets show the optical images of the rGO sheet-based circuits before and after the cyclic bending test. (f) Large-area flexible rGO/PDMS circuits integrated into LED chips those display bright light illumination on twisting by hand and when wrapped on a roller pen. [Reprinted with permission from ref 109. Copyright American Chemical Society.]

0−40% applied strain and stretchability up to 130%. Huang et al.[108] reported inkjet printing from water-soluble single- and few-layered GO on flexible substrates of poly(ethylene terephthalate), polyimide and paper. The graphene patterns printed on flexible polymer surface showed high electrical conductivity after thermal reduction, and no decrease in conductivity after 100 repeated bending cycles. The graphene inks showed high sensitivity to hydrogen peroxide (H_2O_2) as well as good performance for electric circuits. This inkjet printing technique could be used for fabricating flexible graphene-based electronic devices such as LEDs, solar cells, supercapacitors, displays, and gas sensors. For example, Li et al.[109] developed graphene-based flexible circuits and actuators. Patterns of rGO were printed on different substrates including glass, silicon, PDMS, and PET where adhesive forces were the highest between the printed rGO circuits and PET substrate and lowest for PDMS substrate. Figure 1d−f shows the flexibility characteristics of rGO sheet-based circuits in terms of relative resistance change ($\Delta R/R_0$) as a function of the bending radius (2−30 mm) and stability up to 1000 bending cycles. LED chips developed from large-area flexible rGO-based circuits illuminated bright light on twisting and when wrapped around a roller pen. The rGO circuits were developed on flexible PDMS substrate for conducting bending test to evaluate the electrical stability. A slight change in relative resistance ($\Delta R/R_0$) was observed as the bending radius decreased from 30 mm to 2 mm upon compression. The relative resistance changes remained 5% at a bending radius of 5 mm up to 2000 bending cycles. No breakage of rGO circuit was noticed after the bending test though some mechanical deformation appeared as wrinkles which had a slight impact on electrical resistance. The rGO/PDMS-based hand-shaped soft actuators were fabricated using flexible printed rGO electrodes. This study demonstrates that graphene-based materials can be successfully

DOI: 10.1021/acsami.7b07063
ACS Appl. Mater. Interfaces 2017, 9, 34544−34586

used for flexible electronics from flexible electronic circuits to sensors.

Another example of graphene-based flexible and wearable electronics was demonstrated by Yang et al.[110] who fabricated a wearable temperature sensor by depositing graphene nanowalls (GNWs) on flexible PDMS substrate. Figure 2 shows an SEM

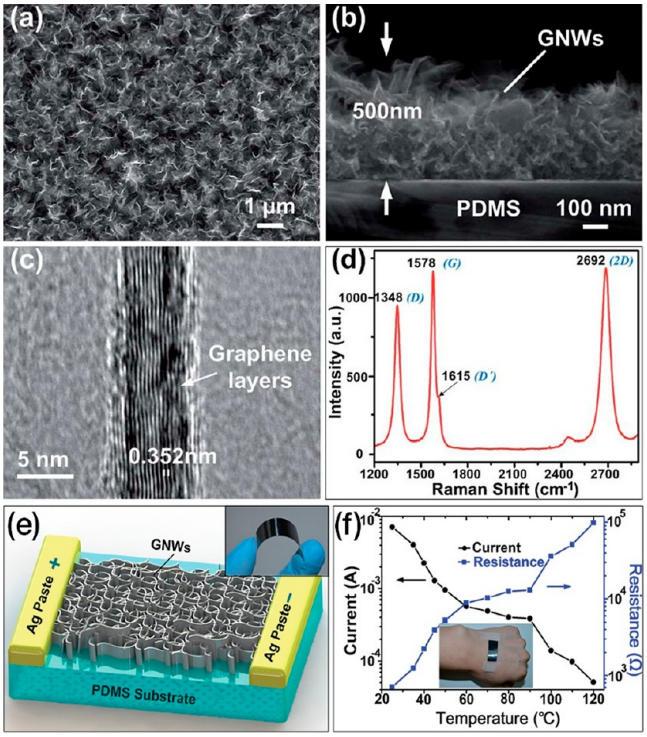

Figure 2. (a) SEM image of sheet-like graphene nanowalls (GNWs) on flexible (PDMS) substrate. The GNWs/PDMS composite sheets were used to fabricate a flexible wearable temperature sensor. (b) SEM image of a cross section of GNWs on PDMS. (c) HRTEM image of GNWs indicating graphene layers. (d) Raman spectrum of GNWs films on PDMS substrate. (e) Schematic structure of flexible GNWs/PDMS temperature sensor. Insert is an optical image showing flexibility of fabricated temperature sensor. (f) Thermal response of GNWs/PDMS sensor. The variation of current and resistance as a function of temperature from 25 °C (room temperature) to 120 °C range at an applied voltage of 5 V. The inset shows a GNWs/PDMS temperature sensor attached on the hand. [Reprinted with permission from ref 110. Copyright Royal Society of Chemistry.]

image of GNWs films on PDMS, an HRTEM image of GNWs showing graphene layers, Raman spectrum of the GNWs films, a schematic structure, photograph and thermal response of flexible GNWs/PDMS sensor. The 500 nm high GNWs are vertically standing graphene nanosheets on a PDMS substrate. The graphene nanosheet has a spacing of 0.35 nm and consists of several graphene layers. Raman spectroscopy showed a strong D-band at 1348 cm^{-1}, G-band at 1578 cm^{-1}, D′-band at 1615 cm^{-1}, and 2D-band at 2692 cm^{-1} indicating huge edges and the presence of defects in the graphene nanosheets. The resistance of GNW films increased by 138-fold as temperature increased from 25 °C (706.2 Ω) to 120 °C (98.04 kΩ). The GNWs/PDMS thermal sensor showed a 3-fold higher positive temperature coefficient of resistivity (0.214 $°C^{-1}$) compared to the carbon nanotube and Pt temperature sensors due to the high thermal sensitivity and stretchability of GNWs and large expansion coefficient of the PDMS film. The GNW/PDMS temperature sensor was used as a wearable device to measure human body temperature. The sensor exhibited fast response time of 1.6 s and recovery time of 8.52 s as well as stability of up to 2 months under ambient environment. The response and recovery times of a sensor device are defined as the time required for achieving 90% of the total electrical resistance change. Such GNWs/PDMS-based stretchable and wearable temperature sensors can be used in field of healthcare.

Flexible strain sensors could find direct applications in wearable electronics to monitor human activities under different physiological motions. The example of a graphene-based wearable strain sensor is provided here. Cheng et al.[111] developed graphene-based composite fiber having compression characteristics and integrated into wearable strain sensors. The sensor structure is a highly elastic yarn made of polyurethane as a core fiber and polyester fibers as the scaffold (denoted as PDCY). The elastic PDCY yarn was dip-coated with GO sheets (PDCY-GO) wrapping on the polyester surface. The PDCY-GO was transformed to PDCY-RGO by hydroiodic acid where GO was reduced to RGO. The conductivity of graphene composite fiber increased from 0.012 to 0.136 S/m as the frequency of dip-coating increased from 2 to 6. Relative resistance change of graphene-based fibers increased monotonically up to 100% tensile strain and thereafter stabilized to 200% strain. The calculated gauge factor (GF) expressed as $(\Delta R/R_0)\ \varepsilon$, where ε represents the strain, was 10 and 3.7 within 1% and 50% strain, respectively. The resistance variation versus torsion level curves showed a broad dynamic range of −280 to +800 rad/m for torsion sensing. The signal changes of 17.7% for 1000 cycles and 37.4% for 5000 cycles were observed at 500 rad/m torsion level than that of 10th cycling. Figure 3 shows graphene composite fiber-based wearable strain sensors tested for human and robotics. The graphene fiber-based strain sensors are capable of monitoring human's knee, hand, elbow motions, speech recognition, heartbeat signal during physical exercise, the quality of sleep during relaxing, turning and trembling, human motions including flexing, walking, jogging, and jumping as well as monitoring of complex robotic motions during a "Gangnam Style" dance; therefore, these sensors could be used for detecting tensile strain, bending and torsion. The graphene composite fiber-based strain sensors were able to detect strain as low as 0.2%, sensing range up to 100% strain, response time of 100 ms and reproducibility up to 10,000 cycles. The graphene composite fiber-based sensors offer high sensitivity, a broad strain sensing range, and the detection for multiple motions and could be used in wearable electronic technologies. The exclusive details focused on the graphene-based flexible and stretchable strain sensors for wearable electronics can be found in a state-of-the-art review chapter recently published by authors.[112]

As discussed above and demonstrated through examples of graphene-based devices including highly flexible LEDs, touch screens, highly sensitive thermal sensor and diverse motions detecting strain sensors that graphene-based materials offer tremendous flexibility, stretchability, and mechanical durability than those of conventional inorganic semiconducting materials such as ITO, Si, Ge, GaAs, etc., currently used in flexible electronics, therefore, could be used in a wide variety of wearable electronic devices.

3. GRAPHENE-BASED FLEXIBLE GAS SENSORS

Graphene-based materials have been explored for developing flexible and stretchable strain and pressure sensors, photodetectors, Hall sensors, electrochemical sensors, and biosensors.[112−119]

DOI: 10.1021/acsami.7b07063
ACS Appl. Mater. Interfaces 2017, 9, 34544−34586

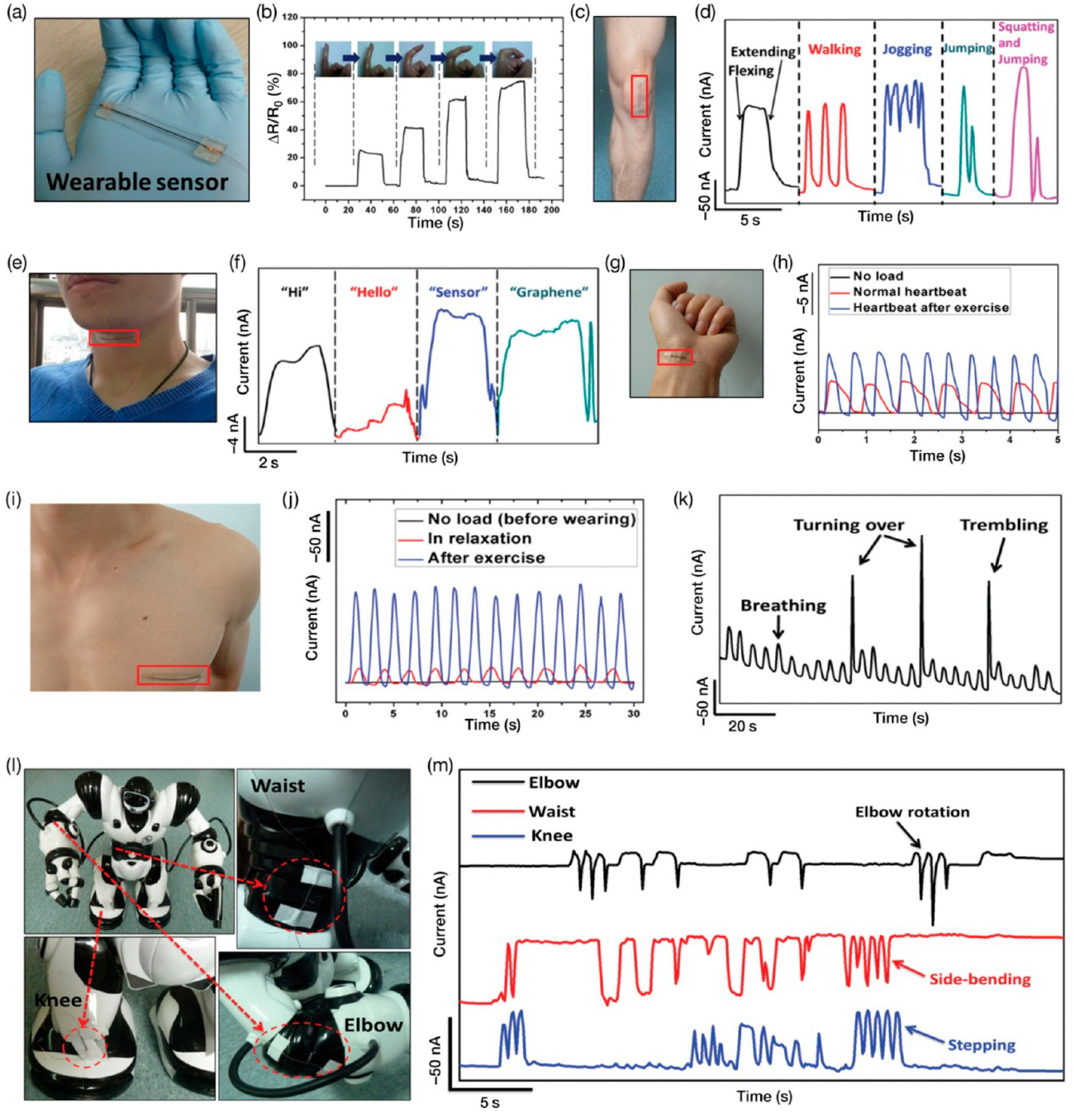

Figure 3. Graphene-based wearable sensors for human and robotics. (a) Photograph of the graphene-based wearable sensor. (b) Response signal originating from wearable sensor during finger bending. Inset shows the photographs of finger bending positions to the corresponding signal. (c) Graphene-based wearable sensor (red box area) attached to the knee. (d) Response of wearable sensor attached to the knee under different motions of flexing/extending, walking, jogging, jumping, and squatting–jumping. (e) Wearable sensor (red box area) attached to the throat. (f) Responsive curves of wearable sensor attached to the throat after sensor-wearer spoke words "Hi", "Hello", "Sensor", and "Graphene". (g) Wearable sensor (red box area) attached to the wrist. (h) Response of wearable sensor attached to the wrist before wearing (no load), and heartbeat under normal and exercise conditions. (i) Wearable sensor (red box area) attached to the chest. (j) Response of wearable sensor attached to the chest before wearing, during relaxation, and after exercise. (k) Response of wearable sensor attached to the chest during deep sleep and light sleep while turning over and trembling. (l) A robot wearing graphene-fiber-based sensors at different movable joints (marked in the red boxes) including elbow, waist, and knee. (m) Response of wearable sensors from elbow (black line), waist (red line), and knee (blue line) during the robot's "Gangnam Style" dance. [Reprinted with permission from ref 111. Copyright Wiley-VCH.]

The oxygenated functional groups in GO impart amphiphilicity, which facilitate the reactivity toward different types of molecules on the graphene surface. Furthermore, the sensitivity toward particular gaseous molecules is induced using catalysts such as nanoparticles of Pd, Pt, Au, Ag, etc. The electrical resistance of graphene changes depending on the nature of the gas (electron donor or acceptor) by the formation of a charge-transfer complex, which is basically a doping process. Graphene-based gas

DOI: 10.1021/acsami.7b07063
ACS Appl. Mater. Interfaces 2017, 9, 34544−34586

and chemical sensors have been of interest due to their industrial applications.[120,121] Some et al.[122] used one-headed polymer optical fiber (POF) sensor arrays made of hydrophilic GO and hydrophobic rGO films for selectively detecting the VOCs including hydrazine, nitromethane, diethylamine, methanol, ethanol, acetone, dichloromethane, and tertahydrofuran (THF). The hydrophilic GO-based POF sensors showed higher sensitivity toward VOCs in the air atmosphere at room temperature compared to hydrophobic rGO-based POF sensors under high humidity as well as in the strong acidic (pH = 1) or basic (pH = 11) conditions due to the existence of copious oxygenated functional groups. Both GO- and rGO-based POF sensor arrays distinguishly identified between THF and dichloromethane at very low concentrations, respectively. The GO prepared at a pH value of 5 exhibited high sensitivity for methanol, ethanol, and THF at 90% RH, acetone at 80% RH, diethylamine and hydrazine at 60% RH, and nitromethane at 50% RH at a concentration of 500 ppb. GO sensors prepared under different pH values also showed sensitivity toward VOCs under high humidity conditions. The VOCs contributed to the swelling of GO layers as evidenced from the measurements of thickness by optical microscopy and the interlayer spacing by the X-ray diffraction (XRD). The interfering effect of humidity over VOCs on GO POF-based sensors was found to be negligible. Rumyantsev et al.[123] demonstrated that the low-frequency noise spectra in graphene-based transistors can be used for sensing vapors of chloroform, methanol, ethanol, acetonitrile, and tetrahydrofuran, though a large resistance change was observed for both toluene and methylene chloride vapors but no change in noise spectra was noticed. Toda et al.[124] reviewed the recent progress on GO-based gas sensors where oxygen functional groups on GO nanosheets interact with polar gas molecules, allowing detection of H_2, NO_2, NH_3, H_2S, water, and organic vapors. The use of graphene-based materials in gas/vapor sensing has been extensively studied in recent years.[125−144]

3.1. Nitrogen Dioxide (NO_2) Sensors. NO_2 is an environmental pollutant arising from industrial emissions, vehicles exhaust, and others, posing a public health hazard. Different types of nanomaterials have been used for efficient detection of NO_2 gas.[145−154] The schematic of a multilayer graphene-based gas sensor and its time-dependent sensitivity toward NH_3 and NO_2 gas molecules are shown in Figure 4. The sensitivity increases with an NO_2 concentration from 25 to 200 ppm for 120 s gas exposure followed by UV irradiation for 120 s. The sensitivity toward 25 ppm of NO_2 was one-fourth compared with that for 200 ppm of NO_2. The transfer-free grown multilayer graphene was tested as a gas sensor for NO_2 and NH_3 gas molecules where opposite sensing responses were observed. The NO_2 molecule is an electron acceptor (*p*-type dopant) so it strongly withdraws electrons from graphene whereas the NH_3 molecule acts an electron donor (*n*-type dopant) so it donates electrons to graphene; therefore, the electrical conductivity of graphene is increased by NO_2 whereas conductivity is decreased by NH_3. The sensors showed long-term stability because no degradation in response was observed after 100 days in an air atmosphere. The sensor after 50 cycles showed a slight decrease in sensitivity due to the accumulated NO_2 gas molecules on the surface of graphene films; however, the sensitivity was recovered after UV irradiation cleaning. Other methods such as thermal annealing, ultraviolet (UV) light, UV/ozone, etc. can be used for clearing the sensing layer for detecting the gas and chemical species. To add a point here, atomic layer etching (ALE) is also one of the most powerful tools to precisely control the layer thickness and

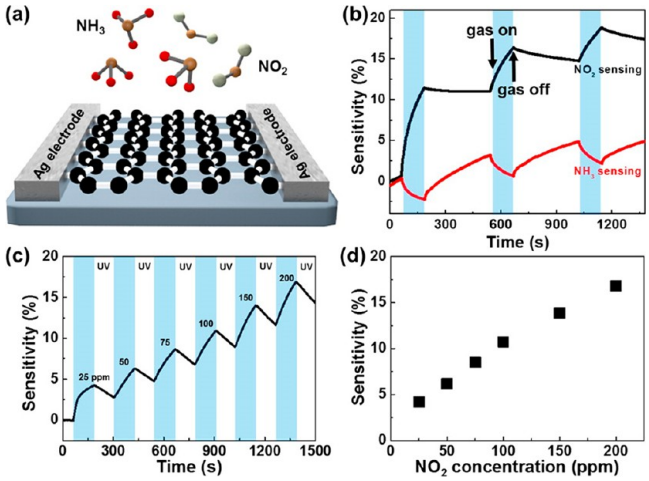

Figure 4. (a) Schematic illustration of the graphene-based sensor toward NH_3 and NO_2 gas molecules. (b) Time-dependent sensitivity of a graphene sensor toward NH_3 and NO_2 gas molecules. (c) Time-dependent sensitivity of graphene sensor with increasing NO_2 concentration from 25 to 200 ppm. (d) Maximum sensitivity of the graphene sensor with increasing NO_2 concentration after exposure to NO_2 gas for 120 s and UV irradiation for 120 s. [Reprinted with permission from ref 70. Copyright American Chemical Society.]

sequentially remove even an atomic layer through the chemical adsorption and physical desorption in cyclic steps in 2D materials such as graphene and MoS_2 without any structural damage and contamination.[52,83] Ricciardella et al.[155] developed a graphene film-based room temperature gas sensor that showed sensitivity to NO_2 up to 50 parts-per-billion (ppb). The sensor was fabricated by drop-casting an *N*-methyl-pyrrolidone solution of graphene nanosheets on an alumina substrate with gold (Au) electrodes. The sensor response was found to be correlated to NO_2 concentrations ranging from 100 to 1000 ppb. In addition to pristine graphene, rGO/Cu_2O nanowire mesocrystals have been used as NO_2 gas sensor.[156] In this case, the rGO network increased the electrical conductivity whereas Cu_2O nanowire mesocrystals induced a high surface area-to-volume ratio, which synergically improved the detection limit to 64 ppb for NO_2 compared to 81 ppb for Cu_2O and 82 ppb for rGO counterparts.

Su and Shieh[157] developed flexible NO_2 sensors by covalently attaching GO to a gold electrode using a layer-by-layer (LbL) procedure together with a peptide chemical protocol. Gold electrodes treated with cysteamine hydrochloride were deposited on a polyethylene terephthalate substrate. *N*-Hydroxysuccinimide (NHS) and *N*-(3-(dimethylamino)propyl)-*N*-ethylcarbodiimide hydrochloride (EDC) were used as the peptide coupling reagent where Au electrodes were reacted with GO. Anchored rGO films were characterized by scanning electron microscopy (SEM), atomic force microscopy (AFM), Fourier transform infrared spectroscopy (FTIR), and electrochemical impedance spectroscopy. The rGO-based flexible NO_2 gas sensor showed a strong response compared with sensors made of CVD-grown graphene. The sensor showed flexibility with 4% deviation in its response when it was bent at a 30° angle. The detection limit was found to be 5 ppm in a binary mixture containing 200 ppm of NH_3. The flexible NO_2 gas sensor showed long-term stability retaining 86% of the original response after 43 days when exposed to 5 ppm of NO_2 gas. Yang et al.[158] developed flexible NO_2 sensors from graphene on a paper substrate, which showed 32−39% response to 200 ppm of NO_2 gas under a strain of 0.5%. In this case, the CVD-grown graphene supported by a

DOI: 10.1021/acsami.7b07063
ACS Appl. Mater. Interfaces 2017, 9, 34544−34586

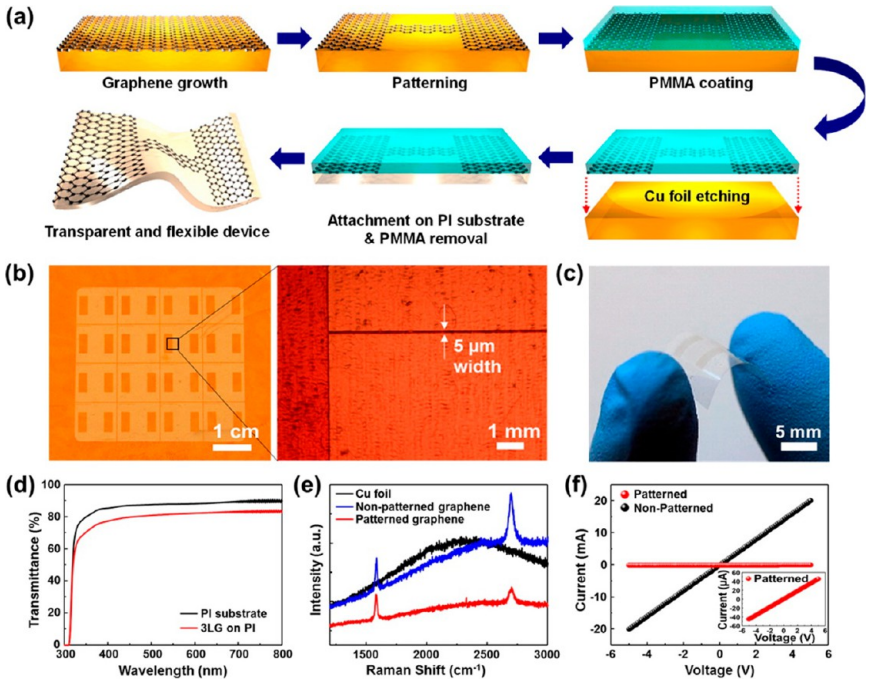

Figure 5. (a) Fabrication procedure of all-graphene-based gas sensor. (b) Optical microscopic images of graphene after patterned on a copper foil. (c) Flexible all-graphene gas sensor fabricated on a polyimide (PI) substrate. (d) Optical transmittance spectra of three-layer graphene deposited on PI and pristine PI substrate. (e) Raman spectra of copper (Cu) foil, nonpatterned, and patterned graphene on the copper foil. (f) Current−voltage (I−V) characteristics of all-graphene sensors before and after patterning. [Reprinted with permission from ref 160. Copyright American Chemical Society.]

poly(methyl methacrylate) layer was transferred onto a paper substrate where two silver paste electrodes served as contacts. The inkjet-printing technique was used for fabricating flexible sensors of rGO films on a PET substrate for detecting NO_2 and Cl_2 gases at ppb level.[159]

Kim et al.[160] fabricated transparent and flexible all-graphene sensors consisting of graphene for both sensor electrodes and active sensing channel, which showed operation under high relative humidity (RH) and mechanical bending. A CVD method was used to grow three-layer graphene (3LG) on a copper (Cu) foil. All-graphene gas sensors were fabricated on a PI substrate. Figure 5 shows the fabrication procedure of these sensors, optical microscopic images of graphene with an electrical channel of 5 mm length and 5 μm width after patterned on a Cu foil, flexibility of the sensor on a PI substrate, transmittance over the 300−800 nm wavelength range, Raman spectra, and current−voltage (I−V) characteristics before and after patterning on a Cu foil. The optical transmittance measured at 550 nm was ∼88% for the PI substrate and ∼80% for 3LG deposited on PI substrate. The sensor exhibits a significant enhancement in resistance after increasing the bias voltage. The response of the patterned sensor to 5 ppm of NO_2 was found to be 4.47% at 1 V and 12.49% at 60 V. The response to 5 ppm of NO_2 for the nonpatterned sensor was not enhanced by applying 10 V with 4.67% at 1 V and 4.35% at 10 V. The nonpatterned sensor also exhibited a noticeable deviation of the response compared with the patterned sensor. When the bias voltage was increased from 1 to 60 V for the patterned graphene sensor, the response time decreased from 328 to 89 s, whereas the recovery time decreased from 1941 to 579 s. The response to 5 ppm of NO_2 for nonpatterned graphene sensor was measured from 27 to 180 °C at an applied voltage of 1 V. The resistance of the sensor reached to ∼240 Ω with increasing temperatures for patterned graphene sensor as a function of bias voltage. The sensor exhibited faster response time and improved recovery with increasing temperature.

The response time of 168 s for the nonpatterned sensor at 180 °C was found to be longer compared with 82 s for the patterned sensor operating with 60 V. The Joule heating may occur in the graphene grain boundaries, which contribute to the local heating spots in the patterned sensor. Graphene grain boundaries dramatically influence the thermal, electrical, optical, and mechanical properties of polycrystalline graphene films. For example, the effect of grain boundaries on gas sensing behavior of graphene has been reported by Yasaei et al.[115] where higher resistance and 300 times higher sensitivity have been measured for isolated grain boundary (GB) in polycrystalline graphene compared to a single graphene grain because graphene GBs function as the main adsorption sites for gaseous molecules. The graphene GB sensors showed 14 times higher sensitivity toward dimethyl methylphosphonate (DMMP) (39.5%) compared with graphene grain sensors (2.8%). Likely, 5 times higher sensitivity toward 1,2-dichlorobenzene was observed for GB sensors than that of grain sensors. The sensitivity of GB sensors also increased from 17 to 70% at 50 ppb DMMP concentration as the distance between electrodes was reduced from 43.6 to 2.8 μm. The sensing mechanism has been explained viewing the closing or opening of local conduction channels by the adsorbed gaseous molecules through the GB, which can be useful for developing future generation of nanosensors.

The relative resistance responses ($\Delta R/R_0$) of the all-graphene sensor to different concentrations of NO_2 at an applied voltage of 60 V, 50% RH, and 50 ppm of ammonia (NH_3), ethanol, and acetone at room temperature are presented in Figure 6. The response to NO_2 at 5 ppm was 13%, while the response to 50 ppm of NH_3 was 5.4%, 1.71% for ethanol (C_2H_5OH), 0.17% for acetone (CH_3COCH_3), and 0.9% for 50% RH in air. The power consumption of the all-graphene sensor increased

DOI: 10.1021/acsami.7b07063
ACS Appl. Mater. Interfaces 2017, 9, 34544−34586

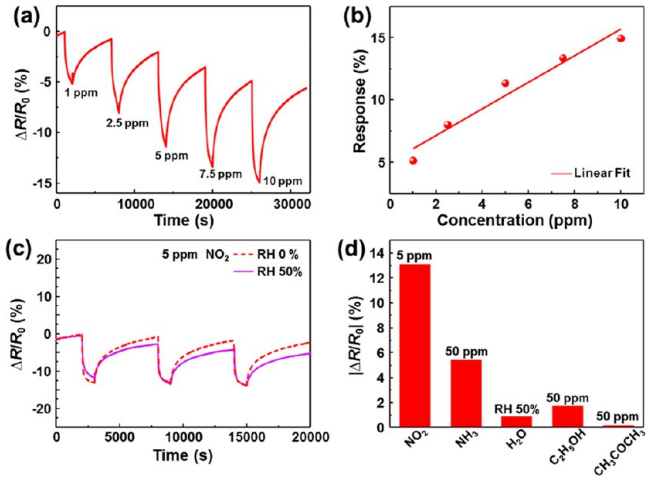

Figure 6. (a) Responses of the all-graphene sensor to different concentrations of NO_2 gas at 60 V. (b) Linear fit showing responses to NO_2 gas concentration at applied voltage of 60 V. (c) Relative resistance responses ($\Delta R/R_0$) of the all-graphene sensor when exposed to 5 ppm of NO_2 in 0% and 50% of relative humidity (RH) at 60 V. (d) Relative resistance responses ($\Delta R/R_0$) of all-graphene sensor to 5 ppm of NO_2, 50 ppm of ammonia (NH_3), 50% RH, 50 ppm of ethanol (C_2H_5OH), and 50 ppm of acetone (CH_3COCH_3) at room temperature. [Reprinted with permission from ref 160. Copyright American Chemical Society.]

from 12 μW to 14.2 mW after applying voltage from 1 to 60 V. The sensor is self-activated with low power consumption, highest sensitivity and selectivity to NO_2. The all-graphene bent sensor exhibited~ 3% degradation under a bending radius of 1 mm.

All-organic NO_2 gas sensor by laser patterning of graphite oxide films deposited on a flexible PET substrate was developed by Strong et al.[161] The highly reduced laser-scribed graphene (hr-LSG) electrodes act as an electrode as well as a current collector. Figure 7 shows all-organic interdigitated electrodes with

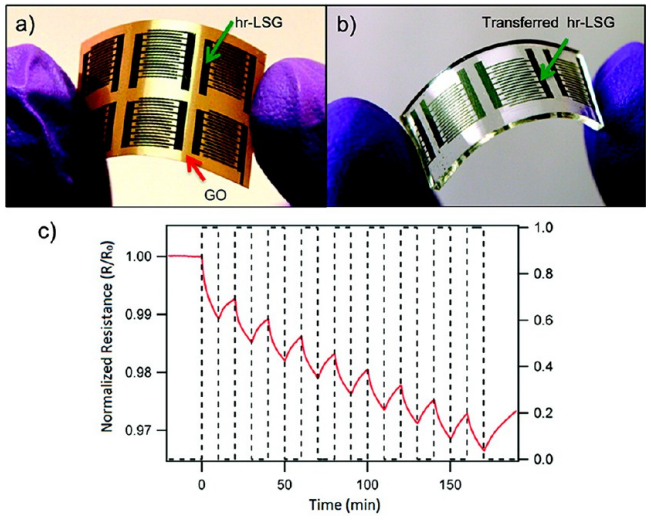

Figure 7. (a) All-organic flexible interdigitated electrodes produced from highly reduced laser-scribed graphene (hr-LSG). (b) Same interdigitated electrodes transferred onto flexible PDMS. (c) Detection of NO_2 gas using flexible all-organic interdigitated electrodes. [Reprinted with permission from ref 161. Copyright American Chemical Society.]

dimensions of 6 mm × 6 mm and ~500 μm spacing, which are directly patterned onto the graphite oxide thin film deposited on a flexible PET substrate. This method allows tuning of the electrical conductivity over 5 orders of magnitude by varying the laser intensity. The hr-LSG was used as the active electrodes whereas the marginally laser-reduced graphite oxide was used as a detecting media. The all-organic interdigitated electrodes were transferred onto a flexible PDMS substrate and thereafter used as flexible gas sensor for NO_2 detection. The sensor response for patterned flexible interdigitated electrodes was recorded after exposing to 20 ppm of NO_2 gas in dry air. The all-organic flexible electrode showed 238% electrochemical activity compared to graphite toward the electron transfer of the ferri-/ferrocyanide redox couple. The low content of oxygen in hr-LSG (~3.5%) benefits the electrochemical activity because higher content of oxygen at the edge plane sites has been found to slow down and limit the electron transfer for the ferri-/ferrocyanide $[Fe(CN)_6^{3-}]/[Fe(CN)_6^{4-}]$ redox couple.

In another study, Jeong et al.[162] developed a flexible NO_2 sensor using vertical carbon nanotubes/reduced graphene hybrid films. The sensor device was made of PI substrate, Au electrode, Ni/Cu microheater, and CNTs/reduced graphene hybrid films. No noticeable NO_2 sensing activity was observed for reduced graphene films as resistance did not change upon exposure to NO_2. However, when vertical CNT arrays were grown on the reduced graphene surface, 20% sensitivity to NO_2 was recorded after 60 min exposure. The sensitivity showed an increase up to 200 °C, thereafter, it decreased until 350 °C. The effect of bending was also measured and the resistance increased with a bending radius of 15 mm. Yun et al.[163] developed a wearable, washable, and bendable electronic textile (e-textile) gas sensor from reduced GO-decorated yarn (RGOY) using commercial textile yarn. RGOY gas sensors were fabricated from RGO-decorated polyester yarn (RGOPY) and RGO-decorated cotton yarn (RGOCY). Figure 8 shows a flexible and wearable gas sensor developed from reduced RGOY, a photograph of RGOCY and RGOPY on a plastic bobbin, and RGOCY-based wearable gas sensing and a LED alarm system integrated into a fabric for NO_2 detection. The RGOCY and RGOPY sensors selectively detected NO_2 at 1.25 ppm with a −12% response compared with a very small response to ethanol (EtOH), ethylene, acetone, and CO_2 at room temperature. The RGOCY sensor responded to 100 ppb NO_2 in the presence of 1 ppm ethanol or 1 ppm ethylene. RGO-based e-textile gas sensors showed durability against detergent and mechanical stability up to 1000 bending cycles at a bending radius of 1.0 mm and high sensitivity of 250 ppb toward NO_2 at room temperature. RGOCY sensor was not sensitive to ethanol or ethylene gas. The stability of the RGOCY sensor was monitored by exposure to 0.25 ppm of NO_2 for 30 min each day for 1 week, where the time for both the response and recovery was found to be constant. RGO/e-textile-based gas sensors can be used for flexible and wearable electronics.

Chemically functionalized graphene films have been used for gas sensing. Huang et al.[164] developed a flexible NO_2 sensor on a PI substrate using sulfonated reduced graphite oxide (S-RGO) decorated with silver nanoparticles (AgNPs). Figure 9 shows the chemical synthesis procedure of Ag-S-RGO inks using graphite oxide followed by the prereduction of GO with sodium borohydride, sulfonation of RGO using aryl diazonium salt, decoration of S-RGO with $AgNO_3$ and thereafter obtaining sulfonated RGO decorated with AgNPs (Ag-S-RGO) via postreduction using hydrazine. The final product Ag-S-RGO consisted of copious amounts of 10−20 nm size AgNPs and was hydrophilic in nature due to attached $-SO_3H$ functional groups

DOI: 10.1021/acsami.7b07063
ACS Appl. Mater. Interfaces 2017, 9, 34544−34586

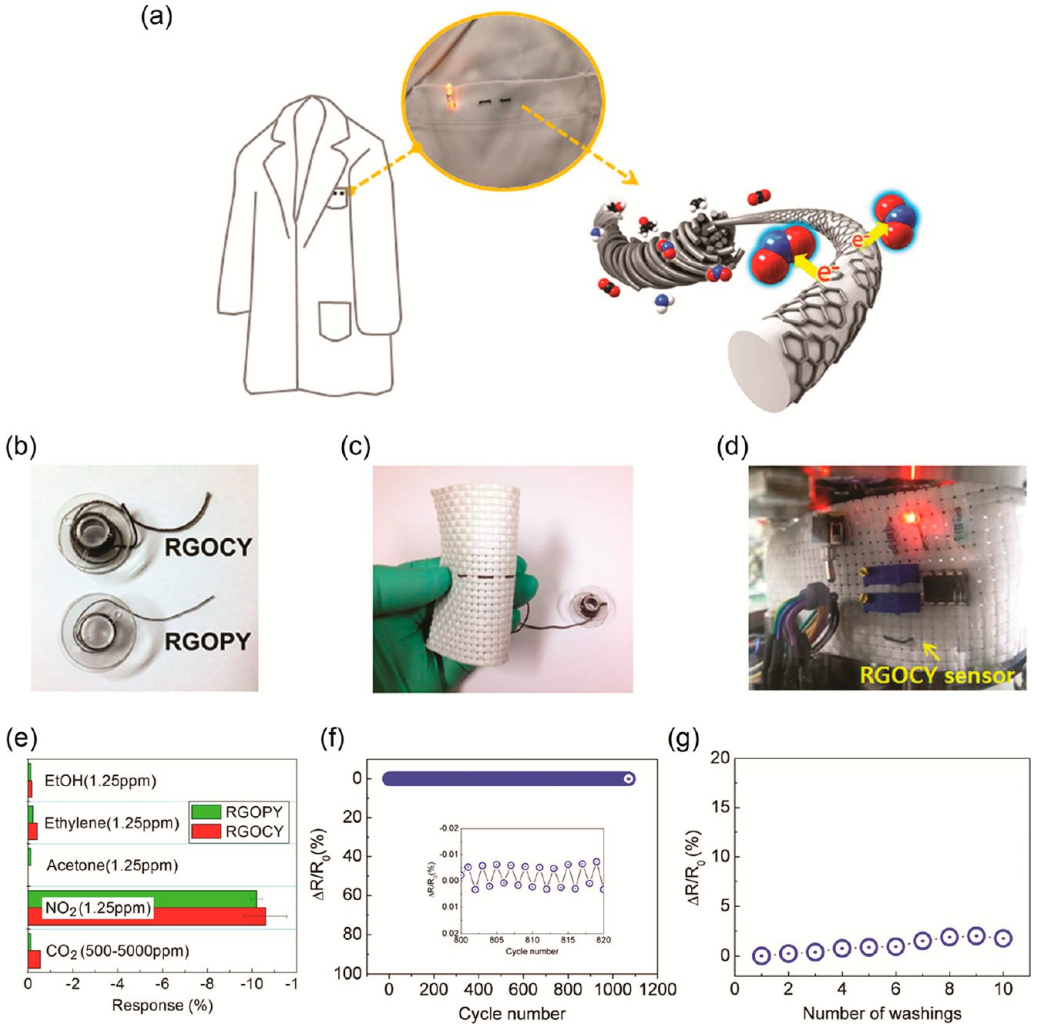

Figure 8. Flexible and wearable gas sensor developed from reduced graphene oxide-decorated with commercial textile yarn (RGOY). (a) Schematic illustration of the RGOY-based gas sensor prepared from microfiber bundles denoted by light gray cylinders, which were wrapped with RGO denoted by dark gray hexagon patches. The red, blue, black, and white spheres represent oxygen (O), nitrogen (N), carbon (C), and hydrogen (H) atoms, respectively. (b) Photograph of RGO-decorated cotton yarn (RGOCY) and RGO-decorated polyester yarn (RGOPY) on a plastic bobbin. (c) RGOCY-based gas sensor integrated into a fabric. (d) Demonstration of RGOCY-based wearable gas sensing and alarm system. (e) Response of RGOCY- and RGOPY-based sensors to different gases at 1.25 ppm concentration. (f) Relative resistance change ($\Delta R/R_0$) of RGOCY-based sensor during repeated bending/straightening process to 1 mm radius over 1000 cycles. (g) Relative resistance change ($\Delta R/R_0$) of RGOCY- and RGOPY-based wearable sensors as a function of the number of washings. [Reprinted with permission from ref 163. Copyright Nature Publishing Group.]

on RGO sheets, therefore imparting a high sensitivity of 0.5 to 50 ppm of NO_2 at room temperature. The Ag-S-RGO sensors were developed by printing Ag interdigitated electrodes and Ag-S-RGO ink on the flexible PI substrate. Figure 10 compares the normalized resistance change ($\Delta R/R$) of Ag-S-RGO sensors to 100 ppm of NO_2, 1 mL concentration each of ammonia (NH_3), methanol (CH_3OH), ethanol (C_2H_5OH), toluene (C_7H_8), and 40−80% RH showing gas selectivity toward various gases. The gas vapors induce changes in electrical resistivity, which shows different magnitudes for each type of gas. The normalized resistance change ($\Delta R/R$) in Ag-S-RGO sensor measured as a function of time for different concentrations of NO_2 under ambient conditions (25 °C, 30% RH) increased from 3.4% for 500 ppb of NO_2 gas to 74.6% for 50 ppm. The printed Ag-S-RGO sensor exhibited fast response and recovery times of 12 and 20 s, respectively when exposed to 50 ppm of NO_2 at room temperature. Comparatively, the S-RGO-based NO_2 sensors showed slow response and recovery times of over 10 min. The Ag-S-RGO sensors showed response of 90, 101, 5, 4, and 10 for 100 ppm of NO_2, 1 mL concentration each of NH_3, CH_3OH, C_2H_5OH, and C_7H_8 respectively. The sensing response of 11, 21, and 21 were recorded for Ag-S-RGO sensors toward 40, 60, and 80% RH, respectively, which indicate that the sensitivity to NO_2 is not much influenced by different RH. The electrical resistance of the Ag-S-RGO sensor increased when exposed to NH_3, which is a reducing agent, contrary to NO_2, which is an oxidizing agent. NO_2 is an electron acceptor so it attracts electrons from a *p*-type Ag-S-RGO layer whereas NH_3 is an electron donor so it injects electrons to the layer. Figure 11 shows the photograph of a printed flexible Ag-S-RGO sensor and the changes in normalized resistance ($\Delta R/R$) as a function of bending cycles. The flexibility of Ag-S-RGO sensors was measured as a function of bending cycles where no change in resistance was observed up to 1000 bending cycles for 1 cm bending radius indicating high electromechanical stability of the flexible Ag-S-RGO sensors.

DOI: 10.1021/acsami.7b07063
ACS Appl. Mater. Interfaces 2017, 9, 34544−34586

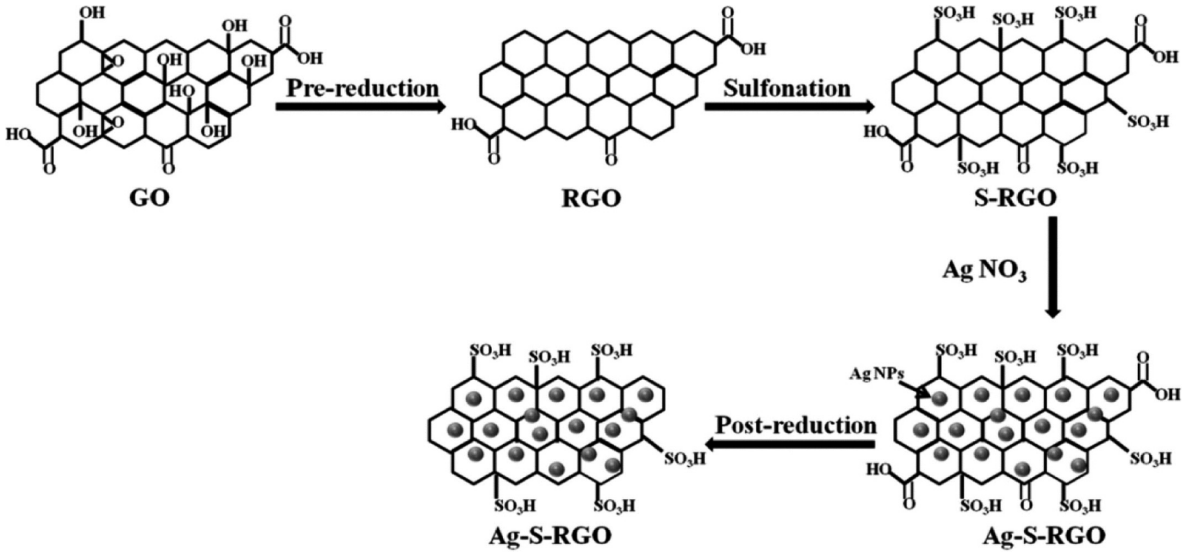

Figure 9. Illustration for the chemical synthesis procedure of Ag-S-RGO inks using graphite oxide. [Reprinted with permission from ref 164. Copyright American Chemical Society.]

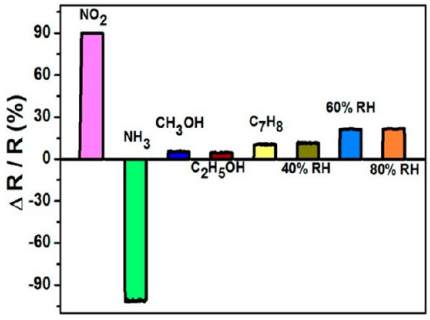

Figure 10. Change in resistance ($\Delta R/R$) of Ag-S-RGO sensors for different concentrations of vapors including 100 ppm of NO_2, 1 mL (13 ppt) of ammonia (NH_3), 1 mL (46 ppt) of methanol (CH_3OH), 1 mL (32 ppt) of ethanol (C_2H_5OH), 1 mL (18 ppt) of toluene (C_7H_8), 40%, 60%, and 80% of relative humidity (RH). [Reprinted with permission from ref 164. Copyright American Chemical Society.]

The nanocomposites of AgNPs/rGO with poly(ionic liquid) (PIL) were used by Tung et al.[165] to fabricate chemoresistive sensors for volatile organic compounds (VOCs). The Ag-RGO/PIL nanocomposite fabricated by the LbL method was used to detect polar vapors of methanol, ethanol, acetone, methyl acetate, and water and nonpolar vapors of chloroform, toluene, dichlorobenzene, and styrene. The sensitivity of the sensors showed a trend toward polar vapors: methanol > ethanol > methyl acetate > acetone > water. The higher sensitivity and selectivity were observed toward polar vapors over those of nonpolar vapors. The sensors showed a signal-to-noise ratio of 168 for 1 ppm of methanol and less than 3% degradation over 3 months. The Ag-RGO/PIL nanocomposite-based sensors showed higher chemoresistive response than that of bare RGO-based sensors toward different polar vapors. This provides evidence that AgNPs play a significant role in enhancing the sensitivity of RGO nanosheets. Cho et al.[166] incorporated metal nanoparticles on the graphene surface to develop a flexible gas sensor for NO_2 and NH_3. The synergistic effect of metal nanoparticles and graphene alters the electronic properties of graphene film, which enhances the selectivity and sensitivity toward gases. Palladium (Pd) nanoparticles on graphene build up hole carriers on graphene, which results in the sensitization of the material by adsorbed NH_3 molecules. On the other hand, aluminum (Al) nanoparticles deplete the hole carriers of graphene, which significantly improves the sensitivity for NO_2 molecules. A similar approach was used for flexible graphene-based gas sensors where the sensitivity was retained after

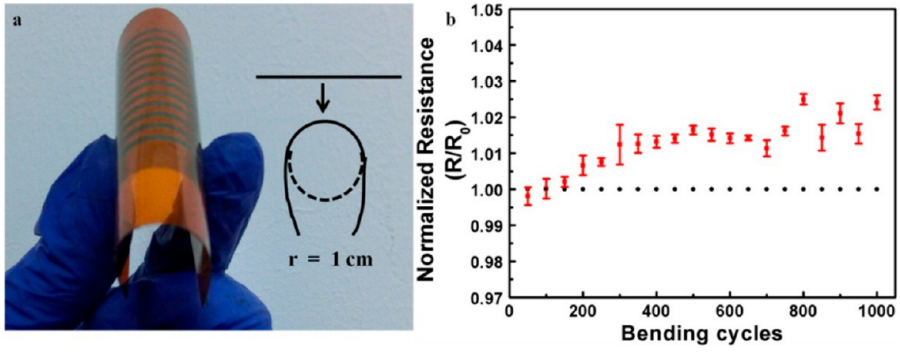

Figure 11. (a) Photograph of a printed flexible Ag-S-RGO sensor and mechanical testing at 1 cm bending radius. (b) Changes in normalized resistance ($\Delta R/R_0$) of the normalized resistance as a function of bending cycles for the Ag-S-RGO sensor. [Reprinted with permission from ref 164. Copyright American Chemical Society.]

DOI: 10.1021/acsami.7b07063
ACS Appl. Mater. Interfaces 2017, 9, 34544−34586

10 000 bending cycles and even after 3 months. The details of graphene-based materials used for developing NO_2 sensors are listed in Table 1. An excellent review on graphene-based gas sensors has been written by Wang et al.[121]

The hybrids of ethylenediamine-modified rGO and polythiophene (PTh) were used by Bai et al.[228] to develop flexible sensors onto a PET film. The rGO-PTh hybrids were characterized by SEM, XRD, TG, UV−visible, and FTIR techniques. The sensing behavior was studied with different rGO weight ratios (1.5, 3, 5, 8, and 10 wt %) in response to 1−10 ppm of NO_2 where the highest response to 10 ppm of NO_2 was observed for 5 wt % rGO hybrid. This also indicates that the excessive loading of rGO contents leads to lower gas-sensitivity. The selectivity and sensitivity of rGO/PTh hybrid film-based sensors were examined for NO_2, NH_3, Cl_2, C_2H_5OH, and CH_2O at a fixed concentration of 10 ppm at room temperature. The 5% rGO/PTh sensor showed both higher response and higher selectivity toward NO_2 than other gases. The response of the hybrid with 5 wt % rGO to 10 ppm of NO_2 was found to be 4 times higher compared with pure PTh due to a synergistic effect. The rGO/PTh hybrid-based flexible sensors were also fabricated using PET thin film substrate. They not only show higher sensitivity and selectivity toward NO_2 but also exhibit flexibility and, therefore, can be used for wearable and portable electronics to detect toxic gases in the environment. In another interesting study, gas sensors were developed from 3D rGO hydrogel using an integrated microheater that was able to detect 200 ppb NO_2 and 20 ppm of NH_3 at room temperature.[185] The microheater was used to enhance the selectivity of NO_2 because the sensor response for NH_3 can be suppressed by increased temperature whereas NO_2 showed no such sensitivity, thus enabling selectively between NO_2 and NH_3 at substrate temperature elevated by the microheater. A limit of detection as low as ∼300 parts per trillion (ppt) for NO_2 was achieved by flexible graphene-based papers, where graphene layers were deposited onto paper.[229]

3.2. Ammonia (NH_3) Sensors. Ammonia is a toxic gas, hazardous to human health; therefore, its monitoring by sensors is very important. A general introduction to ammonia gas, its sources, and detection at low concentrations of parts per billion (ppb) in air is summarized by Timmer et al.[230] Different nanostructured materials including carbon nanotubes,[148,231−234] polyaniline,[235] polypyrrole,[236−239] ZnO,[240−242] tungsten trioxide (WO3),[243,244] SnO_2,[245,246] TiO_2,[247] α-Fe_2O_3,[248] vanadium oxide,[249,250] transition metal dichalcogenides,[251,252] and graphene,[253−259] have been investigated for ultralow-level detection of NH_3. Wang et al.[259] chemically reduced GO sheets on Au electrodes to rGO sheets by hydrazine or pyrrole vapors, which consequently provided a gas sensor based on self-assembled rGO sheets. The rGO reduced by pyrrole vapors exhibited 2.7 times higher response to 50 ppm concentration of NH_3 compared to rGO reduced by hydrazine vapors. The change in resistance was clearly observed when the sensor was exposed to a wide range of concentrations from 5 ppb to 100 ppm. The resistance changed by 22% at 100 ppm concentration of NH_3. However, as the concentration was decreased to a minimum level of 5 ppb, the resistance changed only by 4.2%. The rGO reduced by pyrrole showed excellent sensitivity and long-term reproducibility to NH_3 over a period of several months. The rGO sensor showed 2.3 times higher response to 100 ppm of NH_3 compared with 1% saturated vapor concentrations of DMMP, methanol, dichloromethane, hexane, chloroform, and xylene, indicating selectivity of self-assembled rGO (pyrrole reduced)-based sensors over different gases. Karaduman et al.[194] used Ag, Pt, and Au

Table 1. Gas Sensors Developed from Graphene-Based Materials[a]

Graphene-based gas sensors	Sensor type	Gas analyte	Limit of detection	Ref.
NO_2 sensors				
Pristine graphene (CVD-grown) *in situ* cleaning with UV light	Chemiresistor	NO_2	2.06 ppt	167
Graphene (mechanical exfoliation)	Chemiresistor	NO_2	1.5 ppm	168
Graphene (CVD-grown)	Chemiresistor	NO_2	100 ppb	169
3D porous graphene hydrogel	Chemiresistor	NO_2	200 ppb	170
Graphitic carbon nitride (g-C_3N_4)/graphene composite	Chemiresistor	NO_2	5 ppm	171
Graphene single-layer/SiC	FET	NO_2	2.5 ppm	172
Graphene/MoS_2 hybrid aerogel	Chemiresistor	NO_2	14 ppb	173
Ozone-treated graphene (CVD-grown)	Chemiresistor	NO_2	1.3 ppb	174
Multilayer graphene films (CVD-grown)	Chemiresistor	NO_2	1 ppm	175
Nitrogen-doped graphene nanosheets	Chemiresistor	NO_2	120 ppb	176
Graphene oxide doped with cesium (GO-Cs)	Chemiresistor	NO_2	90 ppb	177
ZnO nanorods/rGO) mesoporous nanocomposites	Chemiresistor	NO_2	50 ppb	178
rGO/SnO_2 nanoparticles	Chemiresistor	NO_2	5 ppm	179
Nitrogen-doped reduced graphene oxide/SnO_2 nanoparticles	Chemiresistor	NO_2	5 ppm	180
Graphene aerogel-supported SnO_2 nanoparticles	Chemiresistor	NO_2	50 ppm	181
Reduced graphene oxide (rGo)	Chemiresistor	NO_2	82 ppb	156
rGO/Cu_2O nanowire mesocrystals	Chemiresistor	NO_2	64 ppb	156
rGO nanosheet/SnO_2 monocrystals	Chemiresistor	NO_2	50 ppb	182
rGO/WO_3 nanocomposite	Chemiresistor	NO_2	5 ppm	183
rGO/α-Fe_2O_3 nanocomposite	Chemiresistor	NO_2	180 ppb	184
3D rGO hydrogel with integrated microheater		NO_2	200 ppm	185
rGO/polyuethane nanofiber nanocomposites (flexible)	Chemiresistor	NO_2	50 ppb	186
Graphene (CVD-grown) on PET substrate (flexible)	Chemiresistor	NO_2	200 ppm	187
rGO/$NaBH_4$ on PET substrate (flexible)	Chemiresistor	NO_2	5 ppm	157
Single-layer graphene on PES substrate (flexible)	Chemiresistor	NO_2	500 ppb	188
Sulfonated rGO decorated with AgNPs on PI substrate (flexible)	Chemiresistor	NO_2	500 ppb	164
Flower-like ZnO/flexible rGO sheets	Chemiresistor	NO_2	5 ppb	189

DOI: 10.1021/acsami.7b07063
ACS Appl. Mater. Interfaces 2017, 9, 34544−34586

Table 1. continued

Graphene-based gas sensors	Sensor type	Gas analyte	Limit of detection	Ref.
NH_3 sensors				
Pristine graphene (CVD-grown) *in situ* cleaning with UV light		NH_3	33.2 ppt	167
Graphene (CVD-grown)	Chemiresistor	NH_3	500 ppb	169
3D porous graphene hydrogel with integrated microheater	-	NH_3	20 ppm	185
NO_2-doped graphene (CVD-grown)	FET	NH_3	200 ppb	190
Single-layer graphene (CVD-grown) on mica substrate	FET	NH_3	50 ppm	131
Graphene (CVD-grown) FET gated by ionic liquid	FET	NH_3	130 ppb	191
Cobalt porphyrin functionalized graphene	-	NH_3	100 ppb	192
Graphene nanoplatelets/polyaniline nanocomposite	Chemiresistor	NH_3	1 ppm	144
Graphene/PEDOT:PSS composite (flexible)	Chemiresistor	NH_3	5 ppm	261
Graphene (CVD-grown) with gold nanoparticles	Chemiresistor	NH_3	6 ppm	193
rGO/AgNPs nanocomposite	Chemiresistor	NH_3	1.2 ppb	194
rGO/PtNPs nanocomposite	Chemiresistor	NH_3	1.6 ppb	194
rGO/AuNPs nanocomposite	Chemiresistor	NH_3	16 ppb	194
rGO/1,8,15,22-tetra-(4-*tert*-butylphenoxyl)-leadphthalocyanine hybrid	Chemiresistor	NH_3	300 ppb	195
Pyrrole-reduced graphene oxide (rGO)	Chemiresistor	NH_3	1 ppb	196
rGO/poly(3-hexylthiophene) composite	Chemiresistor	NH_3	10 ppm	197
rGO/polyaniline (PANI) composite	Chemiresistor	NH_3	5 ppm	198
Polyaniline (PANI)/graphene oxide (GO)/ZnO hybrid LbL film	Chemiresistor	NH_3	25 ppm	199
H_2 sensors				
Graphene oxide (dielectrophoresis process)	Chemiresistor	H_2	100 ppm	200
Graphene monolayer (CVD-grown)/Pd nanoparticles	Chemiresistor	H_2	25 ppm	201
Graphene nanoribbons/Pd nanoparticles	Chemiresistor	H_2	30 ppm	202
Pd-functionalized multilayer graphene nanoribbon	Chemiresistor	H_2	40 ppm	203
Graphene monolayer (CVD-grown)/Pd nanoparticles on PET (flexible)	Chemiresistor	H_2	20 ppm	204
Graphene monolayer (CVD-grown)/Pd nanoclusters on PEN (flexible)	Chemiresistor	H_2	0.1 ppm	205
rGO/Pt nanoparticles composite (flexible) H_2	RFID	H_2	1 ppm	206
Multiwalled carbon nanotubes (MWCNTs)/Pd nanocubes/rGO	Chemiresistor	H_2	10 ppm	207
Graphene/ZnO nanotubes (self-assembled)	Chemiresistor	H_2	10 ppm	208
rGO/TiO_2 decorated by Pd/Pt nanoparticles	Chemiresistor	H_2	500 ppm	209
Graphene (mechanical exfoliation) decorated by SnO_2 nanoparticles	FET	H_2	1 ppm	210
PtNPs decorated graphene oxide (GO) hybrid	FET	H_2	200 ppm	211
PdNPs decorated graphene composite	Chemiresistor	H_2	0.2 ppm	212
CO_2 sensors				
Pristine graphene (CVD-grown) *in situ* cleaning with UV light	Chemiresistor	CO_2	136 ppt	167
Graphene sheet prepared by mechanical cleavage	Chemiresistor	CO_2	10 ppm	213
Hydrogen plasma reduced GO (CVD-grown)	Chemiresistor	CO_2	750 ppm	214
Graphene/Sb_2O_3 quantum dots (QDs) composites	Chemiresistor	CO_2	50 ppm	215
Graphene/Al_2O_3 QDs composites	Chemiresistor	CO_2	100 ppm	216
SO_2 sensors				
Pristine graphene (CVD-grown) *in situ* cleaning with UV light	Chemiresistor	SO_2	67.4 ppt	167
Graphene (CVD-grown)	FET	SO_2	50 ppm	217
Reduction of graphene oxide (rGO)	Chemiresistor	SO_2	5 ppm	218
TiO_2/rGO hybrid film (layer-by-layer self-assembly)	Chemiresistor	SO_2	1 ppb	219
H_2S sensors				
Chemically converted graphene/ZnO nanorods	Chemiresistor	H_2S	2 ppm	220
Nonoxidized graphene flakes/porous WO_3 nanofibers composite	Chemiresistor	H_2S	100 ppb	221
Cu_2O nanocrystals grown on functionalized graphene sheets	Chemiresistor	H_2S	5 ppb	222
Poly(4-styrenesulfonic acid)-doped PANI/graphene nanocomposites	Chemiresistor	H_2S	1 ppm	223
SnO_2 nanofibers/rGO nanosheets	Chemiresistor	H_2S	1 ppm	224
		Acetone	100 ppb	224
SnO_2 nanorods/graphene nanosheets	Chemiresistor	H_2S	1 ppm	225
SnO_2 quantum wire/rGO nanocomposites	Chemiresistor	H_2S	43 ppb	226
rGO/polyimide flexible substrate	Chemiresistor	H_2S	1 ppm	227
	Chemiresistor	H_2	1 ppm	227
	Chemiresistor	CO	1 ppm	227
Pristine graphene (CVD-grown) *in situ* cleaning with UV light	Chemiresistor	NO	158 ppq	167
Pristine graphene (CVD-grown) *in situ* cleaning with UV light	Chemiresistor	N_2O	103 ppt	167
Pristine graphene (CVD-grown) *in situ* cleaning with UV light	Chemiresistor	O_2	38.8 ppt	167

[a]Sodium borohydride ($NaBH_4$), poly(ether sulfone) (PES), 2,4,6-trinitrotoluene (TNT), liquid petroleum gas (LPG).

DOI: 10.1021/acsami.7b07063
ACS Appl. Mater. Interfaces 2017, 9, 34544−34586

nanoparticles decorated rGO films for NH_3 sensing. The AgNPs-rGO nanocomposite shows the higher sensitivity and selectivity toward NH_3 gas compared with PtNPs-rGO and AuNPs-rGO nanocomposites and excludes the interference from CO, H_2, and CO_2 gases (Figure 12). The sensitivity of 6.52, 2.87, and 0.5%

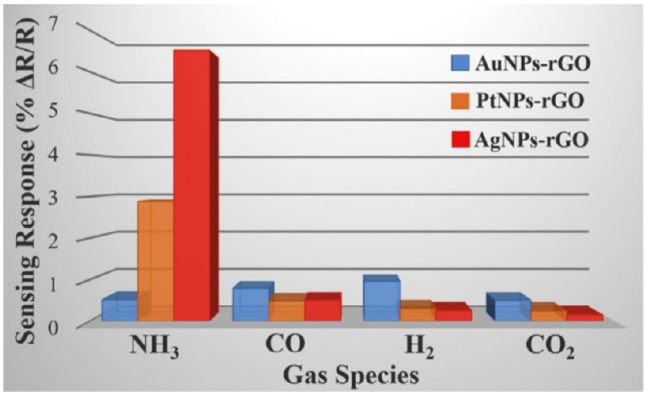

Figure 12. Selectivity of NH_3 gas by the AuNPs-rGO, AgNPs-rGO, and PtNPs-rGO nanocomposite-based sensors over interfering CO, H_2, and CO_2 gases at 1 ppm. [Reprinted with permission from ref 194. Copyright Elsevier.]

were measured for the AgNP-rGO, PtNPs-rGO, and AuNPs-rGO nanocomposites at 1 ppm concentration of NH_3 gas at room temperature, respectively. The AgNPs-rGO, PtNP-rGO, and AuNPs-rGO nanocomposites showed the linear range of 5−15 ppm, 4−15 ppm, and 4−13 ppm; and response/recovery times of 5/6 s, 7/8 s, and 13/17 s for the NH_3 gas, respectively. The higher sensitivity of AgNPs seemingly originated from the stronger molecular interactions, lower ionization energy of Ag that improved catalytic adsorption and also more surface active sites accessible to NH_3 gas molecules.

In order to make sensors cost-effective, multilayered graphene on a 3 in. diameter filter paper was used to develop highly sensitive and flexible ammonia sensor.[260] The sensor was able to detect ammonia concentrations as low as 430 ppb. The response of the graphene sensor was measured as a function of ammonia concentrations, varying from 400 to 4000 ppm. The variation in sensitivity was recorded for both flat and bent positions. Seekaew et al.[261] used inkjet-printing technique for fabricating flexible sensors consisting of graphene/poly(3,4-ethylenedioxythiophene):poly-(styrenesulfonate) (PEDOT:PSS) composite film for detecting ammonia at room temperature. The electronic ink made of graphene dispersion in PEDOT:PSS solution was inkjet-printed on a transparent substrate with prefabricated electrodes. TEM, FTIR, UV−visible and Raman spectroscopy were used to confirm a few-layer graphene in PEDOT:PSS matrix and $\pi-\pi$ interactions occurring between graphene and PEDOT:PSS. The sensor exhibited high selectivity to NH_3 in the concentration range of 25−1000 ppm at room temperature, which may be due to the increased specific surface area by graphene and increased π electron interactions between the sensing film and molecular NH_3.

Polyanline (PANI) is an interesting π-conjugated polymer that has been investigated for sensor applications. Guo et al.[262] used graphene/PANI composite films for fabricating flexible and transparent gas sensors for foldable and wearable electronic devices. The nanocomposite film was prepared by anchoring PANI nanoparticles into the rGO surface and simultaneously depositing PANI nanofibers on a flexible PET substrate to form a nanocomposite network. The flexible gas sensor showed high sensitivity toward NH_3 from 100 ppb to 100 ppm, fast response (36 s)/recovery time (18 s), and strong mechanical flexibility over 1000 bending cycles. The high sensitivity arises from the synergetic effects and a high surface area of 47.9 m^2/g of the graphene/PANI composite films. Gavgani et al.[263] reported flexible ammonia sensor using sulfur (S) and nitrogen (N) codoped graphene quantum dots (GQDs)/PANI composite deposited on flexible poly(ethylene terephthalate) PET thin film. The S and N doped GQDs/PANI hybrid showed 5-fold higher sensitivity compared with pure PANI for 100 ppm of NH_3. The incorporation of S- and N-doped GQDs in PANI increased NH_3 response (42% at 100 ppm and 385% at 1000 ppm) and showed fast response time of 115 s and recovery time of 44 s at room temperature. Furthermore, the sensitivity of flexible gas sensors was found to increase as the bending angle was increased. Duy et al.[264] developed flexible and transparent sensors using rGO coupled with organic dye bromophenol blue. The flexible sensors showed high mechanical flexibility, workability >5000 bending cycles with 0.95 cm bending radius and 60% transparency in the visible region. The water-trapping dye layer on rGO facilitates higher sensitivity and operation in 80% humidity, and detection of NH_3 (5−40 ppm). The flexible and transparent rGO sensor coupled with bromophenol blue dye can be used for real-time monitoring of chemical vapors in wearable electronics.

Two-dimensional TMDs are emerging as a new class of electronic and optoelectronic materials.[82−84] Cho et al.[265] fabricated a 2D heterostructured gas sensor using graphene/molybdenum disulfide (MoS_2) prepared by CVD. For developing flexible sensors, exfoliated MoS_2 flakes were used as the channel whereas patterned graphene lines were used as the electrodes. Figure 13 shows an optical image of the flexible

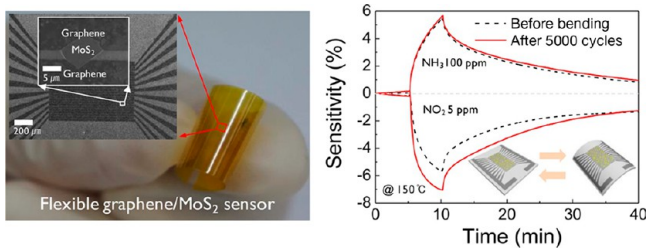

Figure 13. (Left) Optical image of flexible graphene/MoS_2 heterostructured sensor on a bent polyimide substrate. SEM image of the MoS_2 sensor with patterned graphene electrodes. MoS_2 flake is bridged by two graphene lines. (Right) Comparison of NO_2 and NH_3 gas response characteristics of the flexible sensor before and after 5000 bending cycles. The inset is 3D schematic images of the sensor under the bending test. [Reprinted with permission from ref 265. Copyright American Chemical Society.]

graphene/MoS_2 heterostructured sensor device on a PI substrate and NO_2 gas response characteristics before and after 5000 bending cycles. Patterned graphene was employed for charge collection in place of metal electrodes in the sensor, which detected NO_2 as low as 1.2 ppm. For Au/Ti/MoS_2 sensor device, the sensitivity to NO_2 was saturated at a concentration of 20 ppm whereas NH_3 elicited sensitivity up to 100 ppm. The NO_2 molecules caused negative sensitivity so the resistance was found to decrease whereas NH_3 molecules increased the resistance. Furthermore, as the concentration of NH_3 increased from 5 to 100 ppm, the sensitivity of graphene/MoS_2 gas sensor increased. The limit of detection for NO_2 was much lower compared with

DOI: 10.1021/acsami.7b07063
ACS Appl. Mater. Interfaces 2017, 9, 34544−34586

NH_3. For comparison, Au/Ti/MoS_2 gas sensor showed *n*-type behavior whereas graphene/MoS_2 heterojunction gas sensor a *p*-type behavior. The flexible graphene/MoS_2 heterostructured sensor device showed no significant degradation up to 5000 bending cycle tests and gas sensing could be performed at 150 °C; the sensor also showed long-term stability, performing well even after 19 months. Huang et al.[266] reported SiO_2@graphene core−shell hybrids for increasing sensitivity to different gases. The hybrid showed higher performance compared to bare rGO films due to large surface area and less agglomeration. The response of SiO_2@graphene hybrid-based sensors for 50 ppm of NH_3 was increased by 8 times whereas to 50 ppm of NO_2 gas was increased by 5 times. The graphene layers also helped to increase the stability of the sensors. The SiO_2@graphene core−shell hybrid showed 25% decay in performance compared to a 92% decay observed for the bare rGO films. NH_3 sensors have been developed from rGO/PANI hybrids[198] and characterized by TEM, SEM, IR, UV−visible, and Raman spectroscopy. These sensors exhibited 3.4 and 10.4 times higher sensitivity to 50 ppm of NH_3 compared with sensors based on bare PANI nanofibers and bare graphene sheet, respectively. The synergetic interaction between the rGO sheets and PANI nanoparticles led to enhanced sensing behavior of the rGO/PANI hybrids.

The kinetics of NH_3 adsorption/desorption on the surface of graphene thin film has been studied using graphene field effect transistors.[267] The desorption process involves a rapid loss of NH_3 from the top graphene surface with a slower removal of NH_3 from the bottom surface that interfaces with SiO_2/Si substrate identified as a Fickian diffusion process. Adsorption kinetics of NH_3 onto Pt nanoparticle-decorated graphene films has been studied.[268] Both sensitivity and the sensor recovery time were enhanced by the Pt nanoparticles dispersed on the graphene surface. The adsorption/desorption process was evaluated using Langmuir kinetic theory for NH_3 adsorption whereas the effect of surface inhomogeneity was analyzed through Freundlich isotherm. The heat of adsorption and the activation energy indicated that the Pt NP-decorated graphene surface had two different adsorption sites whereas the bare graphene surface had only one adsorption site. This phenomenon yielded 80%−85% increase in sensitivity for Pt NP-decorated graphene surface compared to that of bare graphene surface.

3.3. Hydrogen (H_2) Sensors. Hydrogen is widely used in transportation and aerospace applications, but its safety is a serious concern because it is a highly flammable and explosive gas. Therefore, highly sensitive H_2 detectors are in a great demand to monitor possible hydrogen leaks. Metal oxides such as tin oxide (SnO_2), zinc oxide (ZnO), titanium oxide (TiO_2), vanadium dioxide (VO_2), tungsten trioxide (WO_3), molybdenum trioxide (MoO_3), indium oxide (In_2O_3), niobium pentoxide (Nb_2O_5), nickel(II) oxide (NiO), and metal oxides doped with gold (Au), platinum (Pt), palladium (Pd), and ruthenium (Ru) show a significant change in their resistance after exposure to hydrogen.[269−278] In this regard, graphene-based materials have also been investigated for their low-cost and ease of fabricating sensors. Wu et al.[201] prepared graphene film on Cu foils by CVD under ambient pressure. The large-area (4 in. × 4 in.) graphene film was transferred onto a 6 in. silicon wafer. Raman spectroscopy indicated the formation and transfer of a monolayer graphene film. A 4 mm × 3 mm size graphene film was used for fabricating hydrogen sensors with 1 nm Pd nanoparticle film. Hydrogen in air with 25−10 000 ppm (0.0025%−1%) concentrations was used to measure the sensitivity. A 10% increase in resistance was observed when exposed to 1% hydrogen concentration whereas for lower hydrogen concentration of 0.0025% (25 ppm), the resistance increased only by 0.2%. A response time of 213 s was measured for 0.05% (500 ppm) hydrogen concentration where the resistance increased by 1% in less than 30 s. The Pd-decorated graphene films showed high sensitivity, fast response and recovery, and usability for multiple cycles.

It has been demonstrated that surfaces of Pd and Pt nanoparticles selectively adsorb H_2 molecules; hence Pd and Pt NPs-decorated graphene films are attractive materials for H_2 sensing. Lange et al.[279] prepared Pd nanoparticle-decorated graphene composite by LbL deposition on gold electrodes. The incorporation of Pd nanoparticles increased the sensitivity over 1 order of magnitude in their study for hydrogen, nitrogen dioxide, and humidity. The sensitivity depended on the number of bilayers of graphene/Pd nanoparticles where nanocomposites with seven bilayers showed a stronger response to H_2 dissolved in wet air than ten bilayers. Pristine graphene without Pd nanoparticles exhibited a very little response to H_2. Therefore, Pd nanoparticles play a catalytic role in the *n*-doping of graphene by H_2 molecules. The effect of humidity was measured on both pristine graphene and graphene/Pd nanoparticle composite, and the resistance was found to decrease when switching from humid air to dry air. However, the graphene/Pd nanoparticles composite showed a faster response. For nitrogen dioxide (NO_2), the graphene sensor showed more sensitivity than that based on graphene/Pd nanoparticles composite. Johnson et al.[203] fabricated Pd-functionalized multilayer graphene nanoribbon (MLGN) networks for H_2 sensing at room temperature with fast response as well as recovery time. When the MLGN network sensor was exposed to 2000 ppm hydrogen, the maximum relative resistance response ($\Delta R/R$) increased from 72% to 113% whereas the response time decreased from 8 to 3 s and recovery time from 35 to 7 s as the operating temperature was raised from 20 to 100 °C.

Metallic Pd and Pt nanoparticles show an excellent sensitivity toward hydrogen gas. Pak et al.[202] prepared residue-free graphene nanoribbons (GNRs) of 200 nm width at 1 μm pitch using laser interference lithography. AFM, micro-Raman spectroscopy, and XPS measurements showed the formation of high-quality GNRs. The Pd nanoparticles were deposited on the GNRs as a catalyst for H_2 sensing, and the GNR array acts as a conductive path. The Pd-decorated GNR array showed 90% response within 60 s to 1000 ppm of H_2 and 80% recovery within 90 s in nitrogen. The repeatable sensitivity of GNRs array was observed even at a low H_2 concentration of 30 ppm. The sensitivity as a function of time was compared for pristine graphene and 200 nm-wide GNR sensors with H_2 concentration ranging from 30 to 1000 ppm. The pristine graphene sensor showed 80% recovery in 18 min 40 s compared to the GNR sensor that recovered by 80% within 90 s. In order to compare the repeatability, 22 cycles of 2 min on-state and then 2 min off-state were conducted at 1000 ppm, and the GNR sensor exhibited good repeatability, and fast and stable on/off switching behavior in each cycle while the pristine sensor saturated after 5 cycles and only recovered over 30% within 2 min. In comparison to graphene, Mubeen et al.[280] used Pd nanoparticle-decorated single-walled carbon nanotube films for H_2 nanosensors, which showed 0.42% sensitivity at 100 ppm detection limit, 90% response time of 18 min for H_2 concentrations up to 300 ppm, and 20 min recovery time at 100 ppm in air.

To demonstrate the role of PdNPs in H_2 gas sensing, Chung et al.[204] fabricated flexible sensors using a single-layer graphene-decorated with Pd nanoparticles on a flexible substrate. The Pd

DOI: 10.1021/acsami.7b07063
ACS Appl. Mater. Interfaces 2017, 9, 34544−34586

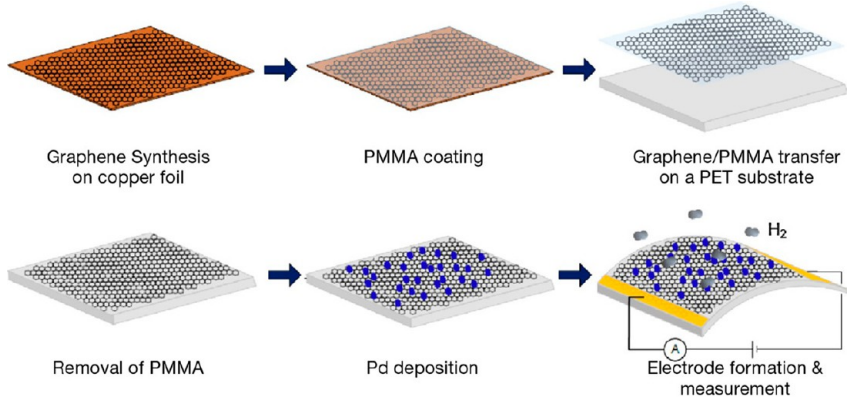

Figure 14. Fabrication procedure of flexible hydrogen gas sensor using graphene decorated with palladium nanoparticles. [Reprinted with permission from ref 204. Copyright Elsevier.]

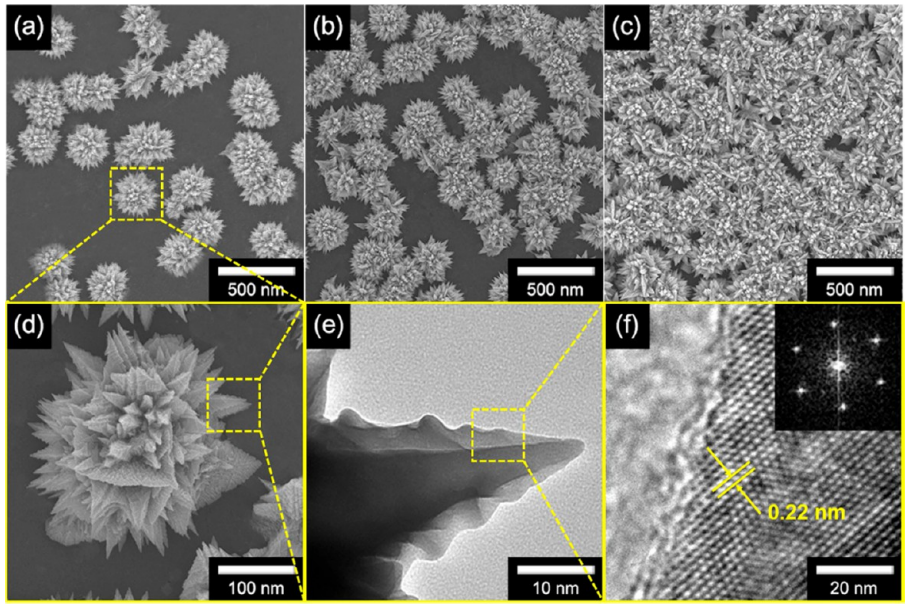

Figure 15. FE-SEM images of flower-like palladium (Pd) nanoclusters onto a CVD-grown graphene layer with different populations of Pd nanoclusters ((a) low, (b) medium, and (c) high). (d) High-resolution SEM, (e) TEM images, (f) HR-TEM, and inset is an FFT pattern. [Reprinted with permission from ref 205. Copyright Nature Publishing Group.]

nanoparticles were deposited on the graphene surface by thermal evaporation. Figure 14 shows the fabrication procedure of graphene-based H_2 sensor. The single-layer graphene was deposited on both sides of the Cu foil using CVD. One side of the Cu foil was spin-coated with PMMA in order to provide support to the graphene layer while transferring to a substrate whereas the graphene was removed from other side by oxygen plasma treatment. The graphene/PMMA layer was separated and transferred onto a flexible PET substrate, and the PMMA layer was removed using chloroform. Palladium with a thickness of 1−10 nm was deposited on the graphene surface using thermal evaporation. The density of Pd nanoparticles on the graphene surface can be controlled during deposition, which is important for the performance of the gas sensor. The sensor with 3 nm thick Pd showed 33% gas response after exposing to 1000 ppm of H_2. The sensor is capable of detecting noise level as low as 20 ppm of H_2 at 22 °C (room temperature). The gas response was found to saturate during consecutive cycles with slow recovery. The sensor based on graphene decorated with Pd nanoparticles is highly flexible and showed no significant degradation after bending with a 3 mm bending radius and exposing to 1000 and 500 ppm of H_2 gas. This indicates that Pd-decorated graphene sensors are suitable for flexible sensing applications.

Shin et al.[205] electrodeposited flower-like Pd nanoclusters onto a CVD-grown graphene electrode. The graphene layer was transferred onto flexible poly(ethylene naphthalate) (PEN) thin film substrate to induce flexibility and mechanical stability. The surface of the graphene layer was functionalized with 1,5-diaminonaphthalene (DAN) to mediate the formation of flower-shaped Pd nanoclusters, which grow in size with reaction time. The population density of the flower-like Pd nanoclusters, which is responsible for H_2 sensitivity, can be controlled by adjusting the concentration of DAN (Figure 15). The population of Pd nanoclusters increased as the DAN concentration is increased from 0.01 to 0.1 M due to the higher number of PdNPs as nuclei; therefore, a high population of Pd nanoclusters eventually leads to higher sensitivity because of more reactive sites for H_2 molecules. Pd nanoclusters were 300 nm in size and consisted of long needles of hexagonal pyramids. The HR-TEM images indicated a highly crystallized structure of Pd nanoclusters and fast Fourier transform (FFT) diffractogram exhibited a 6-fold symmetry of diffraction spots. H_2 sensitivity as low as 0.1 ppm

DOI: 10.1021/acsami.7b07063
ACS Appl. Mater. Interfaces 2017, 9, 34544−34586

was observed for Pd nanoclusters deposited graphene layer which was 2 orders of magnitude lower compared with Pd-based hybrid chemical sensors. The resistance of the flexible Pd nanoclusters/graphene-based H_2 sensor for different bending radius varying from 10 to 30 mm did not change. Furthermore, 2% change in relative resistance was noticed after 100 bending cycles to 10 ppm concentration of H_2 gas. This indicates excellent flexibility and mechanical flexibility of flower-like Pd nanoclusters/graphene electrodes to be useful for wearable electronics.

Like Pd nanoparticle-decorated graphene, PtNPs/graphene nanocomposites have been studied for H_2 sensing. Lee et al.[206] fabricated a radio frequency identification (RFID)-based sensor tag from PtNP-decorated rGO (PtNPs/rGO) nanocomposite system to detect H_2. The nanocomposites were developed by a chemical reduction process and spin-coated on an antenna pattern in the RFID sensor tag. PtNP-decorated graphene-based wireless sensor system has two components, ultrahigh frequency (UHF) RFID sensor tag made of Pt/rGO composite and a RFID-reader antenna-connected network analyzer. Figure 16 shows the

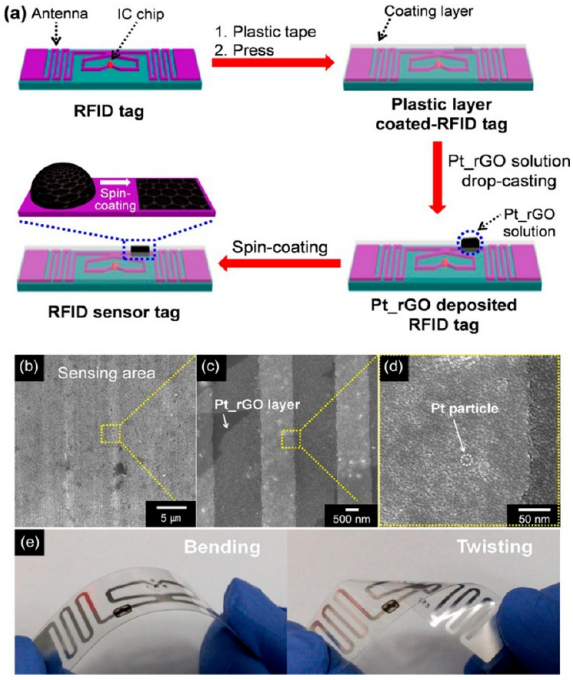

Figure 16. (a) Schematic diagram for fabricating PtNPs/rGO nanocomposite-based flexible radio frequency identification (RFID)-based wireless sensor system made of two components, Pt/rGO composite-based ultrahigh frequency (UHF) sensor tag and a RFID-antenna-connected network analyzer. Field effect scanning electron microscopy (FE-SEM) (b) low-, (c) middle-, and (d) high-resolution images of the PtNPs/rGO nanocomposites sensing area. (e) Photographs of the flexible RFID sensor tag under bending and twisting. [Reprinted with permission from ref 206. Copyright American Chemical Society.]

schematic illustration for fabricating the nanocomposite-based flexible RFID sensor tag, field effect scanning electron microscopy (FE-SEM) images of the sensing area and flexibility of the RFID sensor tag under bending and twisting. The sensor tag showed high sensitivity to H_2 at a very low concentration of 1 ppm via wireless communication between the RFID-reader antenna and the sensor tag. The sensor has a linear range of 1−50 ppm and a response time of 15 s. The change in electrical resistivity of the antenna occurs due to the strong interactions between the uniformly dispersed PtNPs on the rGO surface and H_2 molecules, which cause a shift in the reflectance of the RFID sensor tag resulting in hydrogen detection. The wireless sensor tag also exhibited flexibility and mechanical stability after bending and twisting due to the flexible substrate.

The graphene hybrid materials with ZnO nanostructures have been used to fabricate flexible H_2 sensors. Kathiravan et al.[208] used self-assembled hierarchical ZnO nanotubes/graphene to fabricate H_2 sensors. This sensor exhibits sensitivity at a low detection level of 10−100 ppm and long-term stability up to 90 days under hydrogenation/dehydrogenation conditions. Yi et al.[281] fabricated flexible gas sensors containing ZnO layer in the bottom on a metal foil, a channel of vertically aligned ZnO nanorods, and top conductive electrode made of graphene. Both ZnO nanorods and graphene exhibited good flexibility without any electrical or mechanical deformation or failure for repeated bending and releasing up to 100 times for a bending radius of less than 0.8 cm. The hybrid showed 70% optical transmittance. The gas sensors fabricated using flexible ZnO/graphene hybrid materials were able to detect ethanol vapors with high sensitivity of ∼9 for 10 ppm ethanol. Yang et al.[282] developed H_2 sensors from orthorhombic MoO_3 nanoribbon grown on the surface of graphene sheet. The MoO_3 nanoribbon/graphene composite showed improved sensitivity, and fast response and recovery times at room temperature. A response time of 10 s and recovery time of 30 s were measured for the MoO_3 nanoribbon/graphene sensor with 1.5 wt % graphene content.

The above section discussed the specific examples of detecting NO_2, NH_3, and H_2 gases using graphene-based flexible gas sensors in detail. However, significant advances have been made on the detection of these gases over past years; therefore, more reports are briefly summarized. The pristine CVD-grown graphene films using *in situ* cleaning with UV light were utilized to fabricate the chemiresistor-type high sensitivity sensors for detecting NO_2, NH_3, O_2, CO_2, SO_2, N_2O, and NO gases at the ppt and ppq levels.[167] Different types of graphene-based materials have been used for developing chemiresister-type NO_2 gas sensors including mechanically exfoliated graphene sheets,[168] CVD-graphene,[169] 3D porous graphene hydrogel,[170] graphitic carbon nitride/graphene composite,[171] graphene monolayer/SiC composite (FET sensor),[172] graphene/MoS_2 hybrid aerogel,[173] ozone-treated CVD-graphene,[174] multilayer CVD-graphene films,[175] N-doped graphene nanosheets,[176] cesium (Cs)-doped GO films,[177] rGO/ZnO nanorods composites,[178] rGO/SnO_2NPs composite,[179] N-doped rGO/SnO_2NPs,[180] graphene aerogel/SnO_2NPs,[181] rGO and rGO/Cu_2O nanowire mesocrystals,[156] rGO/SnO_2 monocrystals,[182] rGO/WO_3 nanocomposite,[183] rGO/α-Fe_2O_3 nanocomposite,[184] 3D rGO hydrogel with integrated microheater,[185] rGO/polyurethane nanofiber,[186] CVD-graphene/PET,[187] rGO/$NaBH_4$/PET,[157] graphene monolayer/PES,[188] sulfonated rGO/AgNPs/polyimide,[164] and rGO/ZnO composite.[189]

The chemiresistor-type NH_3 gas sensors with high sensitivity were prepared using graphene-based materials including CVD-graphene,[169] 3D porous graphene hydrogel with integrated microheater,[185] NO_2-doped CVD-graphene,[190] CVD-graphene monolayer/mica (FET device),[131] CVD-graphene/ionic liquid (FET device),[191] cobalt porphyrin functionalized graphene,[192] graphene/polyaniline nanocomposite,[144] CVD-graphene/AuNPs,[193] rGO/rose bengal nanocomposite,[194] rGO/1,8,15,22-tetra-(4-*tert*-butylphenoxyl)-lead-phthalocyanine hybrid,[195] pyrrole-reduced graphene oxide (rGO),[196] rGO/poly(3-hexylthiophene) composite,[197] rGO/PANI composite,[198] and GO-PANI/ZnO hybrid film.[199]

DOI: 10.1021/acsami.7b07063
ACS Appl. Mater. Interfaces 2017, 9, 34544−34586

Similarly, H_2 gas sensors showing high sensitivity were fabricated using graphene-based materials including GO with dielectrophoresis process,[200] multiwalled carbon nanotubes (MWCNTs)/Pd nanocubes/rGO,[207] rGO/TiO_2 decorated by Pd/PtNPs,[209] mechanically exfoliated graphene decorated by SnO_2NPs,[210] GO decorated with PtNPs,[211] and graphene decorated with PdNPs.[212] The sensitivity data on graphene-based NO_2, NH_3, and H_2 sensors reported in literature by different research groups have been compiled in Table 1.

3.4. Sensors for Carbon Dioxide (CO_2), Sulfur Dioxide (SO_2), and Hydrogen Sulfide (H_2S). Table 1 lists the details of graphene-based materials used for developing different types of gas sensors including carbon dioxide (CO_2), sulfur dioxide (SO_2), hydrogen disulfide (H_2S), and their related sensing characteristics. Graphene sheet prepared by mechanical cleavage,[213] few-layer and sheets of graphene,[214] Sb_2O_3/graphene composites,[215] and Al_2O_3 quantum dots/graphene composites[216] have been explored for carbon dioxide (CO_2) gas sensing. Graphene field effect transistor[217] and rGO-based chemiresistive gas sensors[218] have been studied for detecting sulfur dioxide (SO_2). Zhang et al.[219] reported LbL self-assembled titania (TiO_2)/rGO hybrid composite film-based *n*-type sensor that displayed a response of 6.05% to 11.14% when exposed to a concentration of 1−5000 ppb of SO_2. The response of TiO_2/rGO hybrid film sensor was found to be 9.54% compared to a response of 1.77% for rGO and 4.47% for TiO_2 sensors toward 500 ppb SO_2. The resistance of both rGO and TiO_2 sensors decreased upon SO_2 gas exposure. The TiO_2/rGO hybrid displayed response/recovery times of 71−73 s and 95−128 s at 1, 50, 250 ppb and 1 ppm concentrations of SO_2 gas, respectively. The normalized response of 6.05, 6.81, 7.24, 8.39, 9.57, 10.08, and 11.14% was recorded for 1, 50, 100, 250,500, 1000, and 5000 ppb concentrations of SO_2 gas, respectively. The sensor response was increased with the increase of SO_2 gas concentration. The TiO_2/rGO hybrid composite film showed n-type behavior toward electron donating SO_2 molecules which increased its electrical conductivity. The TiO_2/rGO hybrid composite film also exhibited the highest selectivity for SO_2 when exposed to 1 ppm of various gases including CH_4, C_2H_2, H_2, CO, NO_2, and SO_2 at room temperature.

Graphene-based materials, including graphene/ZnO nanorods,[220] graphene/porous WO_3 nanofibers composite,[221] Cu_2O nanocrystals/graphene sheets,[222] poly(4-styrenesulfonic acid)-doped PANI/graphene nanocomposites,[223] SnO_2 nanofibers/rGO hybrids,[224] SnO_2 nanorods/graphene,[225] and SnO_2 quantum wire/rGO nanocomposites[226] have been studied as H_2S sensing elements. Choi et al.[227] developed flexible wearable chemical sensors using RGO and transparent colorless polyimide (CPI) substrate. The irradiation by intense pulsed light (IPL) formed RGO sheets on flexible CPI film within 4 ms, resulting into a 100-fold increase in electrical conductivity due to the reduction of GO sheets. The intense pulse light (IPL) irradiation onto GO-coated CPI film formed IPL-RGO/CPI film. The bare CPI film showed 89% optical transmittance at 550 nm, which decreased to 78% for the GO-coated CPI film. The IPL-RGO-coated CPI film exhibited 78% optical transmittance at 550 nm similar to that of GO-coated CPI film. The optical transmittance can be controlled by varying the GO film thickness on the CPI substrate. The IPL-RGO sheets showed significantly improved sensitivity toward C_2H_5OH, H_2S, and H_2, whereas negligible gas sensitivity was noticed for the pristine GO sheets. Figure 17 shows the dynamic resistance change of GO and IPL-RGO sensors toward 5−20 ppm concentration of H_2S gas, the response of IPL-RGO sensor in the flat state and bent state at 30° bending angle and under repeated 10 000 bending cycles. The performance of IPL-RGO sensor was also evaluated for H_2,

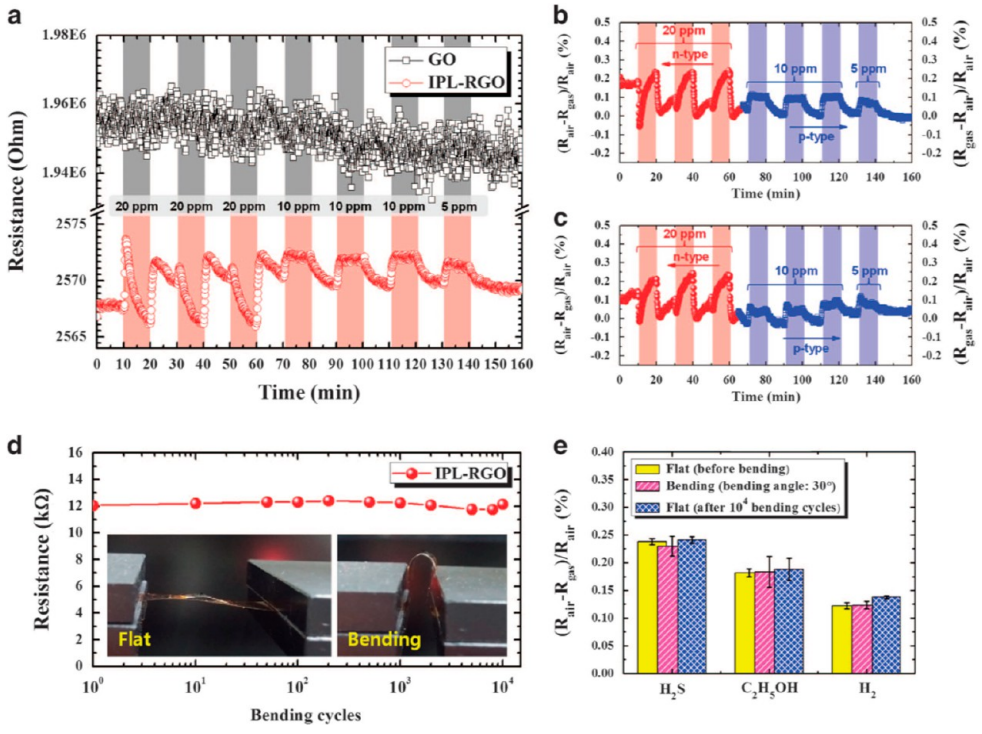

Figure 17. (a) Dynamic resistance change of GO and IPL-RGO sensors toward H_2S for 5−20 ppm concentration at room temperature. Dynamic response change of the IPL-RGO film sensor to 5−20 ppm of H_2S gas at room temperature in the flat state (b) and the bent state (c) at 30° bending angle. (d) Resistance change of the IPL-RGO sensor up to 10 000 bending cycles. (e) Comparison of H_2, H_2S, and ethanol sensing by the IPL-RGO film sensor at 20 ppm before and after bending at 30° angle. [Reprinted with permission from ref 227. Copyright Springer Nature.]

DOI: 10.1021/acsami.7b07063
ACS Appl. Mater. Interfaces 2017, 9, 34544−34586

Figure 18. (a) Photograph of a wearable sensor module (wrist) integrated with the intense pulsed light-reduced graphene oxide (IPL-RGO) sensor (denoted by blue dotted box). (b) Dynamic resistance change of the IPL-RGO-based wearable sensor module to 20 ppm of H_2S gas at room temperature. [Reprinted with permission from Professor I.-D. Kim from Korea Advanced Institute of Science and Technology (KAIST), ref 227. Copyright Springer Nature.]

H_2S, and ethanol at 20 ppm before and after bending. The IPL-RGO sensor showed sensitivity of 0.238% at 20 ppm and 0.107% at 10 ppm toward H_2S. The sensitivity slightly changed to 0.224% when exposed to 20 ppm of H_2S during the bending test. The IPL-RGO/CPI film-based sensors retained their sensitivity up to 10 000 bending cycles at 30° bending angle without any mechanical deformation and ±3% resistance change than that of initial resistance after repeated bending. This indicated the excellent long-term mechanical stability of IPL-RGO film sensor on CPI substrate. The sensing performance of IPL-RGO film sensor was compared before and after bending for three different analytes at 20 ppm where negligible variations were observed toward H_2, H_2S, and C_2H_5OH in the flat and bent states even after 10 000 bending cycles which again confirmed the long-term endurance of the IPL-RGO film sensors. Figure 18 shows the photograph of a wearable sensor module developed from IPL-RGO/CPI film and resistance change upon exposure for 7 cycles at 20 ppm of H_2S at room temperature. The selectivity of IPL-RGO sensor was studied for H_2S, H_2, carbon monoxide (CO), methane (CH_4), ethanol (C_2H_5OH), acetone (CH_3COCH_3), and toluene ($C_6H_5CH_3$) at 20 ppm, which showed very low sensitivity of 0.1% for other interfering analytes compared to H_2S. The resistance of IPL-RGO sensor changed from 1873.7 Ω in 1.5% relative humidity to 2722.4 Ω in 97% relative humidity for H_2S. Moreover, H_2S at 10 ppm behaved as a *p*-type sensor in 1.5% RH and an *n*-type sensor in 63% RH. The sensitivity was retained both in flat and bent states. The resistance of the IPL-RGO sensor was found to increase from 2568 to 6780 Ω after 7 months for 20 ppm of H_2S in air showing 0.231% difference in sensitivity due to the oxidation and high stability. Figure 19 shows the comparative sensitivity of IPL-RGO sensor toward different gaseous species at 20 ppm concentration in the flat state. The IPL-RGO sensor showed a gas sensing trend of H_2S > ethanol > H_2 > toluene > acetone > CO > CH_4 where H_2S gas showed the highest sensitivity and methane (CH_4) as the lowest sensitivity. This RGO-based sensor can be integrated on flexible printed circuit boards for wireless communication and used as portable sensors for healthcare and environmental monitoring systems.

The results reported from various research groups on graphene-based gas sensors for detecting NO_2, NH_3, H_2, CO_2, SO_2, and H_2S gases have been discussed above in detail giving specific examples. Table 1 summarizes the sensor-type such as chemiresistor or FET or RFID devices and detection limit of different graphene-based gas sensors.

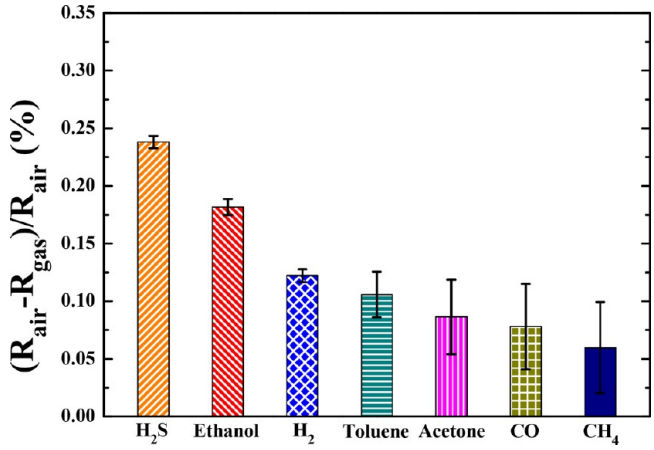

Figure 19. Selectivity of IPL-RGO-based flexible sensor toward various gaseous molecules (H_2S, ethanol, H_2, toluene, acetone, CO, and CH_4) at 20 ppm gas concentration in the normal flat state. [Reprinted with permission from ref 227. Copyright Springer Nature.]

3.5. Humidity Sensors. The amount of humidity has a great influence in our daily life including physiological activities, climate, building constructions, storage facilities for medicines and foods, electronic devices, chemical refineries, corrosion and degradation of instruments, etc. Therefore, humidity sensors with high sensitivity, accuracy, selectivity, repeatability, long-term stability under ambient conditions, corrosion resistance to pollutants, and low cost of manufacturing are in great demand. The basic introduction, principles, materials, fabrication techniques, and applications of humidity sensors have been summarized in the literature.[283−287] 1D, 2D, and 3D nanostructured materials including porous silicon carbide,[288,289] CeO_2 nanowires,[290,291] ZnO nanorods,[292−294] CdS/ZnO,[295] SnO_2 nanowires,[296] CuO nanowires,[297] $BaTiO_3$ nanofibers and composites,[298−300] sulfonated poly(ether ether ketone),[301] sulfonated polybenzimidazole,[302] polypyrrole,[303−305] PANI nanofibers,[9] carbon nanotubes,[306−311] transitional metal dichalcogenides layers,[312−317] black phosphorus nanosheets,[318−321] and graphene sheets[322−334] have been applied for developing high-sensitivity humidity sensors. Today, flexible and stretchable nanostructured-material-based wearable sensors are gaining attention for applications in ubiquitous health monitoring, electronic textile, e-skin, detecting humidity in food packaging, semiconductor devices, communication systems, etc.[335−341]

Graphene-based materials have emerged as key elements for fabricating humidity sensors with high flexibility as well as

DOI: 10.1021/acsami.7b07063
ACS Appl. Mater. Interfaces 2017, 9, 34544−34586

stretchability. Chi et al.[342] used GO films prepared by the modified Hummer's method for optical humidity sensing where the GO active layer detects humidity change in the entire range of RH with an ultrafast response time of 250 ms. A series of saturated salt solution was used to adjust the vapor pressure where rapid color change was observed when silicon wafer chips with GO film were put into vials. Figure 20 shows a systematic

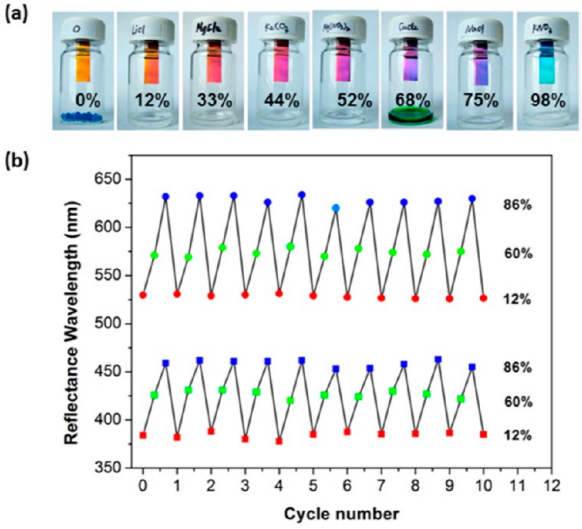

Figure 20. (a) Color change of graphene oxide (GO) film-based sensor when exposure to 0 to 98% ranges of relative humidity. (b) Change of reflectance showing reversible behavior from the dual-colorimetric of GO films after alternately exposing to selected relative humidity of 12, 60, and 86%. [Reprinted with permission from ref 342. Copyright American Chemical Society.]

change of GO films after exposing to RH from 0 to 98% and reflectance peaks of GO film-based humidity sensor with multiple cycles from 12%, 60%, to 86% RH where the sensor had great reversibility over the entire humidity range. UV/vis reflectance spectra show clear shifts as the GO films are exposed to different humidity conditions. Linear optical shifts were detected with increasing humidity from a dry state to 98%. The sensor shows two main reflection peaks at 386 and 526 nm at 12% RH. When RH was increased to 98%, these two reflection peaks shifted to 474 and 645 nm, respectively. A linear relationship was noticed between these two reflection peaks with the change of RH. The response and recovery times were measured at a reflectance wavelength of 550 nm at room temperature from 50% to 98% RH. The response time was found to be 250 ms, whereas the recovery time was 1.2 s. Such a big difference in the response and recovery times of GO films may be due to the hydrophilic groups attached to the GO nanosheets. The spectra changes were seen by the naked eye to be from deep blue to red by GO-based dual-colorimetric humidity sensor. The GO film-based sensors can be used as humidity sensors for health, packaging, and environmental monitoring.

A flexible humidity sensor was fabricated on polyimide (PI) substrate using rGO and poly(diallylimethyammonium chloride) (PDDA) nanocomposite by Zhang et al.[343] The hierarchical nanostructure of GO and PDDA was constructed using an LBL self-assembly approach and then partially reduced by hydrobromic acid treatment to generate chemically active defect sites. The sensing properties of the nanocomposite films were studied in 11−97% RH range at room temperature. The resistance of sensor increased with the increase of RH varying as much as 37.41% at 97% RH. Figure 21 shows an optical image of

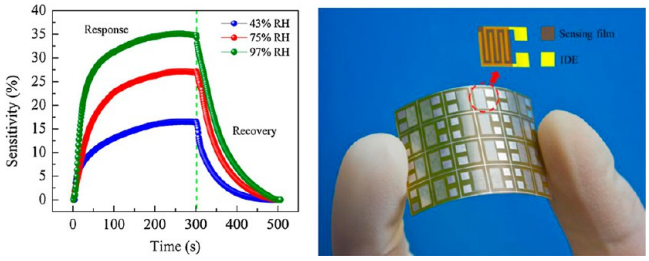

Figure 21. (Left) Time dependent response and recovery curves of the rGO/PDDA nanocomposite film sensor at different relative humidity. (Right) Optical image of 4 × 6 rGO/PDDA nanocomposite film sensors array on a flexible polyimide substrate. [Reprinted with permission from ref 343. Copyright 2014 Elsevier.]

4 × 6 rGO/PDDA nanocomposite film sensor array on a flexible PI substrate and time-dependent response-recovery curves. The hysteresis behavior of the sensor was compared for RH-increasing with absorption of water molecules and RH-decreasing after desorption within 11% to 97% RH range where the maximum hysteresis was noticed at 33% RH. The sensor showed repeatability behavior when measured for five exposure/recovery cycles at 43%, 75%, and 97% RH. A response time of 108−147 s and recovery time of 94−133 s were measured. The standard deviation (SD) derived from six sensors during the humidity exposure was 2.6%, showing a good reproducibility of sensor devices. The long-term stability of the sensor was measured, and no significant change in the sensor response was observed for 23%, 52%, and 75% RH over a period of 60 days. The sensor showed high sensitivity to humidity, a fast response-recovery time, and durability. The rGO/PDDA composite film is highly sensitive toward humidity where water molecules act as electron donors. The concentration of holes in *p*-type rGO films is reduced by the adsorbed water molecules which increases the film resistance. Here, the large density of surface vacancies and the presence of hydrophilic carboxylic groups in rGO film play a significant role in capturing copious water molecules from the environment. The interlayer distance of PDDA/rGO composite film is 3.67 Å compared with 3.60 Å for rGO film because of the surrounding polymer chains. The multilayer films absorb water molecules resulting into swelling of rGO/PDDA interlayers, which increased interlayer distance and deteriorated the connectivity in the composite film causing an increase in electrical resistance. The sensing mechanism is associated with *p*-type behavior of rGO at low RH, and the humidity-induced interlayer swelling of rGO/PDDA composite film at high RH instead of ionic conductivity.

Another flexible humidity sensor was fabricated using two-beam-laser interference (TBLI) method for patterning of GO on a flexible PET substrate as reported by Guo et al.[344] The contents of oxygen functional groups in the GO sheet, which assists in controlling the electrical conductivity, could be changed by tuning the laser power that consequently influences the response and recovery times of the sensor device due to the molecular interactions occurring between oxygen functional groups and the adsorption/desorption process of water molecules on the GO sheets. The pristine GO had 46.5% contents of oxygen atoms and 32% content of carbon which is not bonded to oxygen. After TBLI reduction at 0.15W laser power, C—C percentage was found to increase to 68% whereas C—O percentage was

DOI: 10.1021/acsami.7b07063
ACS Appl. Mater. Interfaces 2017, 9, 34544−34586

decreased to 23%, demonstrating the removal of oxygen functional groups. A significant increase in C—C percentage whereas a decrease in the C—O and C═O percentages was observed with the increasing laser power. Using the TBLI reduction process, the oxygen functional groups from GO sheet can be removed, as a result the conductivity of the RGO thin film could also be tailored within a particular range by controlling the oxygen functional groups. Figure 22 shows the current−voltage

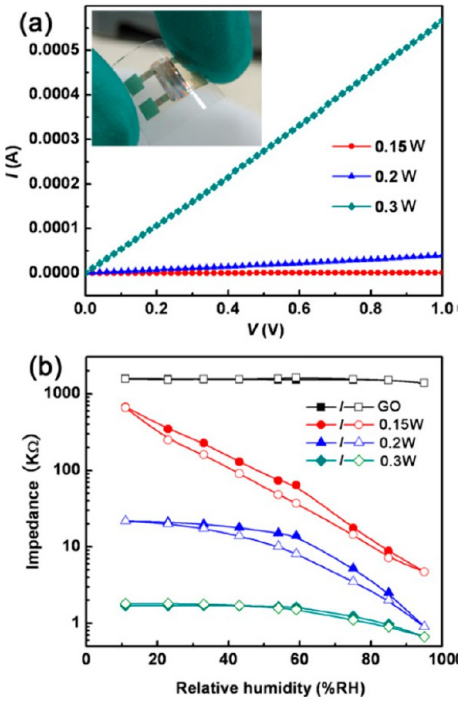

Figure 22. (a) Current−voltage (I−V) curves of RGO sensor prepared by two-beam-laser interference under different laser powers of 0.15, 0.2, and 0.3 W at room temperature. The inset is a photograph of flexible RGO humidity sensor. (b) Humidity hysteresis characteristics of the RGO- and GO-based sensors. [Reprinted with permission from ref 344. Copyright Elsevier.]

curves of the RGO sensors prepared by two-beam-laser interference with laser powers of 0.15, 0.2, and 0.3 W and humidity hysteresis features of RGO and GO sensors where absorption/desorption resistance was measured as a function of RH at room temperature. The resistance for GO did not change over the whole range. However, the resistance of the sensor decreased by 2 orders of magnitude with increasing RH in the 11−95% range after reduction with 0.15W laser power. The response time was 2 s when RH was increased from 11% to 95%, whereas the recovery time was over 100 s when RH was decreasing from 95% to 11%. For sensors fabricated at the laser powers of 0.2 and 0.3 W, the response time was 3 and 50 s, and the recovery time was 10 and 3 s, respectively. This indicates that both response and recovery time of RGO-based flexible humidity sensor was fast.

In addition to chemiresistor-type sensors, Su et al.[345] developed flexible impedance-type humidity sensors using GO and AuNPs by self-assembly and the sol−gel technique. The GO-containing hydrolyzed 3-mercaptopropyltrimethoxysilane (MPTMOS) sol−gel solution was spread out on Au electrodes on a flexible PET substrate. The AuNP/GO/MPTMOS sol−gel film was characterized by SEM and AFM. The effect of the AuNPs and GO amount on the humidity-sensing properties of the AuNPs/GO/MPTMOS sol−gel films was studied. The optimum flexibility, humidity sensitivity, and long-term stability were observed from sensors fabricated with 9.0 wt % GO. The effect of frequency, temperature, and response as well as recovery times on the impedance was studied for flexible humidity sensors. Su et al.[346] also developed impedance-type humidity sensors from diamine-functionalized GO films coated on either alumina or plastic substrates. GO was functionalized by ethylenediamine and 1,6-hexanediamine using *N*-(3-(dimethylamino)propyl)-*N*′-ethylcarbodiimide hydrochloride and *N*-hydroxysuccinimide (EDC/NHS) as a coupling reagent. The effect of the diamine chain length on the electrical and humidity sensitivity was studied where impedance-type humidity sensor fabricated with ethylenediamine-GO film showed great performance in terms of sensitivity, flexibility, rapid response/recovery time, and high long-term stability. The H_3O^+ ions control the conductance of the diamine-functionalized GO film-based sensor. Xuan et al.[347] fabricated flexible Lamb wave humidity sensors using GO microflakes as a sensing layer. The sensor was prepared on piezoelectric ZnO thin films deposited on a flexible PI substrate. The humidity sensitivity of the GO sensors was 145.83 ppm per % relative humidity (at humidity 85% RH). The flexible GO-based humidity sensors showed no degradation under severe bending conditions up to 36° bending angle and showed stability upon repeated bending for 1000 times. The GO-based Lamb wave flexible humidity sensors could be used in flexible electronics. GO biopaper made of GO-silk fiber was used to develop humidity sensors where the reduction of GO was reinforced by silk interlayers. The flexible GO-silk-based chemiresistive sensor showed a fast response time of 3 s, sensitivity range of 20−97% to RH and stability to thousands of folding cycles and chemical solvents.[348]

Table 2 presents the detection range and response time of flexible humidity sensors fabricated using graphene, GO, and rGO. The overall RH detection range is quite wide from 10 to 98% and response from 3.5 s to 2 min depending upon the sensor device structure. Yao et al.[323] developed GO/silicon bilayer flexible structure as humidity sensor with a RH detection range of 10−98%. The sensitivity of GO/Si sensor was influenced by the thickness of GO thin films where sensitivity toward humidity was enhanced by thicker GO films. GO thin films having a thickness

Table 2. Flexible Humidity Sensors Developed from Graphene-Based Materials

Graphene-based sensing material	Sensor type	RH detection range (%)	Response time (s)	ref.
Graphene/polypyrrole nanocomposite	Capacitor	12−90	15	324
GO/PEN substrate	Impedance	35−80	30−120	325
GO/PET substrate	Impedance	30−90	28	327
GO/silicon bilayer	Piezoresistor	10−98	19	323
GO paper	Resistor	30−95	100	350
GO/PSS nanocomposite	Capacitor	20−80	60	351
rGO/PDDA composite/PI substrate	Resistor	11−97	108	343
rGO/PET substrate	Impedance	11−95	2	344
rGO/PU composite/PDMS substrate	Resistor	10−70	3.5	349
rGO/SPS:PEDOT/PET substrate	Resistor	0.13−68.46	39	352

DOI: 10.1021/acsami.7b07063
ACS Appl. Mater. Interfaces 2017, 9, 34544−34586

of 215 nm showed 3 times higher sensitivity compared with a GO thin film of 65 nm thickness. The response of GO/silicon sensor was also found to be related to the deformation of GO films caused by humidity. Lin et al.[324] developed a humidity sensor with 10% graphene/polypyrrole composite that exhibited RH detection range of 12−90%, higher sensitivity (S = 138), the response time of 15 s and recovery time of 20 s, and <0.16% value of humidity hysteresis at all humidity. Borini et al.[325] used GO films to develop humidity sensors having high transparency and flexibility. The GO thin films were coated on the silver screen-printed interdigitated electrodes (IDE) on a flexible PEN substrate The GO/PEN-based flexible sensors showed high sensitivity to humidity and fast response/recovery times of 30 ms for a 15 nm-thick film due to the superpermeability of GO to water molecules. The RH response of GO sensor remained unchanged after 1000 bending cycles conducted at a 10 mm bending radius during the mechanical testing. The impedance and the sensors response were affected by the morphology and thickness of the GO films. Su et al.[327] developed GO-based flexible impedance-type sensors for humidity detection by layer-by-layer (LBL) assembly on a PET substrate. Both electrical conductivity and humidity response were influenced by the reduction process of the GO thin film. The GO humidity sensor showed high sensitivity with a broad linear range dependent on applied frequency, fast response time, and long-term mechanical stability. The impedance data showed that the dominance of ions (H_3O^+) for the conductance of the partially reduced GO thin film. Trung et al.[349] developed transparent and stretchable humidity sensor using rGO/polyurethane (PU) composite and PEDOT:PSS/PU conductive electrodes on a flexible PDMS substrate. The rGO/PU sensor can be stretched up to 60% strain. The rGO/PU sensor showed a RH detection range of 10−70%, response time of 3.5 s and relaxation time of 7 s. The sensitivity and dynamic response of sensor remained almost unchanged up to 60% stretching and even after 10 000 stretching cycles conducted at 40% mechanical strain. Naik and Krishnaswamy[350] developed humidity sensor from 10 mm wide × 30 mm long rectangular GO paper obtained from chemical exfoliation which showed RH detection range of 30−95%.

In order to increase the water absorption, Yu et al.[351] intercalated hydrophilic and electrically insulating poly(sodium 4-styrenesulfonate) (PSS) between GO platelets to develop a capacitive humidity sensor. This sensor device configuration helps in enhancing the water permeation behavior. A significant change in capacitance was observed for the GO/PSS composite film (100 nF) compared with GO film (70 nF) with the increase of RH due to the absorbed water molecules. The GO/PSS composite sensor showed a capacitance of 480 nF compared with 6.4 nF for GO film at 40% RH, which is 75 times higher than the latter one. The GO/PSS composite sensor showed 5.6 times higher voltage and 3 times faster response time compared with GO sensor over a 0−80% RH range. Such a significant improvement in humidity sensing was associated with water absorption capability of both GO and PSS and increased interlayer distance in GO films. Yuan et al.[352] prepared humidity sensor with sulfonate polystyrene:PEDOT NPs (SPS:PEDOT NPs) and GO ink. Multilayers of SPS:PEDOT NPs/GO was obtained using layer-by-layer inkjet printing where one GO layer was followed by one layer of SPS:PEDOT NPs ink on a flexible PET substrate. Thermal annealing was used to obtain SPS:PEDOT NPs-reduced GO (SPS:PEDOT NPs/rGO) nanocomposite-based sensors. The SPS:PEDOT NPs/rGO/PET-based sensor shows high humidity sensing with a 0.13−68.46% range and response and recovery times of 39 and 57 s, respectively. The electrical resistance of sensors remained unchanged after repeated folding for 200 times. The above studies demonstrated that GO- and rGO-based flexible resistance and impedance-type sensors with high sensitivity, a wide detection range and fast response/recovery times can be prepared on different flexible substrates.

4. GRAPHENE-BASED FLEXIBLE CHEMICAL SENSORS

Nanomaterial-based sensors have been studied for detecting environmental pollutants, toxic benzene derivatives, dyes, cosmetics, and byproducts of chemical and pharmaceutical industries as well as for detecting heavy metal ions in water/soil to daily household appliances. These pollutants are also highly toxic and cause cancer because they accumulate in the human body through many different sources. In this regard, graphene-based materials have been used as sensing elements for detecting different types of environmentally harmful volatile organic compounds (VOCs),[26,353−365] pathogens,[366] cancer biomarkers,[367−369] and heavy metal ions.[370,371]

A litmus-type colorimetric sensor fabricated using polydiacetylene (PDA)/graphene stacked composite film exhibited sensitivity to 0.01% concentration of VOCs including methanol (CH_3OH), chloroform ($CHCl_3$), tetrahydrofuran (THF), and dimethylformamide (DMF).[372] The color change caused by the VOCs was visible to the naked eye due to interactions between PDA molecules and different VOCs. Bisphenol A (BPA) is one of the most hazardous industrial chemicals for environment and human health. Zou et al.[373] used heptakis-(2,3,6-tri-*O*-methyl)-β-cyclodextrin (TM-β-CD) functionalized graphene/PtNPs-based sensors for BPA detection due to host−guest supramolecular recognition offered by cyclodextrin and high electrical conductivity, large surface area, and high electrocatalytic activity originating from the graphene/PtNPs networks. The oxidation peak current of BPA was found to be increased by the TM-β-CD-graphene/PtNPs modified glassy carbon electrode (GCE) than those of graphene/PtNPs/GCE and TM-β-CD/graphene/GCE. The lowest limit of detection (LOD) was 1.5 × 10^{-8} mol/L (signal/noise = 3). Graphene-based formaldehyde (HCHO) sensors have been developed using ZnO QD/graphene nanocomposites.[374] The rGO/TiO_2 hybrid film-based sensor detected formaldehyde with high sensitivity at 0.8 ppm level.[375] The polyoxometalate/rGO/AgNPs composite film selectively detected formaldehyde up to 10^{-8} mol/L.[376]

The poly(3,4-ethylenedioxythiophene)/graphene nanocomposite-based sensors simultaneously detected hydroquinone, catechol, resorcinol, and nitrite at lowest limits of 0.06, 0.08, 0.16, and 7 μM, respectively.[377] A Love-wave device developed with GO sensitive layer was used to detect chemical warfare agent (CWA) simulants.[378] The sensors detected 0.2 ppm for dimethyl-methylphosphonate (DMMP), which is a stimulant of sarin nerve gas and 0.75 ppm for dipropylene glycol monomethyl ether (DPGME), which is a simulant of mustard gas. The limit of detection was calculated as 9 ppb for DMMP and 40 ppb for DPGME. The high sensitivity was associated with the hydrogen bonding formation between CWA stimulants and the GO layer. The rGO formed by the reduction of GO by *p*-phenylenediamine (PPD) was used as a sensing material for detecting DMMP at 30 ppm level.[379]

Organophosphates used as pesticides and insecticides in agriculture pose serious food safety and public health concerns. An enzyme-free electronic tongue (e-tongue) was developed for detecting organophosphate pesticides using four sensing units consisting of graphene-based hybrid materials where the

DOI: 10.1021/acsami.7b07063
ACS Appl. Mater. Interfaces 2017, 9, 34544−34586

reduction of GO was accomplished in the presence of PEDOT:PSS, polypyrrole (PPy), and AuNPs as reported by Facure et al.[380] The e-tongue array was composed of rGO, PPy/rGO, PEDOT:PSS/rGO, and PEDOT:PSS/rGO-AuNPs nanocomposite films. The nanocomposite solutions were drop-casted onto the gold-based interdigitated electrodes (IDEs) to analyze different pesticides by the e-tongue system using impedance spectroscopy and then pesticides were selectively classified using the Principal Component Analysis (PCA) technique. Figure 23 presents the PCA plot showing electrical resistance

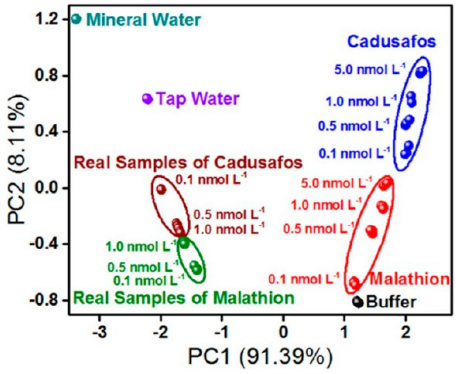

Figure 23. PCA plot showing electrical resistance responses measured with the e-tongue at 100 Hz for analyzing cadusafos and malathion solutions of different nanomolar concentrations (0.1 to 5.0 nmol/L) prepared with phosphate buffer solution (PBS) and tap water (indicated by real samples). [Reprinted with permission from ref 380. Copyright Elsevier.]

responses at a frequency of 100 Hz for analyzing solutions of different nanomolar concentrations (0.1, 0.5, 1.0, and 5.0 nmol/L) with phosphate buffer solution (PBS) and tap water samples having pesticide concentrations of 0.1, 0.5, and 1.0 nmol/L. The PCA showed that the e-tongue array clearly differentiated between PBS buffer and real water samples. The first principal component (PC1) and the second principal component (PC2) components accounted for 99.50% total variance. The PCA plot showed no overlapping between real and buffer samples and both cadusafos and malathion pesticides were selectively identified by the rGO sensor array. The rGO-based nanocomposites exhibited the lowest LOD of 0.1 nmol/L toward pesticide due to the high specific surface area and electrical conductivity. This study indicates that the rGO nanocomposite-based e-tongue sensor array can be used in identifying a mixture of organophosphate pesticides at nanomolar concentrations below the recommended levels by various countries. Likely, other graphene-based sensor arrays can be developed for selectively identifying and classifying other chemical mixtures with PCA method.

The rGO/CNT composites micropatterned on flexible PI films and followed by the bismuth (Bi) electrodeposition on micropatterns was used to detect 0.2 ppb of Pb and 0.6 ppb of Cd ions.[381] Yuan et al.[382] prepared conjugated microporous polymers (CMPs)/PLA-based light-emitting nanofibrous films by electrospinning. The CMP/PLA nanofibrous films exhibited high flexibility, high porosity as well as high surface-area-to-volume ratios, which were used as sensors for detecting nitroaromatic, benzoquinone vapors and oxidizing metal ions. The 4-iodophenyl-substituted graphene sheets were used to prepare graphene-templated CMP sandwiches as flexible chemical sensors. Figure 24 shows the synthetic strategies for preparing CMPs and their graphene-templated CMP (G-CMP) hybrids. PTEPE-TBPE was prepared from their monomers; 1,1,2,2-tetrakis(4-ethynylphenyl)ethene (TEPE) and 1,1,2,2-tetrakis(4-bromophenyl)ethene (TBPE) using the Sonogashira–Hagihara-type cross-coupling reaction. The graphene-templated CMP hybrids namely G-PTBPE and GPTEPE-TBPE were obtained by the reaction of TBPE or TEPE/TBPE mixture with 4-iodophenyl-substituted graphene (RGO-IBz) as templates using Yamamoto-type coupling reaction or Sonogashira–Hagihara-type coupling reactions, respectively. The use of tetraphenylethene (TPE)-cored monomers was based on their inherently high photoluminescence (PL). The morphologies of CMPs and GCMPs were studied by SEM, TEM, and high resolution TEM techniques, which showed porous nanostructures. The PTBPE, G-PTBPE, PTEPE-TBPE, and G-PTEPE-TBPE showed Brunauer–Emmett–Teller (BET) surface areas of 1716, 1477, 1083, and 883 m^2/g, and cumulative pore volumes of 2.34, 1.88, 1.51, and 0.94 cm^3/g, respectively. The graphene-templated G-PTBPE and G-PTEPE-TBPE hybrid materials had lower values of surface area and pore volume compared with their corresponding counterparts. Figure 25 shows the photographs of light-emitting PTBPE/PLA nanofibrous films, morphological images, and fluorescence intensity measured after exposing 1,2-dinitrobenzene (DNB), 1,3,5-trinitrobenzene (TNB), and 1,4-benzoquinone (BQ) vapors and oxidizing metal ions to PTBPE/PLA nanofibrous films. The electrospun PTBPE/PLA-based nanofibrous films are flexible and highly photoemissive under UV light. SEM, TEM, and HRTEM images indicated homogeneous distribution of PTBPE within the PLA matrix with smooth surface of the PTBPE/PLA nanofibers. The normalized fluorescence intensity exhibited by the electrospun PTBPE/PLA nanofibrous films for the 1,2-dinitrobenzene (DNB) was 51% and 29% of the initial intensity after 2 and 30 min exposure, respectively. The 1,3,5-trinitrobenzene (TNB) and 1,4-benzoquinone (BQ) exhibited 52 and 57% PL quenching for 2 min, and 75 and 79% PL quenching for 30 min, respectively. The high-quenching sensitivity resulted from the photoinduced electron transfer occurring between PTBPE and the electron-deficient DNB, TNB, and BQ analytes. The fluorescence quenching of the PTBPE/PLA nanofibrous films for different metal ions including K^+, Ca^{2+}, Mg^{2+}, Ni^{2+}, Co^{2+}, Cu^{2+}, Fe^{3+}, and Ag^+ was recorded in aqueous solutions (10^{-4} mol/L) after immersing for 1 min where enhanced fluorescence quenching of 38% for Ag^+ and 77% for Fe^{3+} was observed due to electron-deficient Ag^+ and Fe^{3+} oxidizing metal ions. The hierarchically porous carbon nanosheets prepared from G-CMP hybrids at 800 °C also showed 48% higher specific capacitance than that of porous carbons without the graphene template due to improved porosity and interfacial interactions. This study supported the fact that light-emitting nanofibrous films of graphene-templated CMPs can be used for flexible chemical sensors and supercapacitors.

An et al.[383] fabricated liquid-ion gated FET-type flexible and transparent graphene-based aptasensor for detecting toxic Hg^{2+} ions in mussels. The surface of single-layer graphene was functionalized with an aptamer that is sensitive specifically to Hg^{2+}. Figure 26 shows HRTEM image, UV–visible spectra of CVD-grown single-layer graphene transferred on flexible PEN film, gold electrodes deposited on a flexible graphene film, real-time response, and high selectivity of graphene/aptamer to Hg^{2+}. Raman spectra of a single-layer graphene showed G-band at 1600 cm^{-1} and 2D band at 2700 cm^{-1}. The UV–visible spectra of the graphene film on flexible PEN substrate showed optical transmittance of 97.73% at 550 nm. The Hg^{2+} ions up to 10 pM concentration were detected in mixed solutions. The flexible

DOI: 10.1021/acsami.7b07063
ACS Appl. Mater. Interfaces 2017, 9, 34544–34586

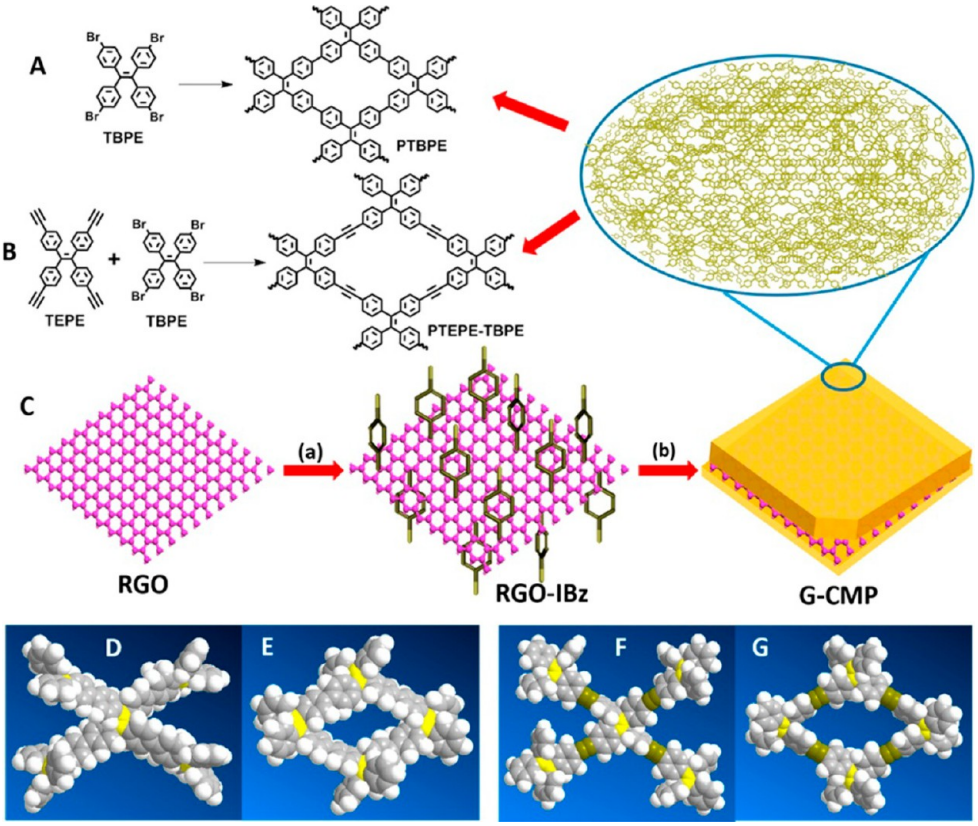

Figure 24. Preparation of conjugated microporous polymers (CMPs): (A) PTBPE was prepared from 1,1,2,2-tetrakis(4-bromophenyl)ethene (TBPE) by the Yamamoto-type coupling reaction and (B) PTEPE-TBPE was synthesized from 1,1,2,2-tetrakis(4-ethynylphenyl)ethene (TEPE) and 1,1,2,2-tetrakis(4-bromophenyl)ethene (TBPE) as monomers by the Sonogashira−Hagihara-type cross-coupling reaction. (C) Process of preparing graphene-templated CMPs involved (a) 4-iodobenzene diazonium salt (b) Yamamoto-type coupling Sonogashira−Hagihara-type coupling reactions; panels D and F are open-frameworks simulated by DFT calculations whereas panels E and G represent closed macrocyclic units showing segments of PTBPE and PTEPE-TBPE, respectively, also simulated by DFT calculations. [Reprinted with permission from ref 382. Copyright American Chemical Society.]

FET-graphene aptasensor showed fast response time of <1 s with different Hg^{2+} ion concentration. The flexible graphene-based aptasensor showed high selectivity to Hg^{2+} in a mixed solution of Cd^{2+}, Co^{2+}, Ni^{2+}, Na^{+}, Pb^{2+}, Sr^{2+}, Li^{2+}, and Zn^{2+}. Negligible variation in resistance of a flexible graphene aptasensor was measured for different bending radius (0−16 mm) up to 100 bending/relaxing cycles. The aptasensor was developed from CVD-grown graphene onto flexible PEN substrate which showed excellent mechanical flexibility and durability for detecting Hg ions.

Table 3 presents a very wide variety of chemical sensors those have been developed using graphene-based materials. Graphene, GO, and rGO have been hybridized with other materials in order to improve sensitivity and selectivity toward a particular chemical analyte. Many different chemical species have been detected with graphene-based materials; Au-PdNPs-loaded graphene for Bisphenol A,[384] Pt/Pd NPs-graphene nanocomposite for formaldehyde,[385] porous graphene/CNT for methotrexate in cancer chemotherapy,[386] rGO/platinum(II)-tetraphenylporphyrin for hydrazine,[387] rGO/nickel-tetraphenyl porphyrin nanocomposite[388] and β-cyclodextrin/graphene oxide[389] for nitrobenzene, rGO/ZnO composite[390] and rGO/SnO_2 aerogels[391] for phenol, glassy carbon electrode/rGO composite for 4-nitrophenol,[392] diamond/graphene/polyaniline composite[393] and molecularly imprinted polymer/graphene oxide for 2,4-dichlorophenol,[394] nitrogen-doped graphene GQDs for 2,4,6-trinitrophenol,[395] GO/chitosan nanocomposite for methylamine, dimethylamine and trimethylamine.[396]

Graphene-based materials have been widely used for detecting toxic metal ions such as rGO/polyethylenimine/Pd hybrids,[397] cobalt sulfide (CoS)/porous rGO,[398] rGO/chitosan/DNA composite[408] and polypyrrole/graphene/β-cyclodextrin composite[409] for Hg^{2+}, AgNPs/rGO for Hg^{2+}, Pb^{2+} and Cr(VI),[400] N-doped graphene/chitosan for Pb^{2+},[399] S-doped graphene QDs for Ag^{+},[410] D-penicillamine-functionalized graphene QDs[401] and rGO/AuNPs composite[402] for Fe^{3+}. The detection of other chemical species include the use of graphene/polyaniline (PANI) nanocomposite for methane,[403] rGO for arsine (AsH_3)[404] and 2,4-dinitrotoluene (DNT),[25] graphene QDs for 2,4,6-trinitrotoluene (TNT),[405] GO/polypyrene for toluene,[406] rGO/AgNPs/ZnO hybrid for acetylene,[407] cerium oxide (CeO_2)/rGO for fenitrothion insecticide,[411] N and S codoped graphene QDs/AgNPs for cyanide,[412] graphene interdigitated microelectrodes for *E. coli* O157:H7,[413] and graphene/PtNPs/Nafion composite for metoprolol associated with cardiovascular disease treatment.[414]

5. SELECTIVITY AND STRATEGIES FOR EXCLUDING INTERFERENTS

Here we emphasize on the sensitivity and selectivity of chemical species by the graphene-based sensors and a few examples of strategies on how to exclude the interference from other analytes

DOI: 10.1021/acsami.7b07063
ACS Appl. Mater. Interfaces 2017, 9, 34544−34586

in order to distinguish the sensitivity response of different analytes through the chemical modification of graphene, GO, and rGO. The selectivity of different analytes is one of the most important factors for evaluating the performance of a sensor. Sensor arrays have also been used for differentiating between various analytes present in a given mixture such as detecting proteins,[415] cancer biomarkers,[416,417] VOCs,[418,419] and other analytes.[420]

Graphene-based sensor arrays have been studied for simultaneously detecting and categorizing a set of chemical elements using the linear discriminant analysis (LDA) for recognizing patterns. Nanographene oxide (NGO)-based sensor arrays have been used for detecting ensemble aptamers (ENSaptamer) proteins with pattern recognition by Pei et al.[421] Figure 27 shows the identification of different proteins using NGO-ENSaptamer as a sensing platform. The nine different proteins including subtilisin A (SubA), fibrinogen (Fib), hemoglobin (Hb), cytochrome *c* (CC), lysozyme (Lyso), horseradish peroxidase (HRP), bovine serum albumin (BSA), lipase, and casein were identified six times against ENSaptamer-5, ENSaptamer-6, and ENSaptamer-7 at 5 μM. A 20-base ssDNA probe series (P1−P7) tagged with 6-carboxyfluorescein (6-FAM) fluorescent dye was used to study the interactions between NGO and DNA. The proteins were analyzed using ENSaptamer sensor containing ENSaptamer-5 (ssDNA probes P1, P2, P5, P6, and P7). Each protein gives rise to different fluorescence response patterns arising from NGO-DNA probes interactions, which were analyzed using classical linear discriminant analysis (LDA). The six replicates of each protein with LDA method yielded four canonical factors with variations of 81.1, 16.4, 1.3, and 1.2%. The 54 canonical fluorescence response patterns (nine proteins × six replicates) were isolated into nine separate groups. The six out of nine proteins were noticeably identified with ENSaptamer-5 in the pattern recognition, however, three remaining BSA, HRP, and Fib proteins showed a significant overlapping, insinuating to the limited differentiation by the use of ENSaptamer-5. By increasing the number of DNA probes to BSA, HRP, Fib, ENSaptamer-6 was able to separate BSA from the HRP and Fib proteins. The jackknifed classification matrix demonstrated classification accuracy enhancement from 96% for ENSaptamer-5 up to 100% for ENSaptamer-6 as well as ENSaptamer-7. Both HRP and Fib still exhibited clear overlap even after increased the classification accuracy in the 2D canonical score plot. One more DNA element was added to prepare ENSaptamer-7, which was able to identify all nine proteins having different surface properties and 3D structures. When Euclidean distance was increased from 2.6 to 4.7 between HRP and Fib, both were separated in the plot. This NGO-ENSaptamer-based sensor array was found to be highly sensitive and selective for detecting nine different proteins at a very low concentration of nanomolar scale. In another study, Chou et al.[422] used the conventional GO and nanographene oxide (NGO)-based nose

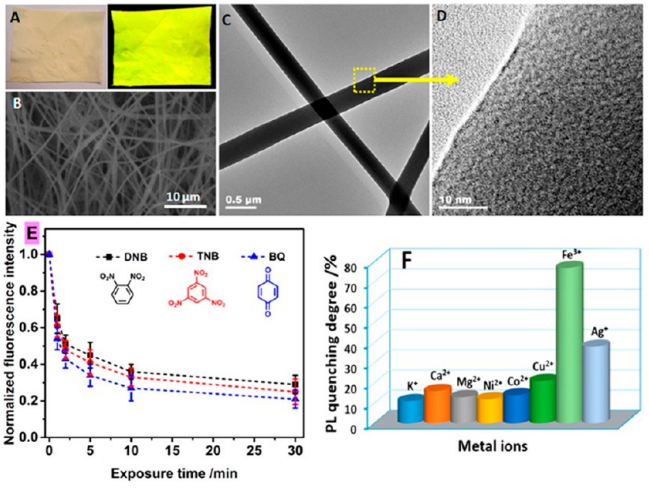

Figure 25. (A) Photographs of light-emitting, electrospun PTBPE/poly(lactic acid) (PLA) nanofibrous films under sunlight (left) and UV lamp excited at 365 nm (right). (B) SEM, (C) TEM, and (D) HRTEM images of the PTBPE/PLA nanofibers. (E) Fluorescence intensity recorded for sensing organic vapors from the electrospun PTBPE/PLA nanofibrous films after exposing to 1,2-dinitrobenzene (DNB), 1,3,5-trinitrobenzene (TNB), and 1,4-benzoquinone (BQ) vapors from 0−30 min. (F) Detection of different types of oxidizing metal ions shown in terms of the degree of fluorescence quenching of the PTBPE/PLA nanofibrous films upon immersing for 1 min in aqueous solutions of metal ions (10^{-4} mol/L). [Reprinted with permission from ref 382. Copyright American Chemical Society.]

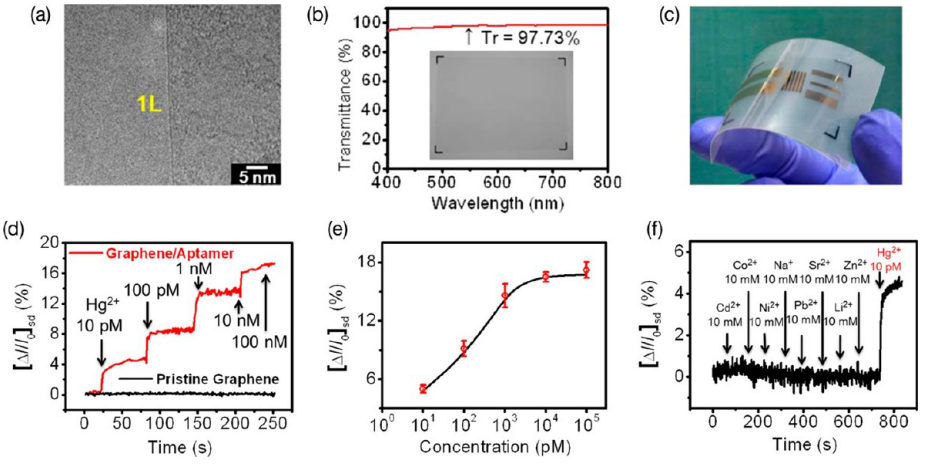

Figure 26. (a) HRTEM image of a single-layer graphene: (b) UV−visible spectra of single-layer graphene (1L) on flexible PEN substrate showing 97.7% optical transmittance at 550 nm; (c) gold electrodes deposited on flexible and transparent graphene aptasensor for detecting Hg^{2+} ions in mussels. (d) Real-time responses of graphene/aptamer and pristine graphene and (e) Sensitivity of aptasensor with varying Hg^{2+} concentrations (10 pM to 100 nM). (f) Aptasensor showing high selectivity toward target metal ion of Hg^{2+} at 10 pM and nontarget metal ions of Cd^{2+}, Co^{2+}, Ni^{2+}, Na^{+}, Pb^{2+}, Sr^{2+}, Li^{2+}, and Zn^{2+} at 10 mM. [Reprinted with permission from ref 383. Copyright American Chemical Society.]

DOI: 10.1021/acsami.7b07063
ACS Appl. Mater. Interfaces 2017, 9, 34544−34586

Table 3. Chemical Sensors Developed from Graphene-Based Materials

Graphene-based electrodes	Analyte	Limit of detection	Ref.
rGO/polyimide flexible substrate	Acetone	1 ppm	227
	Toluene	1 ppm	227
	Ethanol	1 ppm	227
Graphene nanoelectronic heterodyne (FET, 100 kHz)	DMMP	43 ppb	355
	DMF	0.92 ppm	355
	1,4-Dioxane	50 ppm	355
	Chloroform	164 ppm	355
	2-Propanol	105 ppm	355
	Chlorobenzene	12 ppm	355
	Toluene	210 ppm	355
	Dichloromethane	139 ppm	355
	Acetone	58 ppm	355
	Ethanol	65 ppm	355
Cyclodextrin-functionalized graphene/PtNPs	Bisphenol A (BPA)	0.15 nM	373
AuPd nanoparticles-loaded graphene nanosheets	Bisphenol A (BPA)	8 nM	384
Pt/PdNPs-graphene nanocomposite	Formaldehyde	2.85 μM	385
Poly(3,4-ethylenedioxythiophene)/graphene composites	Hydroquinone	0.06 μM	377
	Catechol	0.08 μM	377
	Resorcinol	0.16 μM	377
3D porous graphene/carbon nanotube	Methotrexate	70 nM	386
rGO/platinum(II)-tetraphenylporphyrin nanocomposite	Hydrazine	5 nM	387
rGO/nickel-tetraphenyl porphyrin nanocomposite	Nitrobenzene	0.14 μM	388
β-Cyclodextrin/graphene oxide	Nitrobenzene	0.184 μM	389
rGO/ZnO composite	Phenol	1.94 μM	390
rGO/SnO_2 aerogels	Phenol	10 ppb	391
Glassy carbon electrode/rGO composite	4-Nitrophenol	42 μM	392
Diamond/graphene/polyaniline composite	2,4-Dichlorophenol	0.25 μM	393
Molecularly imprinted polymer/graphene oxide	2,4-Dichlorophenol	0.5 nM	394
Nitrogen-doped graphene quantum dots (N-GQDs)	2,4,6-Trinitrophenol	420 nM	395
Graphene oxide/chitosan nanocomposite	Methylamine	3 ppm	396
	Dimethylamine	3 ppm	
	Trimethylamine	3 ppm	
rGO/polyethylenimine/Pd nanohybrids	Hg^{2+}	10 nM	397
Cobalt sulfide (CoS)/porous rGO nanocomposite	Hg^{2+}	14.23 nM	398
Nitrogen-doped graphene/chitosan nanocomposite	Pb^{2+}	6.64 $\times 10^{-8}$ M	399
AgNPs/rGO nanocomposite (*Moringa oleifera* fruit)	Hg^{2+}	50 nM	400
	Pb^{2+}	15 mM	400
	Cr(VI)	500 nM	400
D-penicillamine-functionalized graphene QDs	Fe^{3+}	1.2 $\times$ 10^{-6} M	401
rGO/gold nanoparticles (AuNPs) composite	Fe^{3+}	3.5 nM	402
Graphene nanosheets/polyaniline (PANI) nanocomposite	CH_4	10 ppm	403
Reduced graphene oxide (rGO)	AsH_3	0.01 ppm	404
Reduced graphene oxide flakes	DNT	52 ppb	25
Graphene quantum dots (GQDs)	TNT	0.495 ppm	405
Graphene oxide/polypyrene composite	Toluene	24 ppm	406
rGO/Ag nanoparticles-loaded ZnO hybrid	Acetylene	100 ppm	407
rGO/chitosan particles/DNA nanocomposite	Hg^{2+}	0.016 nM	408
Polypyrrole-decorated graphene/β-cyclodextrincomposite	Hg^{2+}	0.47 nM	409
Sulfur-doped graphene QDs (fluorescence)	Ag^{+}	30 nM	410
Graphene oxide (GO) layer in Love-wave device	DMMP	9 ppb	378
	DPGME	9 ppb	378
rGO/*p*-phenylenediamine (PPD)	DMMP	30 ppm	379
rGO/PEDOT:PSS/polypyrrole/AuNPs	Pesticide	0.1 nmol/L	380
Cerium oxide (CeO_2)/rGO nanocomposite	Fenitrothion	3 nM	411
N and S codoped graphene QDs/AgNPs (fluorescence)	Cyanide (CN^-)	0.52 μM	412
Graphene interdigitated microelectrodes	*E. coli* O157:H7	10 cells/mL	413
Graphene/PtNPs/Nafion nanocomposite	Metoprolol	4.30 nM	414

arrays with five different fluorescent molecules including acridine orange (AO), rhodamine B (RB), pyronine Y (PY), rhodamine 6G (R6G), His-tagged emerald green fluorescent protein (eGFP) to identify eight different proteins including hemoglobin (Hem), myoglobin (Mayo), ribonuclease A (Rib-A), β-galactosidase (β-Gal), lysozyme (Lys), bovine serum albimin (BSA), histone (His), and lipase (Lip) by the nose arrays at 10 and 100 nM concentrations. The conventional GO arrays showed lower fluorescence response and minor classification at 100 nM protein concentration. The canonical score plot calculated by the linear discriminant analysis (LDA) showed that all eight proteins including Rib-A, His, β-Gal, Hem, Lys, Mayo, BSA, and Lip at 100 nM concentration were 100% accurately categorized by the NGO sensor array whereas the canonical score plot for the conventional GO sensor array was overlapped and not so clear compared to NGO array. The sensing of eight proteins at 10 nM concentration and their canonical score plot obtained from the LDA showed 95% accurate classification for the NGO sensor array but an incomplete classification for the conventional GO sensor array. The 100% classification was achieved with three NGO sensors in the array including eGFP, R6G, and PY for protein detection at 100 nM with LDA/Jackknife analysis. In the case of conventional GO array at 100 nM, 100% classification was achieved with five sensors including AO, RB, eGFP, R6G, and PY and 98% classification using three sensors with eGFP, R6G, and PY. NGO sheets having more oxygenated reactive sites showed enhanced fluorescence response due to their high affinities for different analyte proteins compared to conventional GO associated with the increased charge density of NGO supramolecules. The above studies showed that NGO-aptamer and NGO-based sensor arrays could be used for identifying various proteins at nanomolar concentrations for their potential applications in nanomedicine including bioimgaing, diagnostic and therapeutics.

The PCA is another method of recognizing patterns through graphene-based sensor arrays as used for selectively identifying a

DOI: 10.1021/acsami.7b07063
ACS Appl. Mater. Interfaces 2017, 9, 34544−34586

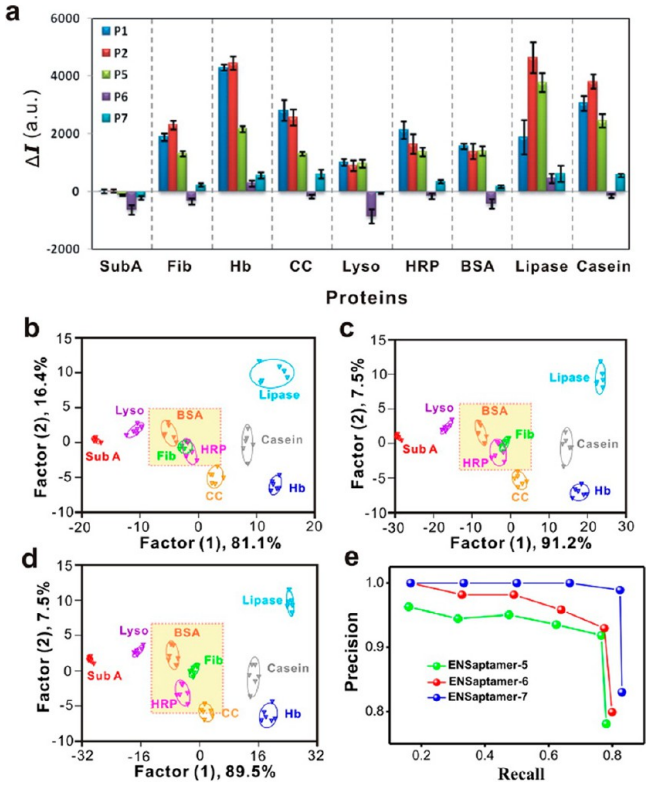

Figure 27. (a) Fluorescence response patterns recorded using ENSaptamer-5 for detecting nine different proteins including subtilisin A (SubA), fibrinogen (Fib), hemoglobin (Hb), cytochrome *c* (CC), lysozyme (Lyso), horseradish peroxidase (HRP), BSA, lipase, and casein at 5 μM. Error bars shows the standard deviations for six measurements. (b) Canonical score plot obtained using the NGO-ENSaptamer-5 sensor array having ssDNA probes P1, P2, P5, P6, and P7. In this plot, six out of nine proteins were clearly identified; however, there was an overlap between BSA, Fib, and HRP proteins. (c) Canonical score plot obtained for NGO-ENSaptamer-6 sensor array containing ssDNA probes P1, P2, P4, P5, P6, and P7. In this case, BSA protein was separated out from Fib and HRP proteins. (d) Canonical score plot obtained for the NGO-ENSaptamer-7 sensor array containing ssDNA probes P1–P7 where all nine proteins were clearly separated and selectively identified. (e) Precision–recall plots for the NGO-ENSaptamer sensor arrays where 99% precision for ENSaptamer-7 was obtained at <83% recalls. [Reprinted with permission from ref 421. Copyright American Chemical Society.]

mixture of organophosphate pesticides.[380] PCA has been extended to selectively discriminate a mixture of gases. Choi et al.[227] demonstrated the selectivity of gas molecules by pattern recognition using principal component analysis (PCA). In order to examine the selectivity of IPL-RGO-based flexible sensors for different gaseous molecules, the PCA was conducted for pattern recognition of H_2S, H_2, acetone, ethanol, methane, toluene, and carbon monoxide at 5–20 ppm both in the flat as well as bent states (Figure 28). The H_2S, H_2, and ethanol were found to cluster in completely different regions without any overlapping in the flat as well as in the bend state, showing that IPL-RGO sensor can distinguish among three different chemical species using pattern recognition. Furthermore, other chemical species including toluene, acetone, methane, and carbon monoxide at 20 ppm in the flat state were also clustered separately in the three-dimensional (3D) PCA pattern recognition domain. The sensitivity and selectivity of IPL-RGO sensor was also evaluated for gaseous molecules at different concentrations.

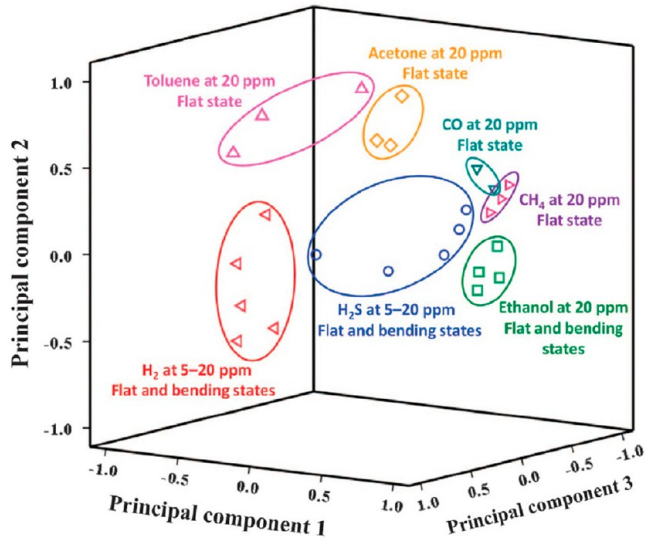

Figure 28. Principal component analysis (PCA) for recognizing pattern of H_2, H_2S, acetone, ethanol, toluene, methane, and carbon monoxide at 5–20 ppm using IPL-RGO-based flexible sensors both in the flat and bent states. [Reprinted with permission from ref 227. Copyright Springer Nature.]

The IPL-RGO sensor showed the highest sensitivity toward H_2S at 20 ppm whereas very low sensitivity of 0.1% was observed toward other interfering chemical species even at this high gas concentration. The ethanol especially displayed the highest sensitivity between 1 and 5 ppm gas concentration whereas hydrogen at 10 ppm. The IPL-RGO sensor showed an *n*-type behavior for H_2S at 20 ppm due to the heavy doping by electron donating H_2S gaseous molecules, which increased the electrical resistance whereas sensor showed a simple *p*-type characteristic below 10 ppm of H_2S concentration without displaying any *p*–*n* transition. Alizadeh and Soltani[423] designed a rGO sensor array for the pattern recognition of DMMP vapors. The rGO chemiresistors were capable of selecting and interfering with DMMP from other vapor analytes. The rGOs were prepared from GO using hydrazine hydrate, ascorbic acid, and sodium borohydride reducing agents. The sodium borohydride and ascorbic acid obtained rGOs were found to be more sensitive to DMMP vapor than rGO reduced by hydrazine hydrate; therefore, synthetic conditions also had a big impact on the selectivity of rGO sensor toward DMMP vapors.

Sensor arrays for selectively detecting proteins by gold nanoclusters[424] and aptamer-based plasmonic element,[425] phosphate anions and metal ions by carbon dots,[426] metal ions by CNTs,[427] explosive vapors by ZnO,[428] and toxic gases by metallic NPs[429] have been reported. Typically, chemiresistive and FET-type sensors with carbon nanotubes, graphene or metal oxides are used to construct an electronic nose system employing a sensor array with the aid of pattern recognition algorithms for selective identification of the analyte of interest. The principles and an example of an e-nose system constructed using CNTs can be found in a review article by Meyyappan.[430]

Though graphene shows self-sensitivity to some analytes such as NO_2 and NH_3 due to their electron exchange properties, but to achieve an absolute selectivity over existing interfering analytes within a working environment is difficult. Therefore, doping of graphene/GCEs with other materials such as metallic nanoparticles of Pt, Pd, Au, etc., polymers such as polyaniline and polypyrrole, semiconducting metal oxides such ZnO, TiO_2,

DOI: 10.1021/acsami.7b07063
ACS Appl. Mater. Interfaces 2017, 9, 34544–34586

SnO_2, and biological species such as DNAzyme oligonucleotides has been found a very effective approach in order to discriminate among various analytes and significantly increasing the selectivity toward a particular analyte by excluding interference by other existing analytes in a given mixture using modified graphene-based sensors. Furthermore, the factors such as temperature, nature and ratio of a dopant, concentration of analyte, morphology, and device structure also assist in differentiating a particular analyte within a mixture. A few examples are discussed in this section.

The semiconducting nanoparticles such as titania, gold nanoparticles (AuNPs) have been used in combination with graphene-based materials for fabricating chemical sensors those can exclude the interference from other chemical species. Chang et al.[431] used self-assembled AuNPs-rGO/chitosan hybrid-modified GCE for catalytic oxidation and electrochemically detection of β-nicotinamide adenine dinucleotide (NADH) coenzyme where chitosan was used as a stabilizing agent for graphene solution and to immobilize AuNPs. The amperometric detection of NADH by the AuNPs-rGO/chitosan film electrode showed a wide linear range from 1.5 to 320 μM, high sensitivity of 0.318 mA μM^{-1} cm^{-2}, 5 s response time and low LOD value of 1.2 μM (S/N = 3). The synergistic effect between AuNPs and rGO started the catalytic oxidation of NADH at 0.05 V and decreased oxidation overpotential by 220 mV compared to a bare electrode, and also significantly enhanced the oxidation current. The interference of ascorbic acid (AA) was investigated through CV analysis for mixtures containing of 0.5 mM AA and different concentrations of NADH on bare and AuNPs-rGO/chitosan film-modified GCEs. The voltammetric signals of a mixture containing 0.5 mM AA and 0.14 mM NADH was hardly discriminated by the bare GCE. In case of AuNs-rGO/chitosan hybrid film modified GCE, two separate oxidative current peaks at 0.36 V for NADH and 0.05 V for AA were observed at 29 μM NADH concentration. The oxidation peak currents of NADH showed a linear increase from 29 μM to 143 μM concentrations in the presence of AA. The anodic peak current for NADH was found to be larger in the presence of AA at particular concentration compared with in the absence of AA. The AuNPs-rGO/chitosan used for detecting NADH showed the exclude effect from the oxidation of AA interference. Yan et al.[432] developed photoelectrochemical sensor for dopamine detection using GQDs dots with TiO_2 nanparticles (GQDs/TiO_2NPs nanocomposites) which showed photocurrent enhancement by 30-time and 12-time for GQDs-TiO_2/GCE under visible-light compared with bare GQDs/GCE and bare TiO_2/GCE, respectively, due to the synergy between GQDs and TiO_2 NPs and excluded the interference of other electrochemical species. Furthermore, the dopamine selectively sensitized GQDs-TiO_2 nanocomposites and enhanced photocurrent with the increasing concentration of dopamine from 0.02 to 105 μM with a LOD of 6.7 nM (S/N = 3) under optimized experimental conditions. Hou et al.[433] used *N*-(trimethoxysilylpropyl) ethylenediamine triacetic acid (EDTA) modified rGO with Nafion to fabricate an electrochemical sensor which detected neurotransmitter dopamine wih LOD of 0.01 μM. The oxygenated functional groups in rGO sheets and their molecular interaction with dopamine eliminate the interference of ascorbic acid.

Wu et al.[434] developed a new approach to detect glucose and efficiently exclude the interference from coexisting chemical species by incorporating glucose oxidase (GOx) into graphene. The electrocatalytic reduction of dissolved oxygen was observed at the GOx-graphene/GC electrode. The reduction current was found to decrease after glucose addition and sensor showed a high sensitivity of 110 ± 3 $\mu A\ mM^{-1}\ cm^{-2}$, a linear range of 0.1−10 mM, and a low LOD of 10 ± 2 μM for glucose detection. This approach excluded the effect of interference of other electroactive species because of a low detection potential used in the experiment (−470 mV, versus SCE). Luo et al.[435] electrodeposited CuNPs on graphene sheets to develop nonenzymatic glucose sensor and studied electrochemical behavior and interference using cyclic voltammetry and chronamperometry. The CuNPs/graphene composite electrode showed a synergistic effect toward glucose oxidation in alkaline solution by displaying a higher oxidation current, a linear range up to 4.5 mM glucose, and response time of (<2 s). The sensor showed high selectivity where the contamination by chloride ions, interference from ascorbic acid, dopamine, uric acid, and carbohydrate was effectively avoided and glucose was selectively detected by the CuNPs/graphene electrode. This study indicated the high selectivity by the sensor toward target glucose detection with LOD of 0.5 μM (S/N = 3) in the presence of other interferents. Kim et al.[436] used single-Si-nanowire (SiNW)-based DNA sensors hybridized with CVD-graphene to develop diode-type biosensors for selectively detecting specific oligonucleotides. This hybridization process leads to a doping effect of SiNWs where the current increased from 19% to 120% as the concentration of DNA was increased from 0.1 to 500 nM. The graphene/SiNWs-based biosensor accurately selected targeted oligonucleotides.

The morphology of a nanostructured material (thin film, nanorods, nanoribbons, nanoflowers, etc.), which controls the surface area and accessible reactive sites to the analytes, plays an important in determining the magnitude of sensitivity toward an analyte. Esfandiar et al.[437] developed H_2 gas sensors by incorporating Pd-WO_3 hybrid into GO and partially reduced graphene oxide (PrGO) sheets using a hydrothermal process. Pd-WO_3 hybrid has ribbon-like morphologies, Pd-WO_3/GO as irregular nanostructure and Pd-WO_3/PrGO a high surface area hierarchical nanostructure. The gas sensitivity was decreased by 50% after adding GO into the Pd-WO_3 because of lower surface area arising from irregular nanostructure compared with the ribbon-like morphology. The Pd-WO_3/PrGO films exhibited 10 times higher sensitivity that of Pd-WO_3/GO. This study demonstrated that the residual oxygenated functional groups of PrGO and a high surface area of Pd-WO_3/PrGO hierarchical nanostructure contributed to higher H_2 gas sensitivity. Huang et al.[198] reported several folds enhancement in sensitivity toward NH_3 gas after adding PANI to rGO sheets (PANI/rGO) compared with pure PANI nanofiber and rGO-based sensors. Feng et al.[253] developed ammonia sensors using electrospun rGO and Co_3O_4 nanofibers that showed sensitivity to ammonia between 5 and 100 ppm and selectivity over interferrents including methanol, ethanol, formaldehyde, acetone, benzene, and methylbenzene. Wang et al.[259] reported the selectivity by self-assembled rGO (pyrrole reduced) sensors for different analytes. Ammonia was detectable at a very low concentration of 100 ppm; however, chloroform, hexane, methanol, dichloromethane, xylene, and DMMP were detectable to 1% of vapor concentrations, which is a much higher concentration compared with ammonia gas. This indicates that the Py-rGO sensors are highly selective for detecting ammonia gas.

In another study, Zou et al.[438] reported much higher sensitivity and selectivity of the Pd-PANI/rGO nanocomposite film (surface area of 71.5 m^2/g) sensor toward H_2 gas compared with PANI/rGO (44.3 m^2/g) and PANI (38.5 m^2/g) due to the

DOI: 10.1021/acsami.7b07063
ACS Appl. Mater. Interfaces 2017, 9, 34544−34586

hydrogen absorption on Pd, and the high surface area offered by the PANI/rGO nanocomposite as shown in Figure 29a.

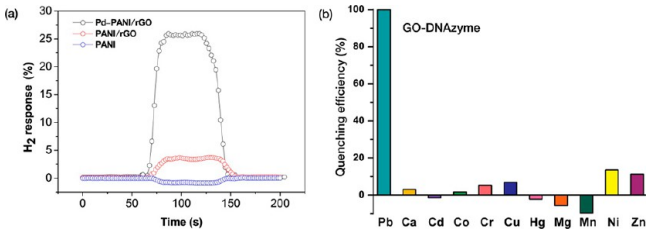

Figure 29. (a) Gas sensing responses of sensors based on the PANI, PANI/rGO, and Pd-PANI/rGO films toward 1% hydrogen at room temperature. [Reprinted with permission from ref 438. Copyright Elsevier.] (b) Selectivity of the GO-DNAzyme oligonucleotide-based sensor toward Pb^{2+} ions over 10 different interference metal ions at 1 μM. [Reprinted with permission from ref 440. Copyright The Royal Society of Chemistry.]

The Pd-PANI/rGO nanocomposite-based sensor showed 25% H_2 gas sensitivity, low detection limit of 0.01 vol %, and response and recovery times of 20 and 50 s, respectively. The electrical conductivity of the Pd-PANI/rGO nanocomposite-based sensor decreased with the increase of H_2 gas concentration due to the adsorption of H_2 molecules on the surface of Pd nanoparticles that formed Pd hydride (PdHx) and reduced the carrier mobility. The selectivity of H_2 was examined over CO_2, CH_3OH, and H_2S gases at 1 vol % concentration, no response was observed for CO_2 and H_2S gases but a slight response occurred for CH_3OH. These studies showed the role of Pd doping on graphene-based sensors in enhancing sensitivity for H_2 gas because Pd can selectively absorb a high amount of H_2 gas. The selective gas sensing has been reported with a single pristine graphene transistor.[123] The CuO-ZnO/rGO hybrid sensors showed highly selective gas-sensing toward acetone at 100 ppm concentrations of various interfering VOCs including methanol, ethanol, chloroform, toluene, ethylene glycol, formic acid, acetic acid, and propionic acid.[439]

The different absorption characteristics, reactivity, and molecular interactions are exhibited by each and every analytes. Wen et al.[440] reported a GO-DNAzyme oligonucleotides-based sensor that demonstrated the molecular interactions between GO and the Pb^{2+}-dependent DNAzyme exclude the interference from 10 different metal ions including Ca, Cd, Co, Cr, Cu, Hg, Mg, Mn, Ni, and Ni ions at 1 μM and selectivity detected Pb^{2+} ions with ultrahigh sensitivity as shown in Figure 29b. This study indicated that the molecular level interactions occurring between GO sheet and the Pb^{2+}-dependent DNAzyme play a major role in selectively detecting Pb^{2+} ions. Zhao et al.[441] used a GO-DNAzyme-based biosensor showing high selectivity and a LOD of 300 pM for Pb^{2+} where the fluorescence detection of Pb^{2+} was selected by the GR-5 DNAzyme oligonucleotide catalytic unit instead of 8−17 DNAzyme oligonucleotide. These biosensors were tested for detecting Pb^{2+} in river water. Li et al.[442] incorporated GO sheets in the aptamer-functionalized CdSe/ZnS QDs to develop GO/aptamer-CdSe/ZnS QDs that functions as a "turn-on" fluorescent sensor for detecting Pb^{2+}. The interaction of Pb^{2+} ions with the aptamer form a complex where the QDs are separated from the GO sheet. This detachment "turns on" the QDs fluorescence. The sensor showed a LOD of 90 pM and Pb^{2+} ions were exclusively selected over a broad range of other metal ions. The ethylenediamine was utilized as a chelating reagent to exclude the effect of interference of other metal ions. This study showed that the fluorescence of CdSe/ZnS QDs was quenched by GO through metal surface energy transfer mechanism instead of Förster resonance energy transfer (FRET) process. Zhao et al.[443] reported selective sensing Pb^{2+} due to the selective adsorption by the polypyrrole/rGO composite toward Hg^{2+}. The sensor showed Pb^{2+} sensitivity of 0.642 μA nM^{-1} and a LOD of 4 pM in the presence of Hg^{2+}. The minimal interference was observed with other ions at high concentrations.

Graphene QDs (GQDs) have been explored for sensing applications. Wei et al.[444] used fluorescent GQDs to detect TNT in a solution using FRET quenching. The fluorescent GQDs and TNT bind together via the $\pi-\pi$ interactions, which suppresses the fluorescence emission due to the FRET from electron donor GQDs to electron acceptor TNT via intermolecular interactions. The unmodified GQDs showed high sensitivity down to 0.495 ppm (2.2 μM) of TNT with 1 mL solution of GQDs. The FRET-based GQDs exhibited high fluorescence without any modification and can detect ultratrace analytes. The high selectivity of potassium (K) ions was achieved by using an ion-selective crown ether and by the transfer of fluorescence resonance energy from carbon dots to graphene. Highly selective detection and visual identification of Fe^{3+} ions in wine was reported using Nile red with partially oxidized graphene film.[445]

The gas sensing material SnO_2 has been used with rGO for selectivity purpose. The SnO_2/rGO-based sensor exhibited up to 33.4% enhancement in sensitivity toward NO_2 gas compared with pure rGO, whereas up to 23.8% reduction in sensitivity of NH_3 compared with pure rGO. Therefore, selectivity of the gas sensors was tuned by SnO_2 nanocrystals as reported by Mao et al.[446] Wei et al.[447] mixed gas sensing semiconductor SnO_2 with rGO for detecting heavy metal ions and to study difference in their sensitivity and mutual interference during simultaneous electrochemical analysis of Cd(II), Pb(II), Cu(II), and Hg(II). The SnO_2/rGO composite modified glass carbon electrode (GCE) were able to simultaneously and selectively detect traces of Cd(II), Pb(II), Cu(II), and Hg(II) in drinking water using square wave anodic stripping voltammetry (SWASV) technique. The detection limit of 1.015×10^{-10} M, 1.839×10^{-10} M, 2.269×10^{-10} M, and 2.789×10^{-10} M were measured for the Cd(II), Pb(II), Cu(II), and Hg(II) respectively, which is below than the recommended value by the World Health Organization. The sensitivity of 5.167 μA μ/M for Cu(II) and 2.766 μA μ/M for Hg(II) were observed during the individual analysis; however, during the simultaneous analysis, the sensitivity of Cu(II) significantly increased to 9.664 μA μ/M whereas sensitivity of Hg(II) remained unchanged at 2.713 μA μ/M. These results were explained in terms of the Hg film formation as well as followed by the formation of a Cu-Hg compound on the SnO_2/rGO surface during the deposition process, which enhanced the sensitivity toward Cu(II). The Cd(II), Pb(II), Cu(II), and Hg(II) showed sensitivity of 18.4, 18.6, 14.98, and 28.2 μA μ/M during simultaneous analysis, respectively. Here, the sensitivity dramatically increased for both Cu(II) and Hg(II) compared with the individual analysis as well as simultaneous analysis of Cu(II) and Hg(II). The effect of the concentrations of Cd(II) was investigated in order to understand the significant enhancement of sensitivity for Cu(II) and Hg(II) during simultaneous analysis. Figure 30 shows the square wave anodic stripping voltammetry (SWASV) response of the SnO_2/rGO electrode at different Cd(II) concentrations in the presence of 0.5 μM Cu(II) and 0.5 μM Hg(II) where an interference on the anodic peak currents was observed. With addition of 1.0 μM Cd(II), the peak current of Hg(II) was noticeably increased

DOI: 10.1021/acsami.7b07063
ACS Appl. Mater. Interfaces 2017, 9, 34544−34586

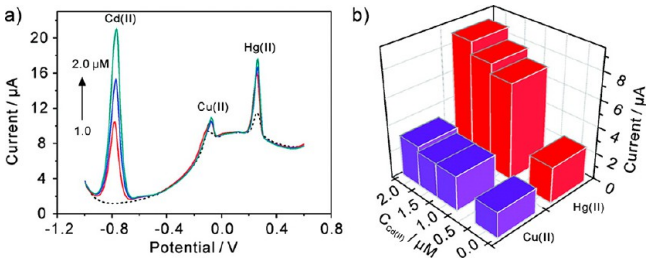

Figure 30. (a) SWASV response of the SnO_2/rGO composite modified glass carbon electrode (GCE) at 0, 1.0, 1.5, and 2.0 μM concentrations of Cd(II) in the presence of 0.5 μM Cu(II) and 0.5 μM Hg(II) in 0.1 M NaAc-HAc (pH 5.0). Here the concentrations of Cd(II) show an interference on the anodic peak currents of 0.5 μM Cu(II) and 0.5 μM Hg(II). (b) Comparison of the voltammetric peak current of Cu(II) and Hg(II) at different Cd(II) concentrations corresponding to SWASV conditions. [Reprinted with permission from ref 447. Copyright American Chemical Society.]

while the increase for the peak current of Cu(II) was lower. Moreover the peak currents of Cu(II) and Hg(II) stabilize with further addition of Cd(II). The sensitivity toward Cu(II) and Hg(II) was increased during deposition process which was interpreted in terms of the formation of Cd film and thereafter the formation of intermetallic Cd compounds with Cu and Hg. The formation of Cd film is prevented at a particular concentration of Cd(II) as a result the peak currents for both Cu(II) and Hg(II) are stabilized. Likely, the SWASV response of the SnO_2/rGO composite modified GCE at 0, 2.5, 3.0, and 3.5 μM concentrations of Pb(II) was studied in the presence of 0.5 μM Cu(II) and 0.5 μM Hg(II) where the Pb(II) concentration also showed an interference on the anodic peak currents of 0.5 μM Cu(II) and 0.5 μM Hg(II). This study clearly explains the mutual interference phenomenon and the effect of concentration of interference. Furthermore, this work indicated the use of SnO_2 in detecting heavy metal ions.

Chemiresistor and FET-type sensors made of modified graphene films have also been investigated by various research groups for selectively detecting gases,[448−452] heavy metal ions,[453,454] fluoride anions,[455] glutathione,[456] depression biomarker,[457] cancer cells,[458] nucleic acid,[459] pesticides,[460] tramadol,[461] quercetin, morin and rutin in grape wine,[462] and other chemicals.[463,464]

6. CHEMICAL SENSING MECHANISMS FOR GRAPHENE

In this section, reported chemical sensing mechanisms for graphene, GO, and rGO are briefly described. The sensitivity of graphene-based materials depends upon the chemical species attached to graphene surfaces and at the edges in the case of GO and rGO films which contains oxygentated functional. GO imparts quite different physical and chemical properties than that of pristine graphene or rGO due to attached oxygenated functional groups which are also the adsorption sites for chemical analytes. The presence of hydroxyl groups play a major role in hydrogen bond formation between GO films and adsorbed chemical molecules depending upon their chemical functionality. For example, water molecule (H_2O) will easily form hydrogen bonds with OH groups of GO or rGO films. For electron accepting NO_2 molecules and electron donating NH_3 and H_2S molecules, the change in electrical resistance is observed due to the electron exchange processes occurring between the gas molecules and the graphene and such chemical sensing mechanisms are discussed in the literature.[70,160−164,198,220−227,259−267] Humidity sensing by the GO and rGO films has been explained in terms of H bonding. Bi et al.[465] reported ultrahigh sensitivity of graphene oxide toward humidity. The graphene oxide (GO) films-based capacitive humidity sensor exhibited sensitivity up to 37 800% at 15% to 95% relative humidity as indicated by the increase of capacitance from 9.8 pF to 3710 pF. The relative capacitance of GO sensor changed from 8000% at 100 Hz to 32 200% at 10 kHz, which was over 10 times higher compared with conventional sensors. Figure 31 shows a schematic illustration of humidity sensing mechanism by the GO films.

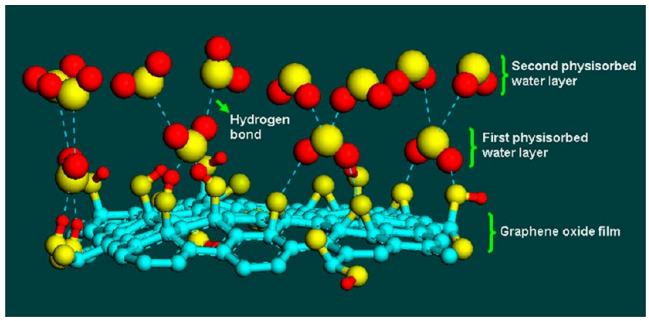

Figure 31. Schematic diagram showing humidity sensing mechanism on the surface of GO films. [Reprinted with permission from ref 465. Copyright 2017 Macmillan Publishers Limited.]

The water molecules are adsorbed following two different hydrogen bonding processes; double hydrogen bonds are formed between the first-layer of water molecules and on the surface of GO films whereas a single hydrogen bond is formed from the second layer of water molecules. The water molecules adsorbed by hydrophilic oxygenated groups on the GO surface form two H bonds at low relative humidity. In this case, the free movement of adsorbed water molecules is restricted by two H bonds. The hopping of protons between adjacent OH groups of GO films gives rise to higher electrical resistance. The multilayer adsorption of water molecules takes place as the RH is increased. The second layer of water molecules forms a single H bond with OH groups, where water molecules have more moving flexibility. With progressing multilayer adsorption, hydronium ions (H_3O^+) can be generated as charge carriers by the ionization of water under an electrostatic field. The adsorbed water layers could behave like a liquid under higher humidity. The higher number of epoxy groups in GO could help in proton migration. All these events could lead to high sensitivity of GO films at high RH.

The sensing mechanisms of NO_2 and H_2S gases with rGO films have been explained in terms of intrasheet and intersheet effects occurring between an individual rGO sheet and interconnections formed among different rGO sheets, respectively.[466] Sun et al.[467] detected physisorption of an individual CO_2 molecule on suspended bilayer graphene (BLG). The density functional theory (DFT) simulation indicated resistance increment of 50 Ω in graphene by the adsorbed single CO_2 molecule whereas experimentally a resistance change of 61 Ω was measured as a result of individual CO_2 adsorption and desorption phenomena in graphene. The CO_2 gas adsorption mechanism was described in terms of van der Waals (vdW) interactions.[467−469] The H_2 sensing mechanisms for the Pd nanocluster-decorated graphene[205] and Pt nanoparticle-decorated rGO surfaces[206] have been proposed. The H_2 molecules are adsorbed onto the Pd or Pt surfaces. and thereafter the H_2 molecule is dissociated into two H atoms. The Pd nanoclusters are transformed from the Pd phase to the palladium hydride (PdHx) phase when exposed to H_2 gas, which causes a change in

DOI: 10.1021/acsami.7b07063
ACS Appl. Mater. Interfaces 2017, 9, 34544−34586

electrical resistance and work function. Likely, the transformation of Pt phase to platinum hydride (PtHx) phase takes place, which also gives rise to resistance change upon exposure to H_2. The molecular interactions of the graphene, GO, and rGO with their doping materials are not fully understood; therefore, more studies are needed to explain the chemical sensing mechanisms of graphene-based materials.

7. LONG-TERM STABILITY OF GRAPHENE-BASED SENSORS

Long-term stability of humidity sensors against oxidative conditions is important for commercial applications. Graphene multilayer-based sensors displayed stability up to 100 days in air for NO_2.[70] The rGO-based flexible gas sensor exhibited stability up to 43 days toward 5 ppm of NO_2.[157] The mechanical stability of up to 5000 bending cycles and long-term stability up to 19 months has been reported for a flexible graphene/MoS_2 gas sensor.[265] The ZnO nanotubes/graphene-based H_2 sensors showed stability up to 90 days under hydrogenation/dehydrogenation conditions.[208] The LbL self-assembled TiO_2/rGO hybrid film-based sensors when exposed to 1, 100, and 500 ppb SO_2 for 30 days showed very little variation in the resistances.[219] The rGO/PDDA composite film-based humidity sensor showed stability in sensitivity under 23%, 52%, and 75% RH for 60 days.[343] Bi et al.[465] fabricated capacitive humidity sensors using GO films as a sensing material, which exhibited sensitivity of 37 800% that was 10 times higher compared with conventional humidity sensors and response and recovery times of 10.5 and 4.1 s, respectively. Long-term stability test of the GO-based sensors conducted in 15%, 35%, 55%, 75%, and 95% RH at 100 Hz and 1 kHz frequencies showed negligible variation over a period of 30 days. Humidity sensors fabricated from graphene modified with naphthalene-1-sulfonic acid sodium salt (NA) and AgNPs showed no degradation in sensitivity and response time when exposed for 110 days in air.[470] The AgNPs-NA-rGO composite-based sensor exhibited fast response/recovery time ($\leq$1 s) under 11% and 95% RH in air at room temperature at 100 Hz and response time remained the same for 110 days. These studies indicate that the humidity sensors based on graphene are quite stable under ambient conditions. Long-term stability of TiO_2/rGO hybrid film-based sensors toward SO_2 and AgNP-NA-graphene composite-based sensor for humidity is shown in Figure 32.

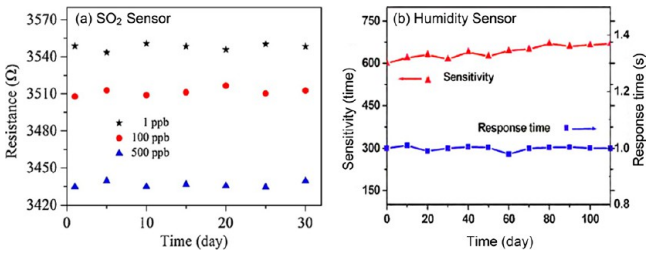

Figure 32. (a) Long-term stability test of TiO_2/rGO hybrid film-based sensors to 1, 100, and 500 ppb SO_2 gas concentrations. [Reprinted with permission from ref 219. Copyright Elsevier.] (b) Long-term stability of humidity sensor fabricated from graphene modified with naphthalene-1-sulfonic acid sodium salt (NA) and AgNPs. [Reprinted with permission from ref 470. Copyright American Chemical Society].

As discussed above, the graphene-based gas and chemical sensors indicate stability for a long period of time under different environmental conditions from oxidative atmosphere to high humidity to mechanical testing.

8. CONCLUSION AND PERSPECTIVE

Graphene-based materials have been used as new sensing elements in developing gas and chemical sensors for wearable electronics due to their unique optical, electrical, mechanical, and thermal properties. We have summarized the status of flexible gas sensors focused on sensing nitrogen dioxide, ammonia, hydrogen, hydrogen disulfide, carbon dioxide, and sulfur dioxide. Furthermore, applications of a graphene sensitive layer in detecting toxic bisphenol A (BPA), formaldehyde, acetone, methanol, ethanol, phenols, nitrobenzene, toluene, amines, explosives such as DNT and TNT, chemical warfare agents such as sarin and mustard nerve gases, heavy metal ions (Cd, Hg, Pb, Cr, Fe, Ni, Co, Cu, Zn, Ag), and other environmental pollutants were also analyzed. The sensors based on hybrids of graphene nanosheets decorated with nanostructured Pd, Pt, SnO_2, TiO_2, ZnO, Cu_2O, WO_3, Fe_2O_3, MoS_2, PANI, and polypyrrole and functionalized with organic moieties provide higher sensitivity and selectivity compared with pristine counterparts. The different types of sensors discussed here indicate that the right combination with doping materials, device architectures and synergetically contributing interfacial effects are important for high-performance sensors.

Both sensitivity and selectivity of chemiresistor and FET-type graphene-based sensors depend upon a number of factors ranging from the synthetic conditions to morphological structures to the concentrations of dopants and analytes. Factors including chemical structures,[122,163,164,170,263] synthetic conditions,[196,259,471] surface area of morphological nanostructures,[262,266,373,382,437,438] defects in graphene layered structures,[168,215,343] graphene interlayer spacing,[122] concentration of analytes,[122,160,164,201,202,205,259−265,380,383,416,431,432,447] intermolecular $\pi-\pi$ interactions,[405] fluorescence resonance energy transfer (FRET) quenching,[405,442,444] etc., control the sensitivity and selectivity of graphene-based sensors. Graphene-based sensor arrays could selectively identify and accurately classify a group of gases[227] and proteins[421,422] from interfering analytes using pattern recognition analysis. Both LDA and PCA methods proved to be significantly instrumental for discriminating a mixture of chemicals with graphene-based sensor arrays. Also, the comparative study between conventional GO and NGO sensor arrays showed that the size of GO sheets, amount, and the location of oxygenated functional groups (−OH, COOH, −CO, −C−O−C) offering reactive sites and their interactions with proteins are important factors for selectively detecting proteins at nanomolar level.[422] GO-based sensors can detect various gases, VOCs, and humidity. The adsorption sites offered by GO are important for sensing analytes, therefore, the control of the oxygenated functional groups on GO surface and the edges is important for tailoring electrical resistance as well as sensitivity and selectivity toward different analytes. The principles of molecular interactions of the graphene, GO, rGO, and their hybrid-based materials with different chemical analytes are not fully understood. The sensitivity and selectivity of graphene sensors should be significantly improved for accurately detecting chemical analytes over interferents at a very low concentration.

Flexible graphene-based materials not only exhibit high sensitivity toward chemicals but also show promise for developing flexible, transparent, and stretchable strain sensors for wearable electronics.[472−475] Graphene, GO, and rGO hybridized with other 2D materials, inorganic, and organic materials for applications in gas and chemical sensors are also advancing rapidly.[476−478] As discussed above, graphene-based materials show potential to fabricate transparent and flexible

DOI: 10.1021/acsami.7b07063
ACS Appl. Mater. Interfaces 2017, 9, 34544−34586

sensors that could be used for wearable electronic devices. The recent advances in flexible gas and chemical sensors for wearable technology are at an early stage, unparallel to the outstanding progress made for graphene-based flexible and wearable strain sensors to monitor various types of human body activities, which may lead to real commercial applications in the near future. Graphene flexible sheets fulfill most requirements for wearable electronic devices. Graphene-based flexible RFID tag sensors having wireless communication system is such an example.[206] The applications of RFID sensor technology are expected to grow significantly in various flexible devices including mobile phones. Furthermore, RFID sensors will have enormous interest in connection with IoT sector. Wearable sensors will be one of the most active research areas in coming years for applications in healthcare, robotics, artificial intelligence, military, space exploration, and in association with IoT by connecting billions of electronic devices through the Internet/cloud to the worldwide population; therefore, there will be enormous demand and growth in developing flexible and stretchable nanomaterials and their based wearable sensors for IoT sector.[479,480] Many challenges remain to find new low-cost and lightweight materials that can be used to manufacture transparent, flexible, and wearable chemical and biological sensors on a large-scale similar to present day conventional semiconductors. The efforts should be devoted to significantly improving the flexibility, stretchability, softness, long-term stability, and durability of graphene gas, chemical and biological sensors under varying environmental conditions such as humidity, temperature, and oxidative chemicals. One of the major challenges of wearable technology is the integration of flexible wearable sensors with wireless technology for the IoT applications as it is critical for future commercial success.

AUTHOR INFORMATION

Corresponding Authors

*E-mail: nalwa@mindspring.com (H. S. Nalwa).
*E-mail: m.meyyappan@nasa.gov (M. Meyyappan).

Notes

The authors declare no competing financial interest.

REFERENCES

(1) Novoselov, K. S.; Geim, A. K.; Morozov, S. V.; Jiang, D.; Zhang, Y.; Dubonos, S. V.; Grigorieva, I. V.; Firsov, A. A. Electric Field Effect in Atomically Thin Carbon Films. *Science* **2004**, *306*, 666−669.

(2) Bolotin, K. I.; Sikes, K. J.; Jiang, Z.; Klima, M.; Fudenberg, G.; Hone, J.; Kim, P.; Stormer, H. L. Ultrahigh Electron Mobility in Suspended Graphene. *Solid State Commun.* **2008**, *146*, 351−355.

(3) Banszerus, L.; Schmitz, M.; Engels, S.; Dauber, J.; Oellers, M.; Haupt, F.; Watanabe, K.; Taniguchi, T.; Beschoten, B.; Stampfer, C. Ultrahigh-Mobility Graphene Devices from Chemical Vapor Deposition on Reusable Copper. *Sci. Adv.* **2015**, *1*, e1500222.

(4) Nair, R. R.; Blake, P.; Grigorenko, A. N.; Novoselov, K. S.; Booth, T. J.; Stauber, T.; Peres, N. M.; Geim, A. K. Fine Structure Constant Defines Visual Transparency of Graphene. *Science* **2008**, *320*, 1308−1308.

(5) Lee, C.; Wei, X.; Kysar, J. W.; Hone, J. Measurement of the Elastic Properties and Intrinsic Strength of Monolayer Graphene. *Science* **2008**, *321*, 385−388.

(6) Kim, K. S.; Zhao, Y.; Jang, H.; Lee, S. Y.; Kim, J. M.; Kim, K. S.; Ahn, J. H.; Kim, P.; Choi, J. Y.; Hong, B. H. Large-Scale Pattern Growth of Graphene Films for Stretchable Transparent Electrodes. *Nature* **2009**, *457*, 706−710.

(7) Lee, Y.; Bae, S.; Jang, H.; Jang, S.; Zhu, S. E.; Sim, S. H.; Song, Y. I.; Hong, B. H.; Ahn, J. H. Wafer-Scale Synthesis and Transfer of Graphene Films. *Nano Lett.* **2010**, *10*, 490−493.

(8) Wang, G.; Yang, J.; Park, J.; Gou, X.; Wang, B.; Liu, H.; Yao, J. Facile Synthesis and Characterization of Graphene Nanosheets. *J. Phys. Chem. C* **2008**, *112*, 8192−8195.

(9) Zhu, C.; Guo, S.; Fang, Y.; Dong, S. Reducing Sugar: New Functional Molecules for the Green Synthesis of Graphene Nanosheets. *ACS Nano* **2010**, *4*, 2429−2437.

(10) Fan, Z. J.; Kai, W.; Yan, J.; Wei, T.; Zhi, L.-J.; Feng, J.; Ren, Y.-M.; Song, L.-P.; Wei, F. Facile Synthesis of Graphene Nanosheets Via Fe Reduction of Exfoliated Graphite Oxide. *ACS Nano* **2011**, *5*, 191−198.

(11) Chen, H.; Müller, M. B.; Gilmore, K. J.; Wallace, G. G.; Li, D. Mechanically Strong, Electrically Conductive, and Biocompatible Graphene Paper. *Adv. Mater.* **2008**, *20*, 3557−3561.

(12) Li, X.; Wang, X.; Zhang, L.; Lee, S.; Dai, H. Chemically Derived, Ultrasmooth Graphene Nanoribbon Semiconductors. *Science* **2008**, *319*, 1229−1232.

(13) Jiao, L.; Zhang, L.; Wang, X.; Diankov, G.; Dai, H. Narrow Graphene Nanoribbons from Carbon Nanotubes. *Nature* **2009**, *458*, 877−880.

(14) Huang, X.; Qian, K.; Yang, J.; Zhang, J.; Li, L.; Yu, C.; Zhao, D. Functional Nanoporous Graphene Foams with Controlled Pore Sizes. *Adv. Mater.* **2012**, *24*, 4419−4423.

(15) Chen, Z.; Xu, C.; Ma, C.; Ren, W.; Cheng, H.-M. Lightweight and Flexible Graphene Foam Composites for High-Performance Electromagnetic Interference Shielding. *Adv. Mater.* **2013**, *25*, 1296−1300.

(16) Le, L. T.; Ervin, M. H.; Qiu, H.; Fuchs, B. E.; Lee, W. Y. Graphene Supercapacitor Electrodes Fabricated by Inkjet Printing and Thermal Reduction of Graphene Oxide. *Electrochem. Commun.* **2011**, *13*, 355−358.

(17) Yoo, J. J.; Balakrishnan, K.; Huang, J.; Meunier, V.; Sumpter, B. G.; Srivastava, A.; Conway, M.; Reddy, A. L. M; Yu, J.; Vajtai, R.; Ajayan, P. M. Ultrathin Planar Graphene Supercapacitors. *Nano Lett.* **2011**, *11*, 1423−1427.

(18) Huang, Y.; Liang, J.; Chen, Y. An Overview of the Applications of Graphene-Based Materials in Supercapacitors. *Small* **2012**, *8*, 1805−1834.

(19) Pumera, M. Graphene-Based Nanomaterials for Energy Storage. *Energy Environ. Sci.* **2011**, *4*, 668−674.

(20) Raccichini, R.; Varzi, A.; Passerini, S.; Scrosati, B. The Role of Graphene for Electrochemical Energy Storage. *Nat. Mater.* **2015**, *14*, 271−279.

(21) Singh, E.; Nalwa, H. S. Graphene-Based Dye-Sensitized Solar Cells: A Review. *Sci. Adv. Mater.* **2015**, *7*, 1863−1912.

(22) Singh, E.; Nalwa, H. S. Graphene-Based Bulk-Heterojunction Solar Cells: A Review. *J. Nanosci. Nanotechnol.* **2015**, *15*, 6237−6278.

(23) Singh, E.; Nalwa, H. S. Stability of Graphene-Based Heterojunction Solar Cells. *RSC Adv.* **2015**, *5*, 73575−73600.

(24) Hernaez, M.; Zamarreño, C.; Melendi-Espina, S.; Bird, L.; Mayes, A.; Arregui, F. Optical Fibre Sensors Using Graphene-Based Materials: A Review. *Sensors* **2017**, *17*, 155.

(25) Fowler, J. D.; Allen, M. J.; Tung, V. C.; Yang, Y.; Kaner, R. B.; Weiller, B. H. Practical Chemical Sensors from Chemically Derived Graphene. *ACS Nano* **2009**, *3*, 301−306.

(26) Liu, Y.; Dong, X.; Chen, P. Biological and Chemical Sensors Based on Graphene Materials. *Chem. Soc. Rev.* **2012**, *41*, 2283−2307.

(27) Hill, E. W.; Vijayaragahvan, A.; Novoselov, K. Graphene Sensors. *IEEE Sens. J.* **2011**, *11*, 3161−3170.

(28) Han, T.-H.; Lee, Y.; Choi, M.-R.; Woo, S.-H.; Bae, S.-H.; Hong, B. H.; Ahn, J.-H.; Lee, T.-W. Extremely Efficient Flexible Organic Light-Emitting Diodes with Modified Graphene Anode. *Nat. Photonics* **2012**, *6*, 105−110.

(29) Li, N.; Oida, S.; Tulevski, G. S.; Han, S.-J.; Hannon, J. B.; Sadana, D. K.; Chen, T.-C. Efficient and Bright Organic Light-Emitting Diodes on Single-Layer Graphene Electrodes. *Nat. Commun.* **2013**, *4*, 2294.

(30) Song, S. H.; Jang, M.-H.; Chung, J.; Jin, S. H.; Kim, B. H.; Hur, S.-H.; Yoo, S.; Cho, Y.-H.; Jeon, S. Highly Efficient Light-Emitting Diode of Graphene Quantum Dots Fabricated from Graphite Intercalation Compounds. *Adv. Opt. Mater.* **2014**, *2*, 1016−1023.

(31) Huang, B.; Li, Z.; Liu, Z.; Zhou, G.; Hao, S.; Wu, J.; Gu, B.-L.; Duan, W. Adsorption of Gas Molecules on Graphene Nanoribbons and

DOI: 10.1021/acsami.7b07063
ACS Appl. Mater. Interfaces 2017, 9, 34544−34586

Its Implication for Nanoscale Molecule Sensor. *J. Phys. Chem. C* **2008**, *112*, 13442−13446.
(32) Wang, J.; Liang, M.; Fang, Y.; Qiu, T.; Zhang, J.; Zhi, L. Rod-Coating: Towards Large-Area Fabrication of Uniform Reduced Graphene Oxide Films for Flexible Touch Screens. *Adv. Mater.* **2012**, *24*, 2874−2878.
(33) Lee, X.; Yang, T.; Li, X.; Zhang, R.; Zhu, M.; Zhang, H.; Xie, D.; Wei, J.; Zhong, M.; Wang, K.; Wu, D.; Li, Z.; Zhu, H. Flexible Graphene Woven Fabrics for Touch Sensing. *Appl. Phys. Lett.* **2013**, *102*, 163117.
(34) Malesevic, A.; Kemps, R.; Vanhulsel, A.; Chowdhury, M. P.; Volodin, A.; Van Haesendonck, C. Field Emission from Vertically Aligned Few-Layer Graphene. *J. Appl. Phys.* **2008**, *104*, 084301.
(35) Wu, Z.-S.; Pei, S.; Ren, W.; Tang, D.; Gao, L.; Liu, B.; Li, F.; Liu, C.; Cheng, H.-M. Field Emission of Single-Layer Graphene Films Prepared by Electrophoretic Deposition. *Adv. Mater.* **2009**, *21*, 1756−1760.
(36) Kuzhir, P.; Volynets, N.; Maksimenko, S.; Kaplas, T.; Svirko, Y. Multilayered Graphene in Ka-Band: Nanoscale Coating for Aerospace Applications. *J. Nanosci. Nanotechnol.* **2013**, *13*, 5864−5867.
(37) Siochi, E. J. Graphene in the Sky and Beyond. *Nat. Nanotechnol.* **2014**, *9*, 745−747.
(38) Shen, H.; Zhang, L.; Liu, M.; Zhang, Z. Biomedical Applications of Graphene. *Theranostics* **2012**, *2*, 283−294.
(39) Cheng, C.; Li, S.; Thomas, A.; Kotov, N. A.; Haag, R. Functional Graphene Nanomaterials Based Architectures: Biointeractions, Fabrications, and Emerging Biological Applications. *Chem. Rev.* **2017**, *117*, 1826−1914.
(40) Muñoz, R.; Gómez-Aleixandre, C. Review of CVD Synthesis of Graphene. *Chem. Vap. Deposition* **2013**, *19*, 297−322.
(41) Yan, K.; Fu, L.; Peng, H.; Liu, Z. Designed CVD Growth of Graphene Via Process Engineering. *Acc. Chem. Res.* **2013**, *46*, 2263−2274.
(42) Lotya, M.; Hernandez, Y.; King, P. J.; Smith, R. J.; Nicolosi, V.; Karlsson, L. S.; Blighe, F. M.; De, S.; Wang, Z.; McGovern, I. T.; Duesberg, G. S.; Coleman, J. N. Liquid Phase Production of Graphene by Exfoliation of Graphite in Surfactant/Water Solutions. *J. Am. Chem. Soc.* **2009**, *131*, 3611−3620.
(43) Ebert, L. B. Intercalation Compounds of Graphite. *Annu. Rev. Mater. Sci.* **1976**, *6*, 181−211.
(44) Dresselhaus, M. S.; Dresselhaus, G. Intercalation Compounds of Graphite. *Adv. Phys.* **2002**, *51*, 1−186.
(45) Bourlinos, A. B.; Safarova, K.; Siskova, K.; Zbořil, R. The Production of Chemically Converted Graphenes from Graphite Fluoride. *Carbon* **2012**, *50*, 1425−1428.
(46) Watanabe, N.; Nakajima, T.; Touhara, H. *Graphite Fluorides*. Elsevier Science: Amsterdam, The Netherlands, 2013.
(47) Zhang, L.; Liang, J.; Huang, Y.; Ma, Y.; Wang, Y.; Chen, Y. Size-Controlled Synthesis of Graphene Oxide Sheets on a Large Scale Using Chemical Exfoliation. *Carbon* **2009**, *47*, 3365−3368.
(48) Parvez, K.; Wu, Z.-S.; Li, R.; Liu, X.; Graf, R.; Feng, X.; Müllen, K. Exfoliation of Graphite into Graphene in Aqueous Solutions of Inorganic Salts. *J. Am. Chem. Soc.* **2014**, *136*, 6083−6091.
(49) Son, D. I.; Kwon, B. W.; Kim, H.-H.; Park, D. H.; Angadi, B.; Choi, W. K. Chemical Exfoliation of Pure Graphene Sheets from Synthesized ZnO−Graphene Quasi Core−Shell Quantum Dots. *Carbon* **2013**, *59*, 289−295.
(50) Gao, L.; Guest, J. R.; Guisinger, N. P. Epitaxial Graphene on Cu (111). *Nano Lett.* **2010**, *10*, 3512−3516.
(51) Riedl, C.; Coletti, C.; Starke, U. Structural and Electronic Properties of Epitaxial Graphene on SiC(0001): A Review of Growth, Characterization, Transfer Doping and Hydrogen Intercalation. *J. Phys. D: Appl. Phys.* **2010**, *43*, 374009.
(52) Kim, K. S.; Ji, Y. J.; Nam, Y.; Kim, K. H.; Singh, E.; Lee, J. Y.; Yeom, G. Y. Atomic Layer Etching of Graphene through Controlled Ion Beam for Graphene-Based Electronics. *Sci. Rep.* **2017**, *7*, 2462.
(53) Zhu, Y.; Murali, S.; Cai, W.; Li, X.; Suk, J. W.; Potts, J. R.; Ruoff, R. S. Graphene and Graphene Oxide: Synthesis, Properties, and Applications. *Adv. Mater.* **2010**, *22*, 3906−3924.
(54) Fang, W.; Hsu, A. L.; Song, Y.; Kong, J. A Review of Large-Area Bilayer Graphene Synthesis by Chemical Vapor Deposition. *Nanoscale* **2015**, *7*, 20335−20351.
(55) Lee, H. C.; Liu, W.-W.; Chai, S.-P.; Mohamed, A. R.; Aziz, A.; Khe, C.-S.; Hidayah, N. M. S.; Hashim, U. Review of the Synthesis, Transfer, Characterization and Growth Mechanisms of Single and Multilayer Graphene. *RSC Adv.* **2017**, *7*, 15644−15693.
(56) Guo, S.; Dong, S. Graphene Nanosheet: Synthesis, Molecular Engineering, Thin Film, Hybrids, and Energy and Analytical Applications. *Chem. Soc. Rev.* **2011**, *40*, 2644−2672.
(57) Oger, N.; Lin, Y. F.; Labrugère, C.; Le Grognec, E.; Rataboul, F.; Felpin, F.-X. Practical and Scalable Synthesis of Sulfonated Graphene. *Carbon* **2016**, *96*, 342−350.
(58) Quan, Q.; Lin, X.; Zhang, N.; Xu, Y.-J. Graphene and Its Derivatives as Versatile Templates for Materials Synthesis and Functional Applications. *Nanoscale* **2017**, *9*, 2398−2416.
(59) Suk, J. W.; Kitt, A.; Magnuson, C. W.; Hao, Y.; Ahmed, S.; An, J.; Swan, A. K.; Goldberg, B. B.; Ruoff, R. S. Transfer of CVD-Grown Monolayer Graphene onto Arbitrary Substrates. *ACS Nano* **2011**, *5*, 6916−6924.
(60) Reina, A.; Jia, X.; Ho, J.; Nezich, D.; Son, H.; Bulovic, V.; Dresselhaus, M. S.; Kong, J. Large Area, Few-Layer Graphene Films on Arbitrary Substrates by Chemical Vapor Deposition. *Nano Lett.* **2009**, *9*, 30−35.
(61) Verma, V. P.; Das, S.; Lahiri, I.; Choi, W. Large-Area Graphene on Polymer Film for Flexible and Transparent Anode in Field Emission Device. *Appl. Phys. Lett.* **2010**, *96*, 203108.
(62) Chandrashekar, B. N.; Deng, B.; Smitha, A. S.; Chen, Y.; Tan, C.; Zhang, H.; Peng, H.; Liu, Z. Roll-to-Roll Green Transfer of CVD Graphene onto Plastic for a Transparent and Flexible Triboelectric Nanogenerator. *Adv. Mater.* **2015**, *27*, 5210−5216.
(63) Bae, S.; Kim, H.; Lee, Y.; Xu, X.; Park, J.-S.; Zheng, Y.; Balakrishnan, J.; Lei, T.; Ri Kim, H.; Song, Y. I.; Kim, Y.-J.; Kim, K. S.; Özyilmaz, B.; Ahn, J.-H.; Hong, B. H.; Iijima, S. Roll-to-Roll Production of 30-Inch Graphene Films for Transparent Electrodes. *Nat. Nanotechnol.* **2010**, *5*, 574−578.
(64) Kobayashi, T.; Bando, M.; Kimura, N.; Shimizu, K.; Kadono, K.; Umezu, N.; Miyahara, K.; Hayazaki, S.; Nagai, S.; Mizuguchi, Y.; Murakami, Y.; Hobara, D. Production of a 100-M-Long High-Quality Graphene Transparent Conductive Film by Roll-to-Roll Chemical Vapor Deposition and Transfer Process. *Appl. Phys. Lett.* **2013**, *102*, 023112.
(65) Vallés, C.; Núñez, J. D.; Benito, A. M.; Maser, W. K. Flexible Conductive Graphene Paper Obtained by Direct and Gentle Annealing of Graphene Oxide Paper. *Carbon* **2012**, *50*, 835−844.
(66) Chen, J.; Bi, H.; Sun, S.; Tang, Y.; Zhao, W.; Lin, T.; Wan, D.; Huang, F.; Zhou, X.; Xie, X.; Jiang, M. Highly Conductive and Flexible Paper of 1D Silver-Nanowire-Doped Graphene. *ACS Appl. Mater. Interfaces* **2013**, *5*, 1408−1413.
(67) Xin, G.; Sun, H.; Hu, T.; Fard, H. R.; Sun, X.; Koratkar, N.; Borca-Tasciuc, T.; Lian, J. Large-Area Freestanding Graphene Paper for Superior Thermal Management. *Adv. Mater.* **2014**, *26*, 4521−4526.
(68) Paliotta, L.; De Bellis, G.; Tamburrano, A.; Marra, F.; Rinaldi, A.; Balijepalli, S. K.; Kaciulis, S.; Sarto, M. S. Highly Conductive Multilayer-Graphene Paper as a Flexible Lightweight Electromagnetic Shield. *Carbon* **2015**, *89*, 260−271.
(69) Ye, X.; Zhou, Q.; Jia, C.; Tang, Z.; Zhu, Y.; Wan, Z. Producing Large-Area, Foldable Graphene Paper from Graphite Oxide Suspensions by in-Situ Chemical Reduction Process. *Carbon* **2017**, *114*, 424−434.
(70) Yang, G.; Kim, H.-Y.; Jang, S.; Kim, J. Transfer-Free Growth of Multilayer Graphene Using Self-Assembled Monolayers. *ACS Appl. Mater. Interfaces* **2016**, *8*, 27115−27121.
(71) Martins, L. G. P.; Song, Y.; Zeng, T.; Dresselhaus, M. S.; Kong, J.; Araujo, P. T. Direct Transfer of Graphene onto Flexible Substrates. *Proc. Natl. Acad. Sci. U. S. A.* **2013**, *110*, 17762−17767.
(72) Gabriel, D.; Sempere, B.; Colominas, C.; Ferrer-Anglada, N. THz-Conductivity of CVD Graphene on Different Substrates. *Phys. Status Solidi B* **2015**, *252*, 2423−2428.

DOI: 10.1021/acsami.7b07063
ACS Appl. Mater. Interfaces 2017, 9, 34544−34586

(73) Lerf, A.; He, H.; Forster, M.; Klinowski, J. Structure of Graphite Oxide Revisited. *J. Phys. Chem. B* **1998**, *102*, 4477−4482.
(74) Gao, W.; Alemany, L. B.; Ci, L.; Ajayan, P. M. New Insights into the Structure and Reduction of Graphite Oxide. *Nat. Chem.* **2009**, *1*, 403−408.
(75) Yang, C.-W.; Park, J.-W. The Cohesive Crack and Buckle Delamination Resistances of Indium Tin Oxide (ITO) Films on Polymeric Substrates with Ductile Metal Interlayers. *Surf. Coat. Technol.* **2010**, *204*, 2761−2766.
(76) Seo, Y. K.; Joo, C. W.; Lee, J.; Han, J. W.; Lee, D. J.; Entifar, S. A. N.; Kim, S.; Cho, N. S.; Kim, Y. H. Enhanced Electrical Properties of PEDOT:PSS Films Using Solvent Treatment and Its Application to ITO-Free Organic Light-Emitting Diodes. *J. Lumin.* **2017**, *187*, 221−226.
(77) Seo, K.-W.; Noh, Y.-J.; Na, S.-I.; Kim, H.-K. Random Mesh-Like Ag Networks Prepared Via Self-Assembled Ag Nanoparticles for ITO-Free Flexible Organic Solar Cells. *Sol. Energy Mater. Sol. Cells* **2016**, *155*, 51−59.
(78) Califórnia, A.; Silva, A. S.; Gonçalves, J.; Branco, A.; Pinheiro, C.; Costa, C. Silver Grid Electrodes for Faster Switching ITO Free Electrochromic Devices. *Sol. Energy Mater. Sol. Cells* **2016**, *153*, 61−67.
(79) Kumar, G.; Li, Y.-D.; Biring, S.; Lin, Y.-N.; Liu, S.-W.; Chang, C.-H. Highly Efficient ITO-Free Organic Light-Emitting Diodes Employing a Roughened Ultra-Thin Silver Electrode. *Org. Electron.* **2017**, *42*, 52−58.
(80) Eising, M.; Cava, C. E.; Salvatierra, R. V.; Zarbin, A. J. G.; Roman, L. S. Doping Effect on Self-Assembled Films of Polyaniline and Carbon Nanotube Applied as Ammonia Gas Sensor. *Sens. Actuators, B* **2017**, *245*, 25−33.
(81) Choi, W.; Choudhary, N.; Han, G. H.; Park, J.; Akinwande, D.; Lee, Y. H. Recent Development of Two-Dimensional Transition Metal Dichalcogenides and Their Applications. *Mater. Today* **2017**, *20*, 116−130.
(82) Singh, E.; Kim, K. S.; Yeom, G. Y.; Nalwa, H. S. Atomically Thin-Layered Molybdenum Disulfide (MoS_2) for Bulk-Heterojunction Solar Cells. *ACS Appl. Mater. Interfaces* **2017**, *9*, 3223−3245.
(83) Kim, K. S.; Kim, K. H.; Nam, Y.; Jeon, J.; Yim, S.; Singh, E.; Lee, J. Y.; Lee, S. J.; Jung, Y. S.; Yeom, G. Y.; Kim, D. W. Atomic Layer Etching Mechanism of MoS_2 for Nanodevices. *ACS Appl. Mater. Interfaces* **2017**, *9*, 11967−11976.
(84) Singh, E.; Kim, K. S.; Yeom, G. Y.; Nalwa, H. S. Two-Dimensional Transition Metal Dichalcogenide-Based Counter Electrodes for Dye-Sensitized Solar Cells. *RSC Adv.* **2017**, *7*, 28234−28290.
(85) Jeong, H. Y.; Kim, J. Y.; Kim, J. W.; Hwang, J. O.; Kim, J.-E.; Lee, J. Y.; Yoon, T. H.; Cho, B. J.; Kim, S. O.; Ruoff, R. S.; Choi, S.-Y. Graphene Oxide Thin Films for Flexible Nonvolatile Memory Applications. *Nano Lett.* **2010**, *10*, 4381−4386.
(86) Kim, S. M.; Song, E. B.; Lee, S.; Zhu, J.; Seo, D. H.; Mecklenburg, M.; Seo, S.; Wang, K. L. Transparent and Flexible Graphene Charge-Trap Memory. *ACS Nano* **2012**, *6*, 7879−7884.
(87) Petrone, N.; Meric, I.; Chari, T.; Shepard, K. L.; Hone, J. Graphene Field-Effect Transistors for Radio-Frequency Flexible Electronics. *IEEE J. Electron Devices Soc.* **2015**, *3*, 44−48.
(88) Lee, J.; Ha, T.-J.; Li, H.; Parrish, K. N.; Holt, M.; Dodabalapur, A.; Ruoff, R. S.; Akinwande, D. 25 GHz Embedded-Gate Graphene Transistors with High-k Dielectrics on Extremely Flexible Plastic Sheets. *ACS Nano* **2013**, *7*, 7744−7750.
(89) Fisichella, G.; Lo Verso, S.; Di Marco, S.; Vinciguerra, V.; Schilirò, E.; Di Franco, S.; Lo Nigro, R.; Roccaforte, F.; Zurutuza, A.; Centeno, A.; Ravesi, S.; Giannazzo, F. Advances in the Fabrication of Graphene Transistors on Flexible Substrates. *Beilstein J. Nanotechnol.* **2017**, *8*, 467−474.
(90) Lee, C.-H.; Kim, Y.-J.; Hong, Y. J.; Jeon, S.-R.; Bae, S.; Hong, B. H.; Yi, G.-C. Flexible Inorganic Nanostructure Light-Emitting Diodes Fabricated on Graphene Films. *Adv. Mater.* **2011**, *23*, 4614−4619.
(91) Wu, J.; Agrawal, M.; Becerril, H. c. A.; Bao, Z.; Liu, Z.; Chen, Y.; Peumans, P. Organic Light-Emitting Diodes on Solution-Processed Graphene Transparent Electrodes. *ACS Nano* **2010**, *4*, 43−48.
(92) Zhang, Z.; Du, J.; Zhang, D.; Sun, H.; Yin, L.; Ma, L.; Chen, J.; Ma, D.; Cheng, H.-M.; Ren, W. Rosin-Enabled Ultraclean and Damage-Free Transfer of Graphene for Large-Area Flexible Organic Light-Emitting Diodes. *Nat. Commun.* **2017**, *8*, 14560.
(93) Xu, Y.; Yu, H.; Wang, C.; Cao, J.; Chen, Y.; Ma, Z.; You, Y.; Wan, J.; Fang, X.; Chen, X. Multilayer Graphene with Chemical Modification as Transparent Conducting Electrodes in Organic Light-Emitting Diode. *Nanoscale Res. Lett.* **2017**, *12*, 254.
(94) Qiu, T.; Luo, B.; Liang, M.; Ning, J.; Wang, B.; Li, X.; Zhi, L. Hydrogen Reduced Graphene Oxide/Metal Grid Hybrid Film: Towards High Performance Transparent Conductive Electrode for Flexible Electrochromic Devices. *Carbon* **2015**, *81*, 232−238.
(95) Ahn, J.-H.; Hong, B. H. Graphene for Displays That Bend. *Nat. Nanotechnol.* **2014**, *9*, 737−738.
(96) Sun, G.; An, J.; Chua, C. K.; Pang, H.; Zhang, J.; Chen, P. Layer-by-Layer Printing of Laminated Graphene-Based Interdigitated Microelectrodes for Flexible Planar Micro-Supercapacitors. *Electrochem. Commun.* **2015**, *51*, 33−36.
(97) Ramadoss, A.; Yoon, K.-Y.; Kwak, M.-J.; Kim, S.-I.; Ryu, S.-T.; Jang, J.-H. Fully Flexible, Lightweight, High Performance All-Solid-State Supercapacitor Based on 3-Dimensional-Graphene/Graphite-Paper. *J. Power Sources* **2017**, *337*, 159−165.
(98) Liu, L.; Niu, Z.; Zhang, L.; Zhou, W.; Chen, X.; Xie, S. Nanostructured Graphene Composite Papers for Highly Flexible and Foldable Supercapacitors. *Adv. Mater.* **2014**, *26*, 4855−4862.
(99) Li, N.; Lv, T.; Yao, Y.; Li, H.; Liu, K.; Chen, T. Compact Graphene/MoS_2composite Films for Highly Flexible and Stretchable All-Solid-State Supercapacitors. *J. Mater. Chem. A* **2017**, *5*, 3267−3273.
(100) Yin, Z.; Sun, S.; Salim, T.; Wu, S.; Huang, X.; He, Q.; Lam, Y. M.; Zhang, H. Organic Photovoltaic Devices Using Highly Flexible Reduced Graphene Oxide Films as Transparent Electrodes. *ACS Nano* **2010**, *4*, 5263−5268.
(101) Konios, D.; Petridis, C.; Kakavelakis, G.; Sygletou, M.; Savva, K.; Stratakis, E.; Kymakis, E. Reduced Graphene Oxide Micromesh Electrodes for Large Area, Flexible, Organic Photovoltaic Devices. *Adv. Funct. Mater.* **2015**, *25*, 2213−2221.
(102) Yoon, J.; Sung, H.; Lee, G.; Cho, W.; Ahn, N.; Jung, H. S.; Choi, M. Superflexible, High-Efficiency Perovskite Solar Cells Utilizing Graphene Electrodes: Towards Future Foldable Power Sources. *Energy Environ. Sci.* **2017**, *10*, 337−345.
(103) Baker, J. A.; Worsley, C.; Lee, H. K. H.; Clark, R. N.; Tsoi, W. C.; Williams, G.; Worsley, D. A.; Gethin, D. T.; Watson, T. M. Development of Graphene Nano-Platelet Ink for High Voltage Flexible Dye Sensitized Solar Cells with Cobalt Complex Electrolytes. *Adv. Eng. Mater.* **2017**, *19*, 1600652.
(104) Yang, J.; Ran, Q.; Wei, D.; Sun, T.; Yu, L.; Song, X.; Pu, L.; Shi, H.; Du, C. Three-Dimensional Conformal Graphene Microstructure for Flexible and Highly Sensitive Electronic Skin. *Nanotechnology* **2017**, *28*, 115501.
(105) Alonso, E. T.; Karkera, G.; Jones, G. F.; Craciun, M. F.; Russo, S. Homogeneously Bright, Flexible, and Foldable Lighting Devices with Functionalized Graphene Electrodes. *ACS Appl. Mater. Interfaces* **2016**, *8*, 16541−16545.
(106) Ryu, J.; Kim, Y.; Won, D.; Kim, N.; Park, J. S.; Lee, E.-K.; Cho, D.; Cho, S.-P.; Kim, S. J.; Ryu, G. H.; Shin, H.-A. S.; Lee, Z.; Hong, B. H.; Cho, S. Fast Synthesis of High-Performance Graphene Films by Hydrogen-Free Rapid Thermal Chemical Vapor Deposition. *ACS Nano* **2014**, *8*, 950−956.
(107) Liang, J.; Li, L.; Tong, K.; Ren, Z.; Hu, W.; Niu, X.; Chen, Y.; Pei, Q. Silver Nanowire Percolation Network Soldered with Graphene Oxide at Room Temperature and Its Application for Fully Stretchable Polymer Light-Emitting Diodes. *ACS Nano* **2014**, *8*, 1590−1600.
(108) Huang, L.; Huang, Y.; Liang, J.; Wan, X.; Chen, Y. Graphene-Based Conducting Inks for Direct Inkjet Printing of Flexible Conductive Patterns and Their Applications in Electric Circuits and Chemical Sensors. *Nano Res.* **2011**, *4*, 675−684.
(109) Li, W.; Li, F.; Li, H.; Su, M.; Gao, M.; Li, Y.; Su, D.; Zhang, X.; Song, Y. Flexible Circuits and Soft Actuators by Printing Assembly of Graphene. *ACS Appl. Mater. Interfaces* **2016**, *8*, 12369−12376.

DOI: 10.1021/acsami.7b07063
ACS Appl. Mater. Interfaces 2017, 9, 34544−34586

(110) Yang, J.; Wei, D.; Tang, L.; Song, X.; Luo, W.; Chu, J.; Gao, T.; Shi, H.; Du, C. Wearable Temperature Sensor Based on Graphene Nanowalls. *RSC Adv.* **2015**, *5*, 25609−25615.
(111) Cheng, Y.; Wang, R.; Sun, J.; Gao, L. A Stretchable and Highly Sensitive Graphene-Based Fiber for Sensing Tensile Strain, Bending, and Torsion. *Adv. Mater.* **2015**, *27*, 7365−7371.
(112) Singh, E.; Meyyappan, M.; Nalwa, H. S. In *Nanomaterials based Flexible and Multifunctional Sensors*; Singh, E., Nalwa, H. S., Eds.; American Scientific Publishers: Los Angeles, 2018; pp 1−50.
(113) Ren, J.; Wang, C.; Zhang, X.; Carey, T.; Chen, K.; Yin, Y.; Torrisi, F. Environmentally-Friendly Conductive Cotton Fabric as Flexible Strain Sensor Based on Hot Press Reduced Graphene Oxide. *Carbon* **2017**, *111*, 622−630.
(114) Liu, Y.; Tao, L.-Q.; Wang, D.-Y.; Zhang, T.-Y.; Yang, Y.; Ren, T.-L. Flexible, Highly Sensitive Pressure Sensor with a Wide Range Based on Graphene-Silk Network Structure. *Appl. Phys. Lett.* **2017**, *110*, 123508.
(115) Yasaei, P.; Kumar, B.; Hantehzadeh, R.; Kayyalha, M.; Baskin, A.; Repnin, N.; Wang, C.; Klie, R. F.; Chen, Y. P.; Král, P.; Salehi-Khojin, A. Chemical Sensing with Switchable Transport Channels in Graphene Grain Boundaries. *Nat. Commun.* **2014**, *5*, 4911.
(116) Kim, M.; Kang, P.; Leem, J.; Nam, S. Stretchable Crumpled Graphene Photodetector with Plasmonically-Enhanced Photoresponsivity. *Nanoscale* **2017**, *9*, 4058−4065.
(117) Wang, Z.; Shaygan, M.; Otto, M.; Schall, D.; Neumaier, D. Flexible Hall Sensors Based on Graphene. *Nanoscale* **2016**, *8*, 7683−7687.
(118) Tao, L.-Q.; Tian, H.; Liu, Y.; Ju, Z.-Y.; Pang, Y.; Chen, Y.-Q.; Wang, D.-Y.; Tian, X.-G.; Yan, J.-C.; Deng, N.-Q.; Yang, Y.; Ren, T.-L. An Intelligent Artificial Throat with Sound-Sensing Ability Based on Laser Induced Graphene. *Nat. Commun.* **2017**, *8*, 14579.
(119) Fan, Z.; Liu, B.; Liu, X.; Li, Z.; Wang, H.; Yang, S.; Wang, J. A Flexible and Disposable Hybrid Electrode Based on Cu Nanowires Modified Graphene Transparent Electrode for Non-Enzymatic Glucose Sensor. *Electrochim. Acta* **2013**, *109*, 602−608.
(120) Singhal, A. V.; Charaya, H.; Lahiri, I. Noble Metal Decorated Graphene-Based Gas Sensors and Their Fabrication: A Review. *Crit. Rev. Solid State Mater. Sci.* **2017**, 1−28.
(121) Wang, T.; Huang, D.; Yang, Z.; Xu, S.; He, G.; Li, X.; Hu, N.; Yin, G.; He, D.; Zhang, L. A Review on Graphene-Based Gas/Vapor Sensors with Unique Properties and Potential Applications. *Nano-Micro Lett.* **2016**, *8*, 95−119.
(122) Some, S.; Xu, Y.; Kim, Y.; Yoon, Y.; Qin, H.; Kulkarni, A.; Kim, T.; Lee, H. Highly Sensitive and Selective Gas Sensor Using Hydrophilic and Hydrophobic Graphenes. *Sci. Rep.* **2013**, *3*, 1868.
(123) Rumyantsev, S.; Liu, G.; Shur, M. S.; Potyrailo, R. A.; Balandin, A. A. Selective Gas Sensing with a Single Pristine Graphene Transistor. *Nano Lett.* **2012**, *12*, 2294−2298.
(124) Toda, K.; Furue, R.; Hayami, S. Recent Progress in Applications of Graphene Oxide for Gas Sensing: A Review. *Anal. Chim. Acta* **2015**, *878*, 43−53.
(125) Meng, F.-L.; Guo, Z.; Huang, X.-J. Graphene-Based Hybrids for Chemiresistive Gas Sensors. *TrAC, Trends Anal. Chem.* **2015**, *68*, 37−47.
(126) Varghese, S. S.; Lonkar, S.; Singh, K. K.; Swaminathan, S.; Abdala, A. Recent Advances in Graphene Based Gas Sensors. *Sens. Actuators, B* **2015**, *218*, 160−183.
(127) Schedin, F.; Geim, A. K.; Morozov, S. V.; Hill, E. W.; Blake, P.; Katsnelson, M. I.; Novoselov, K. S. Detection of Individual Gas Molecules Adsorbed on Graphene. *Nat. Mater.* **2007**, *6*, 652−655.
(128) Shen, J.; Zhu, Y.; Yang, X.; Li, C. Graphene Quantum Dots: Emergent Nanolights for Bioimaging, Sensors, Catalysis and Photovoltaic Devices. *Chem. Commun.* **2012**, *48*, 3686−3699.
(129) Ko, G.; Kim, H. Y.; Ahn, J.; Park, Y. M.; Lee, K. Y.; Kim, J. Graphene-Based Nitrogen Dioxide Gas Sensors. *Current Appl. Phys.* **2010**, *10*, 1002−1004.
(130) Basu, S.; Bhattacharyya, P. Recent Developments on Graphene and Graphene Oxide Based Solid State Gas Sensors. *Sens. Actuators, B* **2012**, *173*, 1−21.
(131) Aziza, Z. B.; Zhang, Q.; Baillargeat, D. Graphene/Mica Based Ammonia Gas Sensors. *Appl. Phys. Lett.* **2014**, *105*, 254102.
(132) Jung, M. W.; Myung, S.; Song, W.; Kang, M.-A.; Kim, S. H.; Yang, C.-S.; Lee, S. S.; Lim, J.; Park, C.-Y.; Lee, J.-O.; An, K.-S. Novel Fabrication of Flexible Graphene-Based Chemical Sensors with Heaters Using Soft Lithographic Patterning Method. *ACS Appl. Mater. Interfaces* **2014**, *6*, 13319−13323.
(133) Cooper, J. S.; Myers, M.; Chow, E.; Hubble, L. J.; Cairney, J. M.; Pejcic, B.; Müller, K.-H.; Wieczorek, L.; Raguse, B. Performance of Graphene, Carbon Nanotube, and Gold Nanoparticle Chemiresistor Sensors for the Detection of Petroleum Hydrocarbons in Water. *J. Nanopart. Res.* **2014**, *16*, 1−13.
(134) Han, T. H.; Huang, Y.-K.; Tan, A. T. L.; Dravid, V. P.; Huang, J. Steam Etched Porous Graphene Oxide Network for Chemical Sensing. *J. Am. Chem. Soc.* **2011**, *133*, 15264−15267.
(135) Lu, G.; Ocola, L. E.; Chen, J. Reduced Graphene Oxide for Room-Temperature Gas Sensors. *Nanotechnology* **2009**, *20*, 445502.
(136) Dan, Y.; Lu, Y.; Kybert, N. J.; Luo, Z.; Johnson, A. T. C. Intrinsic Response of Graphene Vapor Sensors. *Nano Lett.* **2009**, *9*, 1472−1475.
(137) Lu, Y.; Goldsmith, B. R.; Kybert, N. J.; Johnson, A. C. DNA-Decorated Graphene Chemical Sensors. *Appl. Phys. Lett.* **2010**, *97*, 083107.
(138) Ratinac, K. R.; Yang, W.; Ringer, S. P.; Braet, F. Toward Ubiquitous Environmental Gas Sensors: Capitalizing on the Promise of Graphene. *Environ. Sci. Technol.* **2010**, *44*, 1167−1176.
(139) Jiang, Z.; Wang, J.; Meng, L.; Huang, Y.; Liu, L. A Highly Efficient Chemical Sensor Material for Ethanol: Al_2O_3/Graphene Nanocomposites Fabricated from Graphene Oxide. *Chem. Commun.* **2011**, *47*, 6350−6352.
(140) Song, H.; Zhang, L.; He, C.; Qu, Y.; Tian, Y.; Lv, Y. Graphene Sheets Decorated with SnO_2 Nanoparticles: *In Situ* Synthesis and Highly Efficient Materials for Cataluminescence Gas Sensors. *J. Mater. Chem.* **2011**, *21*, 5972−5977.
(141) Lu, G.; Park, S.; Yu, K.; Ruoff, R. S.; Ocola, L. E.; Rosenmann, D.; Chen, J. Toward Practical Gas Sensing with Highly Reduced Graphene Oxide: A New Signal Processing Method to Circumvent Run-to-Run and Device-to-Device Variations. *ACS Nano* **2011**, *5*, 1154−1164.
(142) Lin, Q.; Li, Y.; Yang, M. Tin Oxide/Graphene Composite Fabricated Via a Hydrothermal Method for Gas Sensors Working at Room Temperature. *Sens. Actuators, B* **2012**, *173*, 139−147.
(143) Yuan, W.; Shi, G. Graphene-Based Gas Sensors. *J. Mater. Chem. A* **2013**, *1*, 10078−10091.
(144) Wu, Z.; Chen, X.; Zhu, S.; Zhou, Z.; Yao, Y.; Quan, W.; Liu, B. Enhanced Sensitivity of Ammonia Sensor Using Graphene/Polyaniline Nanocomposite. *Sens. Actuators, B* **2013**, *178*, 485−493.
(145) Choi, S.-W.; Kim, J.; Byun, Y. T. Highly Sensitive and Selective NO_2 Detection by Pt Nanoparticles-Decorated Single-Walled Carbon Nanotubes and the Underlying Sensing Mechanism. *Sens. Actuators, B* **2017**, *238*, 1032−1042.
(146) Lu, Y.; Meyyappan, M.; Li, J. Fabrication of Carbon-Nanotube-Based Sensor Array and Interference Study. *J. Mater. Res.* **2011**, *26*, 2017−2023.
(147) Li, J.; Lu, Y.; Ye, Q.; Cinke, M.; Han, J.; Meyyappan, M. Carbon Nanotube Sensors for Gas and Organic Vapor Detection. *Nano Lett.* **2003**, *3*, 929−933.
(148) Li, J.; Lu, Y.; Ye, Q.; Delzeit, L.; Meyyappan, M. A Gas Sensor Array Using Carbon Nanotubes and Microfabrication Technology. *Electrochem. Solid-State Lett.* **2005**, *8*, H100−H102.
(149) Lu, Y.; Partridge, C.; Meyyappan, M.; Li, J. A Carbon Nanotube Sensor Array for Sensitive Gas Discrimination Using Principal Component Analysis. *J. Electroanal. Chem.* **2006**, *593*, 105−110.
(150) Yang, W.; Gan, L.; Li, H.; Zhai, T. Two-Dimensional Layered Nanomaterials for Gas-Sensing Applications. *Inorg. Chem. Front.* **2016**, *3*, 433−451.
(151) Donarelli, M.; Prezioso, S.; Perrozzi, F.; Bisti, F.; Nardone, M.; Giancaterini, L.; Cantalini, C.; Ottaviano, L. Response to NO_2 and Other Gases of Resistive Chemically Exfoliated MoS_2-Based Gas Sensors. *Sens. Actuators, B* **2015**, *207*, 602−613.

DOI: 10.1021/acsami.7b07063
ACS Appl. Mater. Interfaces 2017, 9, 34544−34586

(152) Urasinska-Wojcik, B.; Vincent, T. A.; Chowdhury, M. F.; Gardner, J. W. Ultrasensitive WO_3 Gas Sensors for NO_2 Detection in Air and Low Oxygen Environment. *Sens. Actuators, B* **2017**, *239*, 1051−1059.
(153) Perrozzi, F.; Emamjomeh, S. M.; Paolucci, V.; Taglieri, G.; Ottaviano, L.; Cantalini, C. Thermal Stability of WS_2 Flakes and Gas Sensing Properties of WS_2/WO_3 Composite to H_2, NH_3 and NO_2. *Sens. Actuators, B* **2017**, *243*, 812−822.
(154) Khan, A. A.; Ahmad, R.; Zeeshan, M. Comparative Sensing of Aldehyde and Ammonia Vapours on Synthetic Polypyrrole-Sn(IV)-Arsenotungstate Nanocomposite Cation Exchange Material. *Anal. Chem. Res.* **2017**, *12*, 52−64.
(155) Ricciardella, F.; Massera, E.; Polichetti, T.; Miglietta, M. L.; Di Francia, G. A Calibrated Graphene-Based Chemi-Sensor for Sub Parts-Per-Million NO_2 Detection Operating at Room Temperature. *Appl. Phys. Lett.* **2014**, *104*, 183502.
(156) Deng, S.; Tjoa, V.; Fan, H. M.; Tan, H. R.; Sayle, D. C.; Olivo, M.; Mhaisalkar, S.; Wei, J.; Sow, C. H. Reduced Graphene Oxide Conjugated Cu_2O Nanowire Mesocrystals for High-Performance NO_2 gas Sensor. *J. Am. Chem. Soc.* **2012**, *134*, 4905−4917.
(157) Su, P.-G.; Shieh, H.-C. Flexible NO_2 Sensors Fabricated by Layer-by-Layer Covalent Anchoring and *in Situ* Reduction of Graphene Oxide. *Sens. Actuators, B* **2014**, *190*, 865−872.
(158) Yang, G.; Lee, C.; Kim, J.; Ren, F.; Pearton, S. J. Flexible Graphene-Based Chemical Sensors on Paper Substrates. *Phys. Chem. Chem. Phys.* **2013**, *15*, 1798−1801.
(159) Dua, V.; Surwade, S. P.; Ammu, S.; Agnihotra, S. R.; Jain, S.; Roberts, K. E.; Park, S.; Ruoff, R. S.; Manohar, S. K. All-Organic Vapor Sensor Using Inkjet-Printed Reduced Graphene Oxide. *Angew. Chem., Int. Ed.* **2010**, *49*, 2154−2157.
(160) Kim, Y. H.; Kim, S. J.; Kim, Y.-J.; Shim, Y.-S.; Kim, S. Y.; Hong, B. H.; Jang, H. W. Self-Activated Transparent All-Graphene Gas Sensor with Endurance to Humidity and Mechanical Bending. *ACS Nano* **2015**, *9*, 10453−10460.
(161) Strong, V.; Dubin, S.; El-Kady, M. F.; Lech, A.; Wang, Y.; Weiller, B. H.; Kaner, R. B. Patterning and Electronic Tuning of Laser Scribed Graphene for Flexible All-Carbon Devices. *ACS Nano* **2012**, *6*, 1395−1403.
(162) Jeong, H. Y.; Lee, D.-S.; Choi, H. K.; Lee, D. H.; Kim, J.-E.; Lee, J. Y.; Lee, W. J.; Kim, S. O.; Choi, S.-Y. Flexible Room-Temperature NO_2 Gas Sensors Based on Carbon Nanotubes/Reduced Graphene Hybrid Films. *Appl. Phys. Lett.* **2010**, *96*, 213105.
(163) Yun, Y. J.; Hong, W. G.; Choi, N. J.; Kim, B. H.; Jun, Y.; Lee, H. K. Ultrasensitive and Highly Selective Graphene-Based Single Yarn for Use in Wearable Gas Sensor. *Sci. Rep.* **2015**, *5*, 10904.
(164) Huang, L.; Wang, Z.; Zhang, J.; Pu, J.; Lin, Y.; Xu, S.; Shen, L.; Chen, Q.; Shi, W. Fully Printed, Rapid-Response Sensors Based on Chemically Modified Graphene for Detecting NO_2 at Room Temperature. *ACS Appl. Mater. Interfaces* **2014**, *6*, 7426−7433.
(165) Tung, T. T.; Castro, M.; Kim, T. Y.; Suh, K. S.; Feller, J.-F. High Stability Silver Nanoparticles−Graphene/Poly(ionic liquid)-Based Chemoresistive Sensors for Volatile Organic Compounds' Detection. *Anal. Bioanal. Chem.* **2014**, *406*, 3995−4004.
(166) Cho, B.; Yoon, J.; Hahm, M. G.; Kim, D.-H.; Kim, A. R.; Kahng, Y. H.; Park, S.-W.; Lee, Y.-J.; Park, S.-G.; Kwon, J.-D.; Kim, C. S.; Song, M.; Jeong, Y.; Nam, K.-S.; Ko, H. C. Graphene-Based Gas Sensor: Metal Decoration Effect and Application to a Flexible Device. *J. Mater. Chem. C* **2014**, *2*, 5280−5285.
(167) Chen, G.; Paronyan, T. M.; Harutyunyan, A. R. Sub-PPT Gas Detection with Pristine Graphene. *Appl. Phys. Lett.* **2012**, *101*, 053119.
(168) Ricciardella, F.; Vollebregt, S.; Polichetti, T.; Miscuglio, M.; Alfano, B.; Miglietta, M. L.; Massera, E.; Di Francia, G.; Sarro, P. M. Effects of Graphene Defects on Gas Sensing Properties Towards NO_2 Detection. *Nanoscale* **2017**, *9*, 6085−6093.
(169) Yavari, F.; Castillo, E.; Gullapalli, H.; Ajayan, P. M.; Koratkar, N. High Sensitivity Detection of NO_2 and NH_3 in Air Using Chemical Vapor Deposition Grown Graphene. *Appl. Phys. Lett.* **2012**, *100*, 203120.
(170) Wu, J.; Tao, K.; Miao, J.; Norford, L. K. In *IEEE 29th International Conference on Micro Electro Mechanical Systems (MEMS)*; IEEE: Shanghai, 2016; pp 889−892.
(171) Zhang, S.; Hang, N. T.; Zhang, Z.; Yue, H.; Yang, W. Preparation of g-C_3N_4/Graphene Composite for Detecting NO_2 at Room Temperature. *Nanomaterials* **2017**, *7*, 12.
(172) Pearce, R.; Iakimov, T.; Andersson, M.; Hultman, L.; Spetz, A. L.; Yakimova, R. Epitaxially Grown Graphene Based Gas Sensors for Ultra Sensitive NO_2 Detection. *Sens. Actuators, B* **2011**, *155*, 451−455.
(173) Long, H.; Harley-Trochimczyk, A.; Pham, T.; Tang, Z.; Shi, T.; Zettl, A.; Carraro, C.; Worsley, M. A.; Maboudian, R. High Surface Area MoS_2/Graphene Hybrid Aerogel for Ultrasensitive NO_2 Detection. *Adv. Funct. Mater.* **2016**, *26*, 5158−5165.
(174) Chung, M. G.; Kim, D. H.; Lee, H. M.; Kim, T.; Choi, J. H.; Seo, D. k.; Yoo, J.-B.; Hong, S.-H.; Kang, T. J.; Kim, Y. H. Highly Sensitive NO_2 Gas Sensor Based on Ozone Treated Graphene. *Sens. Actuators, B* **2012**, *166*, 172−176.
(175) Choi, H.; Jeong, H. Y.; Lee, D.-S.; Choi, S.-Y.; Choi, C.-G. Flexible NO_2 Gas Sensor Using Multilayer Graphene Films by Chemical Vapor Deposition. *Carbon Lett.* **2013**, *14*, 186−189.
(176) Shaik, M.; Rao, V. K.; Gupta, M.; Murthy, K. S. R. C.; Jain, R. Chemiresistive Gas Sensor for the Sensitive Detection of Nitrogen Dioxide Based on Nitrogen Doped Graphene Nanosheets. *RSC Adv.* **2016**, *6*, 1527−1534.
(177) Piloto, C.; Notarianni, M.; Shafiei, M.; Taran, E.; Galpaya, D.; Yan, C.; Motta, N. Highly NO_2 Sensitive Caesium Doped Graphene Oxide Conductometric Sensors. *Beilstein J. Nanotechnol.* **2014**, *5*, 1073−1081.
(178) Xia, Y.; Wang, J.; Xu, J. L.; Li, X.; Xie, D.; Xiang, L.; Komarneni, S. Confined Formation of Ultrathin ZnO Nanorods/Reduced Graphene Oxide Mesoporous Nanocomposites for High-Performance Room-Temperature NO_2 Sensors. *ACS Appl. Mater. Interfaces* **2016**, *8*, 35454−35463.
(179) Zhang, H.; Feng, J.; Fei, T.; Liu, S.; Zhang, T. SnO_2 Nanoparticles-Reduced Graphene Oxide Nanocomposites for NO_2 Sensing at Low Operating Temperature. *Sens. Actuators, B* **2014**, *190*, 472−478.
(180) Wang, Z.; Zhao, C.; Han, T.; Zhang, Y.; Liu, S.; Fei, T.; Lu, G.; Zhang, T. High-Performance Reduced Graphene Oxide-Based Room-Temperature NO_2 Sensors: A Combined Surface Modification of SnO_2 Nanoparticles and Nitrogen Doping Approach. *Sens. Actuators, B* **2017**, *242*, 269−279.
(181) Liu, X.; Cui, J.; Sun, J.; Zhang, X. 3D Graphene Aerogel-Supported SnO_2 Nanoparticles for Efficient Detection of NO_2. *RSC Adv.* **2014**, *4*, 22601−22605.
(182) Xiao, Y.; Yang, Q.; Wang, Z.; Zhang, R.; Gao, Y.; Sun, P.; Sun, Y.; Lu, G. Improvement of NO_2 Gas Sensing Performance Based on Discoid Tin Oxide Modified by Reduced Graphene Oxide. *Sens. Actuators, B* **2016**, *227*, 419−426.
(183) Su, P.-G.; Peng, S.-L. Fabrication and NO_2 Gas-Sensing Properties of Reduced Graphene Oxide/WO_3 Nanocomposite Films. *Talanta* **2015**, *132*, 398−405.
(184) Dong, Y.- L.; Zhang, X.-F.; Cheng, X.-L.; Xu, Y.-M.; Gao, S.; Zhao, H.; Huo, L.-H. Highly Selective NO_2 Sensor at Room Temperature Based on Nanocomposites of Hierarchical Nanosphere-Like α-Fe_2O_3 and Reduced Graphene Oxide. *RSC Adv.* **2014**, *4*, 57493−57500.
(185) Wu, J.; Tao, K.; Miao, J.; Norford, L. K. Improved Selectivity and Sensitivity of Gas Sensing Using a 3D Reduced Graphene Oxide Hydrogel with an Integrated Microheater. *ACS Appl. Mater. Interfaces* **2015**, *7*, 27502−27510.
(186) Trung, T. Q.; Hanif, A.; Siddiqui, S.; Roh, E.; Lee, W.; Lee, N.-E.; Duy, L. T. A Stretchable and Highly Sensitive Chemical Sensor Using Multilayered Network of Polyurethane Nanofibres with Self-Assembled Reduced Graphene Oxide. *2D Mater.* **2017**, *4*, 025062.
(187) Lee, C.; Ahn, J.; Lee, K. B.; Kim, D.; Kim, J. Graphene-Based Flexible NO_2 Chemical Sensors. *Thin Solid Films* **2012**, *520*, 5459−5462.

DOI: 10.1021/acsami.7b07063
ACS Appl. Mater. Interfaces 2017, 9, 34544−34586

(188) Choi, H.; Choi, J. S.; Kim, J. S.; Choe, J. H.; Chung, K. H.; Shin, J. W.; Kim, J. T.; Youn, D. H.; Kim, K. C.; Lee, J. I.; Choi, S. Y.; Kim, P.; Choi, C. G.; Yu, Y. J. Flexible and Transparent Gas Molecule Sensor Integrated with Sensing and Heating Graphene Layers. *Small* **2014**, *10*, 3685−3691.
(189) Liu, J.; Li, S.; Zhang, B.; Xiao, Y.; Gao, Y.; Yang, Q.; Wang, Y.; Lu, G. Ultrasensitive and Low Detection Limit of Nitrogen Dioxide Gas Sensor Based on Flower-Like ZnO Hierarchical Nanostructure Modified by Reduced Graphene Oxide. *Sens. Actuators, B* **2017**, *249*, 715−724.
(190) Zanjani, S. M. M.; Sadeghi, M. M.; Holt, M.; Chowdhury, S. F.; Tao, L.; Akinwande, D. Enhanced Sensitivity of Graphene Ammonia Gas Sensors Using Molecular Doping. *Appl. Phys. Lett.* **2016**, *108*, 033106.
(191) Inaba, A.; Yoo, K.; Takei, Y.; Matsumoto, K.; Shimoyama, I. Ammonia Gas Sensing Using a Graphene Field−Effect Transistor Gated by Ionic Liquid. *Sens. Actuators, B* **2014**, *195*, 15−21.
(192) Iezhokin, I.; Boer, D. d.; Offermans, P.; Ridene, M.; Elemans, J. A. A. W.; Adriaans, G. P.; Flipse, C. F. J. Porphyrin Molecules Boost the Sensitivity of Epitaxial Graphene for NH_3 Detection. *J. Phys.: Condens. Matter* **2017**, *29*, 065001.
(193) Gautam, M.; Jayatissa, A. H. Ammonia Gas Sensing Behavior of Graphene Surface Decorated with Gold Nanoparticles. *Solid-State Electron.* **2012**, *78*, 159−165.
(194) Karaduman, I.; Er, E.; Çelikkan, H.; Erk, N.; Acar, S. 2017. Room-Temperature Ammonia Gas Sensor Based on Reduced Graphene Oxide Nanocomposites Decorated by Ag, Au and Pt Nanoparticles. *J. Alloys Compd.* **2017**, *722*, 569−578.
(195) Yu, Z.; Wang, B.; Li, Y.; Kang, D.; Chen, Z.; Wu, Y. The Effect of Rigid Phenoxyl Substituent on the NH_3-sensing Properties of Tetra-α-(4-*tert*-butylphenoxyl)-Metallophthalocyanine/Reduced Graphene Oxide Hybrids. *RSC Adv.* **2017**, *7*, 22599−22609.
(196) Hu, N.; Yang, Z.; Wang, Y.; Zhang, L.; Wang, Y.; Huang, X.; Wei, H.; Wei, L.; Zhang, Y. Ultrafast and Sensitive Room Temperature NH_3 Gas Sensors Based on Chemically Reduced Graphene Oxide. *Nanotechnology* **2014**, *25*, 025502.
(197) Ye, Z.; Jiang, Y.; Tai, H.; Yuan, Z. The Investigation of Reduced Graphene Oxide/P3HT Composite Films for Ammonia Detection. *Integr. Ferroelectr.* **2014**, *154*, 73−81.
(198) Huang, X.; Hu, N.; Gao, R.; Yu, Y.; Wang, Y.; Yang, Z.; Kong, E. S.-W.; Wei, H.; Zhang, Y. Reduced Graphene Oxide−Polyaniline Hybrid: Preparation, Characterization and its Applications for Ammonia Gas Sensing. *J. Mater. Chem.* **2012**, *22*, 22488−22495.
(199) Andre, R. S.; Shimizu, F. M.; Miyazaki, C. M.; Riul, A.; Manzani, D.; Ribeiro, S. J. L.; Oliveira, O. N.; Mattoso, L. H. C.; Correa, D. S. Hybrid Layer-by-Layer (LbL) Films of Polyaniline, Graphene Oxide and Zinc Oxide to Detect Ammonia. *Sens. Actuators, B* **2017**, *238*, 795−801.
(200) Wang, J.; Singh, B.; Park, J.-H.; Rathi, S.; Lee, I.-y.; Maeng, S.; Joh, H.-I.; Lee, C.-H.; Kim, G.-H. Dielectrophoresis of Graphene Oxide Nanostructures for Hydrogen Gas Sensor at Room Temperature. *Sens. Actuators, B* **2014**, *194*, 296−302.
(201) Wu, W.; Liu, Z.; Jauregui, L. A.; Yu, Q.; Pillai, R.; Cao, H.; Bao, J.; Chen, Y. P.; Pei, S.-S. Wafer-Scale Synthesis of Graphene by Chemical Vapor Deposition and Its Application in Hydrogen Sensing. *Sens. Actuators, B* **2010**, *150*, 296−300.
(202) Pak, Y.; Kim, S.-M.; Jeong, H.; Kang, C. G.; Park, J. S.; Song, H.; Lee, R.; Myoung, N.; Lee, B. H.; Seo, S.; et al. Palladium-Decorated Hydrogen-Gas Sensors Using Periodically Aligned Graphene Nanoribbons. *ACS Appl. Mater. Interfaces* **2014**, *6*, 13293−13298.
(203) Johnson, J. L.; Behnam, A.; Pearton, S. J.; Ural, A. Hydrogen Sensing Using Pd-Functionalized Multi-Layer Graphene Nanoribbon Networks. *Adv. Mater.* **2010**, *22*, 4877−4880.
(204) Chung, M. G.; Kim, D.-H.; Seo, D. K.; Kim, T.; Im, H. U.; Lee, H. M.; Yoo, J.-B.; Hong, S.-H.; Kang, T. J.; Kim, Y. H. Flexible Hydrogen Sensors Using Graphene with Palladium Nanoparticle Decoration. *Sens. Actuators, B* **2012**, *169*, 387−392.
(205) Shin, D. H.; Lee, J. S.; Jun, J.; An, J. H.; Kim, S. G.; Cho, K. H.; Jang, J. Flower-Like Palladium Nanoclusters Decorated Graphene Electrodes for Ultrasensitive and Flexible Hydrogen Gas Sensing. *Sci. Rep.* **2015**, *5*, 12294.
(206) Lee, J. S.; Oh, J.; Jun, J.; Jang, J. Wireless Hydrogen Smart Sensor Based on Pt/Graphene-Immobilized Radio-Frequency Identification Tag. *ACS Nano* **2015**, *9*, 7783−7790.
(207) Yaqoob, U.; Uddin, A. I.; Chung, G.-S. Foldable Hydrogen Sensor Using Pd Nanocubes Dispersed into Multiwall Carbon Nanotubes-Reduced Graphene Oxide Network Assembled on Nylon Filter Membrane. *Sens. Actuators, B* **2016**, *229*, 355−361.
(208) Kathiravan, D.; Huang, B.-R.; Saravanan, A. Self-Assembled Hierarchical Interfaces of ZnO Nanotubes/Graphene Heterostructures for Efficient Room Temperature Hydrogen Sensors. *ACS Appl. Mater. Interfaces* **2017**, *9*, 12064−12072.
(209) Esfandiar, A.; Ghasemi, S.; Irajizad, A.; Akhavan, O.; Gholami, M. R. The Decoration of TiO_2/Reduced Graphene Oxide by Pd and Pt Nanoparticles for Hydrogen Gas Sensing. *Int. J. Hydrogen Energy* **2012**, *37*, 15423−15432.
(210) Zhang, Z.; Zou, X.; Xu, L.; Liao, L.; Liu, W.; Ho, J.; Xiao, X.; Jiang, C.; Li, J. Hydrogen Gas Sensor Based on Metal Oxide Nanoparticles Decorated Graphene Transistor. *Nanoscale* **2015**, *7*, 10078−10084.
(211) Wang, J.; Rathi, S.; Singh, B.; Lee, I.; Joh, H. I.; Kim, G. H. Alternating Current Dielectrophoresis Optimization of Pt-Decorated Graphene Oxide Nanostructures for Proficient Hydrogen Gas Sensor. *ACS Appl. Mater. Interfaces* **2015**, *7*, 13768−13775.
(212) Phan, D.-T.; Chung, G.-S. Characteristics of Resistivity-Type Hydrogen Sensing Based on Palladium-Graphene Nanocomposites. *Int. J. Hydrogen Energy* **2014**, *39*, 620−629.
(213) Yoon, H. J.; Jun, D. H.; Yang, J. H.; Zhou, Z.; Yang, S. S.; Cheng, M. M.-C. Carbon Dioxide Gas Sensor Using a Graphene Sheet. *Sens. Actuators, B* **2011**, *157*, 310−313.
(214) Hafiz, S. M.; Ritikos, R.; Whitcher, T. J.; Md. Razib, N.; Bien, D. C. S.; Chanlek, N.; Nakajima, H.; Saisopa, T.; Songsiriritthigul, P.; Huang, N. M.; Rahman, S. A. A Practical Carbon Dioxide Gas Sensor Using Room-Temperature Hydrogen Plasma Reduced Graphene Oxide. *Sens. Actuators, B* **2014**, *193*, 692−700.
(215) Nemade, K. R.; Waghuley, S. A. Role of Defects Concentration on Optical and Carbon Dioxide Gas Sensing Properties of Sb_2O_3/Graphene Composites. *Opt. Mater.* **2014**, *36*, 712−716.
(216) Nemade, K. R.; Waghuley, S. A. Highly Responsive Carbon Dioxide Sensing by Graphene/Al_2O_3 Quantum Dots Composites at Low Operable Temperature. *Indian J. Phys.* **2014**, *88*, 577−583.
(217) Ren, Y.; Zhu, C.; Cai, W.; Li, H.; Ji, H.; Kholmanov, I.; Wu, Y.; Piner, R. D.; Ruoff, R. S. Detection of Sulfur Dioxide Gas with Graphene Field Effect Transistor. *Appl. Phys. Lett.* **2012**, *100*, 163114.
(218) Kumar, R.; Avasthi, D. K.; Kaur, A. Fabrication of Chemiresistive Gas Sensors Based on Multistep Reduced Graphene Oxide for Low Parts Per Million Monitoring of Sulfur Dioxide at Room Temperature. *Sens. Actuators, B* **2017**, *242*, 461−468.
(219) Zhang, D.; Liu, J.; Jiang, C.; Li, P.; Sun, Y. High-Performance Sulfur Dioxide Sensing Properties of Layer-by-Layer Self-Assembled Titania-Modified Graphene Hybrid Nanocomposite. *Sens. Actuators, B* **2017**, *245*, 560−567.
(220) Cuong, T. V.; Pham, V. H.; Chung, J. S.; Shin, E. W.; Yoo, D. H.; Hahn, S. H.; Huh, J. S.; Rue, G. H.; Kim, E. J.; Hur, S. H.; Kohl, P. A. Solution-Processed ZnO-Chemically Converted Graphene Gas Sensor. *Mater. Lett.* **2010**, *64*, 2479−2482.
(221) Choi, S. J.; Choi, C.; Kim, S. J.; Cho, H. J.; Hakim, M.; Jeon, S.; Kim, I. D. Highly Efficient Electronic Sensitization of Non-Oxidized Graphene Flakes on Controlled Pore-Loaded WO_3 Nanofibers for Selective Detection of H_2S Molecules. *Sci. Rep.* **2015**, *5*, 8067.
(222) Zhou, L.; Shen, F.; Tian, X.; Wang, D.; Zhang, T.; Chen, W. Stable Cu_2O Nanocrystals Grown on Functionalized Graphene Sheets and Room Temperature H_2S Gas Sensing with Ultrahigh Sensitivity. *Nanoscale* **2013**, *5*, 1564−1569.
(223) Cho, S.; Lee, J. S.; Jun, J.; Kim, S. G.; Jang, J. Fabrication of Water-Dispersible and Highly Conductive PSS-Doped PANI/Graphene Nanocomposites Using a High-Molecular Weight PSS Dopant

DOI: 10.1021/acsami.7b07063
ACS Appl. Mater. Interfaces 2017, 9, 34544−34586

and Their Application in H_2S Detection. *Nanoscale* **2014**, *6*, 15181−15195.
(224) Choi, S. J.; Jang, B. H.; Lee, S. J.; Min, B. K.; Rothschild, A.; Kim, I. D. Selective Detection of Acetone and Hydrogen Sulfide for the Diagnosis of Diabetes and Halitosis Using SnO_2 Nanofibers Functionalized with Reduced Graphene Oxide Nanosheets. *ACS Appl. Mater. Interfaces* **2014**, *6*, 2588−2597.
(225) Zhang, Z.; Zou, R.; Song, G.; Yu, L.; Chen, Z.; Hu, J. Highly Aligned SnO_2 Nanorods on Graphene Sheets for Gas Sensors. *J. Mater. Chem.* **2011**, *21*, 17360−17365.
(226) Song, Z.; Wei, Z.; Wang, B.; Luo, Z.; Xu, S.; Zhang, W.; Yu, H.; Li, M.; Huang, Z.; Zang, J.; et al. Sensitive Room-Temperature H_2S Gas Sensors Employing SnO_2 Quantum Wire/Reduced Graphene Oxide Nanocomposites. *Chem. Mater.* **2016**, *28*, 1205−1212.
(227) Choi, S.-J.; Kim, S.-J.; Kim, I.-D. Ultrafast Optical Reduction of Graphene Oxide Sheets on Colorless Polyimide Film for Wearable Chemical Sensors. *NPG Asia Mater.* **2016**, *8*, e315.
(228) Bai, S.; Guo, J.; Sun, J.; Tang, P.; Chen, A.; Luo, R.; Li, D. Enhancement of NO_2-Sensing Performance at Room Temperature by Graphene-Modified Polythiophene. *Ind. Eng. Chem. Res.* **2016**, *55*, 5788−5794.
(229) Kumar, S.; Kaushik, S.; Pratap, R.; Raghavan, S. Graphene on Paper: A Simple, Low-Cost Chemical Sensing Platform. *ACS Appl. Mater. Interfaces* **2015**, *7*, 2189−2194.
(230) Timmer, B.; Olthuis, W.; Van den Berg, A. Ammonia Sensors and Their Applications—A Review. *Sens. Actuators, B* **2005**, *107*, 666−677.
(231) Hannon, A.; Lu, Y.; Hong, H.; Li, J.; Meyyappan, M. Functionalized-Carbon Nanotube Sensor for Room Temperature Ammonia Detection. *Sens. Lett.* **2014**, *12*, 1469−1476.
(232) Han, J.-W.; Kim, B.; Li, J.; Meyyappan, M. A Carbon Nanotube Based Ammonia Sensor on Cotton Textile. *Appl. Phys. Lett.* **2013**, *102*, 193104.
(233) Han, J.-W.; Kim, B.; Li, J.; Meyyappan, M. A Carbon Nanotube Based Ammonia Sensor on Cellulose Paper. *RSC Adv.* **2014**, *4*, 549−553.
(234) Gandhiraman, R. P.; Singh, E.; Diaz-Cartagena, D. C.; Nordlund, D.; Koehne, J.; Meyyappan, M. Plasma Jet Printing for Flexible Substrates. *Appl. Phys. Lett.* **2016**, *108*, 123103.
(235) Kumar, L.; Rawal, I.; Kaur, A.; Annapoorni, S. Flexible Room Temperature Ammonia Sensor Based on Polyaniline. *Sens. Actuators, B* **2017**, *240*, 408−416.
(236) Šetka, M.; Drbohlavová, J.; Hubálek, J. Nanostructured Polypyrrole-Based Ammonia and Volatile Organic Compound Sensors. *Sensors* **2017**, *17*, 562.
(237) Yan, Y.; Zhang, M.; Moon, C. H.; Su, H.-C.; Myung, N. V.; Haberer, E. D. Viral-Templated Gold/Polypyrrole Nanopeapods for an Ammonia Gas Sensor. *Nanotechnology* **2016**, *27*, 325502.
(238) Tavoli, F.; Alizadeh, N. Optical Ammonia Gas Sensor Based on Nanostructure Dye-Doped Polypyrrole. *Sens. Actuators, B* **2013**, *176*, 761−767.
(239) Karmakar, N.; Fernandes, R.; Jain, S.; Patil, U. V.; Shimpi, N. G.; Bhat, N. V.; Kothari, D. C. Room Temperature NO_2 Gas Sensing Properties of p-Toluenesulfonic Acid Doped Silver-Polypyrrole Nanocomposite. *Sens. Actuators, B* **2017**, *242*, 118−126.
(240) Raj, V. B.; Singh, H.; Nimal, A. T.; Sharma, M. U.; Tomar, M.; Gupta, V. Distinct Detection of Liquor Ammonia by ZnO/Saw Sensor: Study of Complete Sensing Mechanism. *Sens. Actuators, B* **2017**, *238*, 83−90.
(241) Ravichandran, K.; Manivasaham, A. Enhanced Ammonia Sensing by Sn Doped ZnO Films Prepared by a Low-Cost Fully Automated Nebulizer Spray Technique. *J. Mater. Sci.: Mater. Electron.* **2017**, *28*, 6335−6344.
(242) Zeng, Y.; Lou, Z.; Wang, L.; Zou, B.; Zhang, T.; Zheng, W.; Zou, G. Enhanced Ammonia Sensing Performances of Pd-Sensitized Flowerlike ZnO Nanostructure. *Sens. Actuators, B* **2011**, *156*, 395−400.
(243) Wang, G.; Ji, Y.; Huang, X.; Yang, X.; Gouma, P.-I.; Dudley, M. Fabrication and Characterization of Polycrystalline WO_3 nanofibers and Their Application for Ammonia Sensing. *J. Phys. Chem. B* **2006**, *110*, 23777−23782.
(244) Wang, Y.; Liu, J.; Cui, X.; Gao, Y.; Ma, J.; Sun, Y.; Sun, P.; Liu, F.; Liang, X.; Zhang, T.; Lu, G. NH_3 Gas Sensing Performance Enhanced by Pt-Loaded on Mesoporous WO_3. *Sens. Actuators, B* **2017**, *238*, 473−481.
(245) Zhang, J.; Wang, S.; Xu, M.; Wang, Y.; Xia, H.; Zhang, S.; Guo, X.; Wu, S. Polypyrrole-Coated SnO_2 hollow Spheres and Their Application for Ammonia Sensor. *J. Phys. Chem. C* **2009**, *113*, 1662−1665.
(246) Wang, L.; Lou, Z.; Zhang, R.; Zhou, T.; Deng, J.; Zhang, T. Hybrid Co_3O_4/SnO_2 Core−Shell Nanospheres as Real-Time Rapid-Response Sensors for Ammonia Gas. *ACS Appl. Mater. Interfaces* **2016**, *8*, 6539−6545.
(247) Rane, S. S.; Kajale, D. A.; Arbuj, S. S.; Rane, S. B.; Gosavi, S. W. Hydrogen, Ethanol and Ammonia Gas Sensing Properties of Nano-Structured Titanium Dioxide Thick Films. *J. Mater. Sci.: Mater. Electron.* **2017**, *28*, 9011−9016.
(248) Abaker, M.; Umar, A.; Baskoutas, S.; Dar, G. N.; Zaidi, S. A.; Al-Sayari, S. A.; Al-Hajry, A.; Kim, S. H.; Hwang, S. W. A Highly Sensitive Ammonia Chemical Sensor Based on α-Fe_2O_3 nanoellipsoids. *J. Phys. D: Appl. Phys.* **2011**, *44*, 425401.
(249) Huotari, J.; Bjorklund, R.; Lappalainen, J.; Lloyd Spetz, A. Pulsed Laser Deposited Nanostructured Vanadium Oxide Thin Films Characterized as Ammonia Sensors. *Sens. Actuators, B* **2015**, *217*, 22−29.
(250) Huotari, J.; Lappalainen, J.; Eriksson, J.; Bjorklund, R.; Heinonen, E.; Miinalainen, I.; Puustinen, J.; Lloyd Spetz, A. Synthesis of Nanostructured Solid-State Phases of V_7O_{16} and V_2O_5 Compounds for ppb-Level Detection of Ammonia. *J. Alloys Compd.* **2016**, *675*, 433−440.
(251) Li, X.; Li, X.; Li, Z.; Wang, J.; Zhang, J. WS_2 Nanoflakes Based Selective Ammonia Sensors at Room Temperature. *Sens. Actuators, B* **2017**, *240*, 273−277.
(252) Yan, H.; Song, P.; Zhang, S.; Zhang, J.; Yang, Z.; Wang, Q. A Low Temperature Gas Sensor Based on Au-Loaded MoS_2 Hierarchical Nanostructures for Detecting Ammonia. *Ceram. Int.* **2016**, *42*, 9327−9331.
(253) Feng, Q.; Li, X.; Wang, J.; Gaskov, A. M. Reduced Graphene Oxide (RGO) Encapsulated Co_3O_4 Composite Nanofibers for Highly Selective Ammonia Sensors. *Sens. Actuators, B* **2016**, *222*, 864−870.
(254) Khalaf, A. L.; Mohamad, F. S.; Rahman, N. A.; Lim, H. N.; Paiman, S.; Yusof, N. A.; Mahdi, M. A.; Yaacob, M. H. Room Temperature Ammonia Sensor Using Side-Polished Optical Fiber Coated with Graphene/Polyaniline Nanocomposite. *Opt. Mater. Express* **2017**, *7*, 1858−1870.
(255) Yu, C.; Wu, Y.; Liu, X.; Fu, F.; Gong, Y.; Rao, Y.-J.; Chen, Y. Miniature Fiber-Optic NH_3 Gas Sensor Based on Pt Nanoparticle-Incorporated Graphene Oxide. *Sens. Actuators, B* **2017**, *244*, 107−113.
(256) Kumar, R.; Kushwaha, N.; Mittal, J. Superior, Rapid and Reversible Sensing Activity of Graphene-SnO Hybrid Film for Low Concentration of Ammonia at Room Temperature. *Sens. Actuators, B* **2017**, *244*, 243−251.
(257) Sivalingam, M. M.; Balasubramanian, K. Influence of the Concentration of Reducing Agent on Gold Nanoparticles Decorated Reduced Graphene Oxide and Its Ammonia Sensing Performance. *Appl. Phys. A: Mater. Sci. Process.* **2017**, *123*, 281.
(258) Sysoev, V. I.; Okotrub, A. V.; Asanov, I. P.; Gevko, P. N.; Bulusheva, L. G. Advantage of Graphene Fluorination Instead of Oxygenation for Restorable Adsorption of Gaseous Ammonia and Nitrogen Dioxide. *Carbon* **2017**, *118*, 225−232.
(259) Wang, Y.; Zhang, L.; Hu, N.; Wang, Y.; Zhang, Y.; Zhou, Z.; Liu, Y.; Shen, S.; Peng, C. Ammonia Gas Sensors Based on Chemically Reduced Graphene Oxide Sheets Self-Assembled on Au Electrodes. *Nanoscale Res. Lett.* **2014**, *9*, 251.
(260) Ghosh, R.; Singh, A.; Santra, S.; Ray, S. K.; Chandra, A.; Guha, P. K. Highly Sensitive Large-Area Multi-Layered Graphene-Based Flexible Ammonia Sensor. *Sens. Actuators, B* **2014**, *205*, 67−73.
(261) Seekaew, Y.; Lokavee, S.; Phokharatkul, D.; Wisitsoraat, A.; Kerdcharoen, T.; Wongchoosuk, C. Low-Cost and Flexible Printed

DOI: 10.1021/acsami.7b07063
ACS Appl. Mater. Interfaces 2017, 9, 34544−34586

Graphene−PEDOT:PSS Gas Sensor for Ammonia Detection. *Org. Electron.* **2014**, *15*, 2971−2981.
(262) Guo, Y.; Wang, T.; Chen, F.; Sun, X.; Li, X.; Yu, Z.; Wan, P.; Chen, X. Hierarchical Graphene-Polyaniline Nanocomposite Films for High-Performance Flexible Electronic Gas Sensors. *Nanoscale* **2016**, *8*, 12073−12080.
(263) Gavgani, J. N.; Hasani, A.; Nouri, M.; Mahyari, M.; Salehi, A. Highly Sensitive and Flexible Ammonia Sensor Based on S and N Co-Doped Graphene Quantum Dots/Polyaniline Hybrid at Room Temperature. *Sens. Actuators, B* **2016**, *229*, 239−248.
(264) Duy, L. T.; Trung, T. Q.; Dang, V. Q.; Hwang, B.-U.; Siddiqui, S.; Son, I.-Y.; Yoon, S. K.; Chung, D. J.; Lee, N.-E. Flexible Transparent Reduced Graphene Oxide Sensor Coupled with Organic Dye Molecules for Rapid Dual-Mode Ammonia Gas Detection. *Adv. Funct. Mater.* **2016**, *26*, 4329−4338.
(265) Cho, B.; Yoon, J.; Lim, S. K.; Kim, A. R.; Kim, D. H.; Park, S. G.; Kwon, J. D.; Lee, Y. J.; Lee, K. H.; Lee, B. H.; Ko, H. C.; Hahm, M. G. Chemical Sensing of 2D Graphene/MoS_2 Heterostructure Device. *ACS Appl. Mater. Interfaces* **2015**, *7*, 16775−16780.
(266) Huang, D.; Yang, Z.; Li, X.; Zhang, L.; Hu, J.; Su, Y.; Hu, N.; Yin, G.; He, D.; Zhang, Y. Three-Dimensional Conductive Networks Based on Stacked SiO_2@ Graphene Frameworks for Enhanced Gas Sensing. *Nanoscale* **2017**, *9*, 109−118.
(267) Romero, H. E.; Joshi, P.; Gupta, A. K.; Gutierrez, H. R.; Cole, M. W.; Tadigadapa, S. A.; Eklund, P. C. Adsorption of Ammonia on Graphene. *Nanotechnology* **2009**, *20*, 245501.
(268) Gautam, M.; Jayatissa, A. H. Adsorption Kinetics of Ammonia Sensing by Graphene Films Decorated with Platinum Nanoparticles. *J. Appl. Phys.* **2012**, *111*, 094317.
(269) Hübert, T.; Boon-Brett, L.; Black, G.; Banach, U. Hydrogen Sensors−A Review. *Sens. Actuators, B* **2011**, *157*, 329−352.
(270) Gu, H.; Wang, Z.; Hu, Y. Hydrogen Gas Sensors Based on Semiconductor Oxide Nanostructures. *Sensors* **2012**, *12*, 5517−5550.
(271) Bie, L.-J.; Yan, X.-N.; Yin, J.; Duan, Y.-Q.; Yuan, Z.-H. Nanopillar ZnO Gas Sensor for Hydrogen and Ethanol. *Sens. Actuators, B* **2007**, *126*, 604−608.
(272) Phan, D.-T.; Chung, G.-S. Surface Acoustic Wave Hydrogen Sensors Based on ZnO Nanoparticles Incorporated with a Pt Catalyst. *Sens. Actuators, B* **2012**, *161*, 341−348.
(273) Varghese, O. K.; Gong, D.; Paulose, M.; Ong, K. G.; Grimes, C. A. Hydrogen Sensing Using Titania Nanotubes. *Sens. Actuators, B* **2003**, *93*, 338−344.
(274) Mor, G. K.; Varghese, O. K.; Paulose, M.; Ong, K. G.; Grimes, C. A. Fabrication of Hydrogen Sensors with Transparent Titanium Oxide Nanotube-Array Thin Films as Sensing Elements. *Thin Solid Films* **2006**, *496*, 42−48.
(275) Han, C.-H.; Hong, D.-W.; Kim, I.-J.; Gwak, J.; Han, S.-D.; Singh, K. C. Synthesis of Pd or Pt/Titanate Nanotube and Its Application to Catalytic Type Hydrogen Gas Sensor. *Sens. Actuators, B* **2007**, *128*, 320−325.
(276) Simo, A.; Mwakikunga, B.; Maaza, M. One-Dimensional Vanadium Dioxide Nanostructures for Room Temperature Hydrogen Sensors. *Sens. Transducers* **2015**, *189*, 143.
(277) Zhang, C.; Boudiba, A.; Navio, C.; Bittencourt, C.; Olivier, M.-G.; Snyders, R.; Debliquy, M. Highly Sensitive Hydrogen Sensors Based on Co-Sputtered Platinum-Activated Tungsten Oxide Films. *Int. J. Hydrogen Energy* **2011**, *36*, 1107−1114.
(278) Shen, Y.; Wang, W.; Fan, A.; Wei, D.; Liu, W.; Han, C.; Shen, Y.; Meng, D.; San, X. Highly Sensitive Hydrogen Sensors Based on SnO_2 Nanomaterials with Different Morphologies. *Int. J. Hydrogen Energy* **2015**, *40*, 15773−15779.
(279) Lange, U.; Hirsch, T.; Mirsky, V. M.; Wolfbeis, O. S. Hydrogen Sensor Based on a Graphene − Palladium Nanocomposite. *Electrochim. Acta* **2011**, *56*, 3707−3712.
(280) Mubeen, S.; Zhang, T.; Yoo, B.; Deshusses, M. A.; Myung, N. V. Palladium Nanoparticles Decorated Single-Walled Carbon Nanotube Hydrogen Sensor. *J. Phys. Chem. C* **2007**, *111*, 6321−6327.
(281) Yi, J.; Lee, J. M.; Park, W. I. Vertically Aligned ZnO Nanorods and Graphene Hybrid Architectures for High-Sensitive Flexible Gas Sensors. *Sens. Actuators, B* **2011**, *155*, 264−269.
(282) Yang, S.; Wang, Z.; Zou, Y.; Luo, X.; Pan, X.; Zhang, X.; Hu, Y.; Chen, K.; Huang, Z.; Wang, S.; Zhang, K.; Gu, H. Remarkably Accelerated Room-Temperature Hydrogen Sensing of MoO_3 Nanoribbon/Graphene Composites by Suppressing the Nanojunction Effects. *Sens. Actuators, B* **2017**, *248*, 160−168.
(283) Yamazoe, N.; Shimizu, Y. Humidity Sensors: Principles and Applications. *Sens. Actuators* **1986**, *10*, 379−398.
(284) Rittersma, Z. M. Recent Achievements in Miniaturised Humidity Sensors—A Review of Transduction Techniques. *Sens. Actuators, A* **2002**, *96*, 196−210.
(285) Lee, C.-Y.; Lee, G.-B. Humidity Sensors: A Review. *Sens. Lett.* **2005**, *3*, 1−15.
(286) Chen, Z.; Lu, C. Humidity Sensors: A Review of Materials and Mechanisms. *Sens. Lett.* **2005**, *3*, 274−295.
(287) Farahani, H.; Wagiran, R.; Hamidon, M. N. Humidity Sensors Principle, Mechanism, and Fabrication Technologies: A Comprehensive Review. *Sensors* **2014**, *14*, 7881−7939.
(288) Connolly, E. J.; O'Halloran, G. M.; Pham, H. T. M.; Sarro, P. M.; French, P. J. Comparison of Porous Silicon, Porous Polysilicon and Porous Silicon Carbide as Materials for Humidity Sensing Applications. *Sens. Actuators, A* **2002**, *99*, 25−30.
(289) Connolly, E. J.; Pham, H. T. M.; Groeneweg, J.; Sarro, P. M.; French, P. J. Relative Humidity Sensors Using Porous SiC Membranes and Al Electrodes. *Sens. Actuators, B* **2004**, *100*, 216−220.
(290) Fu, X. Q.; Wang, C.; Yu, H. C.; Wang, Y. G.; Wang, T. H. Fast Humidity Sensors Based on CeO_2 Nanowires. *Nanotechnology* **2007**, *18*, 145503.
(291) Zhang, Z.; Hu, C.; Xiong, Y.; Yang, R.; Wang, Z. L. Synthesis of Ba-Doped CeO_2 Nanowires and Their Application as Humidity Sensors. *Nanotechnology* **2007**, *18*, 465504.
(292) Qi, Q.; Zhang, T.; Yu, Q.; Wang, R.; Zeng, Y.; Liu, L.; Yang, H. Properties of Humidity Sensing ZnO Nanorods-Base Sensor Fabricated by Screen-Printing. *Sens. Actuators, B* **2008**, *133*, 638−643.
(293) Zhang, Y.; Yu, K.; Jiang, D.; Zhu, Z.; Geng, H.; Luo, L. Zinc Oxide Nanorod and Nanowire for Humidity Sensor. *Appl. Surf. Sci.* **2005**, *242*, 212−217.
(294) Gu, L.; Zheng, K.; Zhou, Y.; Li, J.; Mo, X.; Patzke, G. R.; Chen, G. Humidity Sensors Based on ZnO/TiO_2 Core/Shell Nanorod Arrays with Enhanced Sensitivity. *Sens. Actuators, B* **2011**, *159*, 1−7.
(295) Feng, M. H.; Wang, W. C.; Li, X. J. Capacitive Humidity Sensing Properties of CdS/ZnO Sesame-Seed-Candy Structure Grown on Silicon Nanoporous Pillar Array. *J. Alloys Compd.* **2017**, *698*, 94−98.
(296) Kuang, Q.; Lao, C.; Wang, Z. L.; Xie, Z.; Zheng, L. High-Sensitivity Humidity Sensor Based on a Single SnO_2 Nanowire. *J. Am. Chem. Soc.* **2007**, *129*, 6070−6071.
(297) Hsueh, H. T.; Hsueh, T. J.; Chang, S. J.; Hung, F. Y.; Tsai, T. Y.; Weng, W. Y.; Hsu, C. L.; Dai, B. T. CuO Nanowire-Based Humidity Sensors Prepared on Glass Substrate. *Sens. Actuators, B* **2011**, *156*, 906−911.
(298) Wang, L.; He, Y.; Hu, J.; Qi, Q.; Zhang, T. DC Humidity Sensing Properties of $BaTiO_3$ Nanofiber Sensors with Different Electrode Materials. *Sens. Actuators, B* **2011**, *153*, 460−464.
(299) Wang, J.; Lin, Q.; Zhou, R.; Xu, B. Humidity Sensors Based on Composite Material of Nano-$BaTiO_3$ and Polymer RMX. *Sens. Actuators, B* **2002**, *81*, 248−253.
(300) Yuk, J.; Troczynski, T. Sol−Gel $BaTiO_3$ Thin Film for Humidity Sensors. *Sens. Actuators, B* **2003**, *94*, 290−293.
(301) Zhuang, Z.; Li, Y.; Qi, D.; Zhao, C.; Na, H. Novel Polymeric Humidity Sensors Based on Sulfonated Poly(ether ether ketone)s: Influence of Sulfonation Degree on Sensing Properties. *Sens. Actuators, B* **2017**, *242*, 801−809.
(302) Park, K.-J.; Gong, M.-S. A Water Durable Resistive Humidity Sensor Based on Rigid Sulfonated Polybenzimidazole and Their Properties. *Sens. Actuators, B* **2017**, *246*, 53−60.

DOI: 10.1021/acsami.7b07063
ACS Appl. Mater. Interfaces 2017, 9, 34544−34586

(303) Zhang, T.; He, Y.; Wang, R.; Geng, W.; Wang, L.; Niu, L.; Li, X. Analysis of DC and AC Properties of Humidity Sensor Based on Polypyrrole Materials. *Sens. Actuators, B* **2008**, *131*, 687−691.
(304) Suri, K.; Annapoorni, S.; Sarkar, A. K.; Tandon, R. P. Gas and Humidity Sensors Based on Iron Oxide−Polypyrrole Nanocomposites. *Sens. Actuators, B* **2002**, *81*, 277−282.
(305) Su, P.-G.; Huang, L.-N. Humidity Sensors Based on TiO_2 Nanoparticles/Polypyrrole Composite Thin Films. *Sens. Actuators, B* **2007**, *123*, 501−507.
(306) Han, J.-W.; Kim, B.; Li, J.; Meyyappan, M. Carbon Nanotube Based Humidity Sensor on Cellulose Paper. *J. Phys. Chem. C* **2012**, *116*, 22094−22097.
(307) Su, P.-G.; Sun, Y.-L.; Lin, C.-C. A Low Humidity Sensor Made of Quartz Crystal Microbalance Coated with Multi-Walled Carbon Nanotubes/Nafion Composite Material Films. *Sens. Actuators, B* **2006**, *115*, 338−343.
(308) Yu, H.; Cao, T.; Zhou, L.; Gu, E.; Yu, D.; Jiang, D. Layer-by-Layer Assembly and Humidity Sensitive Behavior of Poly(ethyleneimine)/Multiwall Carbon Nanotube Composite Films. *Sens. Actuators, B* **2006**, *119*, 512−515.
(309) Yoo, K.-P.; Lim, L.-T.; Min, N.-K.; Lee, M. J.; Lee, C. J.; Park, C.-W. Novel Resistive-Type Humidity Sensor Based on Multiwall Carbon Nanotube/Polyimide Composite Films. *Sens. Actuators, B* **2010**, *145*, 120−125.
(310) Zhang, D.; Wang, K.; Tong, J.; Xia, B. Layer-by-Layer Nanoassembly Fabrication and Humidity Sensing Behaviors of Multi-Walled Carbon Nanotubes/Polyelectrolyte Hybrid Film. *J. Nanosci. Nanotechnol.* **2016**, *16*, 6705−6710.
(311) Itoh, E.; Yuan, Z. Comparative Study of All-Printed Polyimide Humidity Sensors with Single-and Multiwalled Carbon Nanotube Gas-Permeable Top Electrodes. *Jpn. J. Appl. Phys.* **2017**, *56*, 05EC03.
(312) Yang, A.; Gao, J.; Li, B.; Tan, J.; Xiang, Y.; Gupta, T.; Li, L.; Suresh, S.; Idrobo, J. C.; Lu, T.-M.; et al. Humidity Sensing Using Vertically Oriented Arrays of ReS_2 Nanosheets Deposited on an Interdigitated Gold Electrode. *2D Mater.* **2016**, *3*, 045012.
(313) Zhang, S. L.; Jung, H.; Huh, J. S.; Yu, J. B.; Yang, W. C. Efficient Exfoliation of MoS_2 with Volatile Solvents and Their Application for Humidity Sensor. *J. Nanosci. Nanotechnol.* **2014**, *14*, 8518−8522.
(314) Ze, L.; Yueqiu, G.; Xujun, L.; Yong, Z. MoS_2-Modified ZnO Quantum Dots Nanocomposite: Synthesis and Ultrafast Humidity Response. *Appl. Surf. Sci.* **2017**, *399*, 330−336.
(315) Zhang, D.; Sun, Y.; Li, P.; Zhang, Y. Facile Fabrication of MoS_2-Modified SnO_2 Hybrid Nanocomposite for Ultrasensitive Humidity Sensing. *ACS Appl. Mater. Interfaces* **2016**, *8*, 14142−14149.
(316) Pawbake, A. S.; Jadkar, S. R.; Late, D. J. High Performance Humidity Sensor and Photodetector Based on SnSe Nanorods. *Mater. Res. Express* **2016**, *3*, 105038.
(317) Bharatula, L. D.; Erande, M. B.; Mulla, I. S.; Rout, C. S.; Late, D. J. SnS_2 Nanoflakes for Efficient Humidity and Alcohol Sensing at Room Temperature. *RSC Adv.* **2016**, *6*, 105421−105427.
(318) Erande, M. B.; Pawar, M. S.; Late, D. J. Humidity Sensing and Photodetection Behavior of Electrochemically Exfoliated Atomically Thin-Layered Black Phosphorus Nanosheets. *ACS Appl. Mater. Interfaces* **2016**, *8*, 11548−11556.
(319) Late, D. J. Liquid Exfoliation of Black Phosphorus Nanosheets and Its Application as Humidity Sensor. *Microporous Mesoporous Mater.* **2016**, *225*, 494−503.
(320) Chen, W. H.; Huang, J. Q.; Zhu, C. Y.; Huang, Q. A. In *IEEE Sensors*; IEEE: Orlando, FL, 2016; pp 1−3.
(321) Miao, J.; Cai, L.; Zhang, S.; Nah, J.; Yeom, J.; Wang, C. Air-Stable Humidity Sensor Using Few-Layer Black Phosphorus. *ACS Appl. Mater. Interfaces* **2017**, *9*, 10019−10026.
(322) Yao, Y.; Chen, X.; Guo, H.; Wu, Z. Graphene Oxide Thin Film Coated Quartz Crystal Microbalance for Humidity Detection. *Appl. Surf. Sci.* **2011**, *257*, 7778−7782.
(323) Yao, Y.; Chen, X.; Guo, H.; Wu, Z.; Li, X. Humidity Sensing Behaviors of Graphene Oxide-Silicon Bi-Layer Flexible Structure. *Sens. Actuators, B* **2012**, *161*, 1053−1058.
(324) Lin, W.-D.; Chang, H.-M.; Wu, R.-J. Applied Novel Sensing Material Graphene/Polypyrrole for Humidity Sensor. *Sens. Actuators, B* **2013**, *181*, 326−331.
(325) Borini, S.; White, R.; Wei, D.; Astley, M.; Haque, S.; Spigone, E.; Harris, N.; Kivioja, J.; Ryhanen, T. Ultrafast Graphene Oxide Humidity Sensors. *ACS Nano* **2013**, *7*, 11166−11173.
(326) Li, Y.; Deng, C.; Yang, M. Facilely Prepared Composites of Polyelectrolytes and Graphene as the Sensing Materials for the Detection of Very Low Humidity. *Sens. Actuators, B* **2014**, *194*, 51−58.
(327) Su, P.-G.; Chiou, C.-F. Electrical and Humidity-Sensing Properties of Reduced Graphene Oxide Thin Film Fabricated by Layer-by-Layer with Covalent Anchoring on Flexible Substrate. *Sens. Actuators, B* **2014**, *200*, 9−18.
(328) Gao, R.; Lu, D.-F.; Cheng, J.; Jiang, Y.; Jiang, L.; Qi, Z.-M. Humidity Sensor Based on Power Leakage at Resonance Wavelengths of a Hollow Core Fiber Coated with Reduced Graphene Oxide. *Sens. Actuators, B* **2016**, *222*, 618−624.
(329) Alizadeh, T.; Shokri, M. A New Humidity Sensor Based upon Graphene Quantum Dots Prepared Via Carbonization of Citric Acid. *Sens. Actuators, B* **2016**, *222*, 728−734.
(330) Lim, M.-Y.; Shin, H.; Shin, D. M.; Lee, S.-S.; Lee, J.-C. Poly(vinyl alcohol) Nanocomposites Containing Reduced Graphene Oxide Coated with Tannic Acid for Humidity Sensor. *Polymer* **2016**, *84*, 89−98.
(331) Ali, S.; Hassan, A.; Hassan, G.; Bae, J.; Lee, C. H. All-Printed Humidity Sensor Based on Graphene/Methyl-Red Composite with High Sensitivity. *Carbon* **2016**, *105*, 23−32.
(332) Toloman, D.; Popa, A.; Stan, M.; Socaci, C.; Biris, A. R.; Katona, G.; Tudorache, F.; Petrila, I.; Iacomi, F. Reduced Graphene Oxide Decorated with Fe Doped SnO_2 Nanoparticles for Humidity Sensor. *Appl. Surf. Sci.* **2017**, *402*, 410−417.
(333) Han, K. I.; Kim, S.; Lee, I. G.; Kim, J. P.; Kim, J. H.; Hong, S. W.; Cho, B. J.; Hwang, W. S. Compliment Graphene Oxide Coating on Silk Fiber Surface Via Electrostatic Force for Capacitive Humidity Sensor Applications. *Sensors* **2017**, *17*, 407.
(334) Tao, J.; Wang, Y.; Xiao, Y.; Yao, P.; Chen, C.; Zhang, D.; Pang, W.; Yang, H.; Sun, D.; Wang, Z.; Liu, J. One-Step Exfoliation and Functionalization of Graphene by Hydrophobin for High Performance Water Molecular Sensing. *Carbon* **2017**, *116*, 695−702.
(335) Guo, H.; Lan, C.; Zhou, Z.; Sun, P.; Wei, D.; Li, C. Transparent, Flexible, and Stretchable WS_2 Based Humidity Sensors for Electronic Skin. *Nanoscale* **2017**, *9*, 6246−6253.
(336) Jin, H.; Huynh, T.-P.; Haick, H. Self-Healable Sensors Based Nanoparticles for Detecting Physiological Markers Via Skin and Breath: Toward Disease Prevention Via Wearable Devices. *Nano Lett.* **2016**, *16*, 4194−4202.
(337) Li, W.; Xu, F.; Sun, L.; Liu, W.; Qiu, Y. A Novel Flexible Humidity Switch Material Based on Multi-Walled Carbon Nanotube/Polyvinyl alcohol Composite Yarn. *Sens. Actuators, B* **2016**, *230*, 528−535.
(338) Zhou, G.; Byun, J. H.; Oh, Y.; Jung, B. M.; Cha, H. J.; Seong, D. G.; Um, M. K.; Hyun, S.; Chou, T. W. Highly Sensitive Wearable Textile-Based Humidity Sensor Made of High-Strength, Single-Walled Carbon Nanotube/Poly(vinyl alcohol) Filaments. *ACS Appl. Mater. Interfaces* **2017**, *9*, 4788−4797.
(339) Jang, J.; Han, J. I. High Performance Cylindrical Capacitor as a Relative Humidity Sensor for Wearable Computing Devices. *J. Electrochem. Soc.* **2017**, *164*, B136−B141.
(340) Yao, S.; Myers, A.; Malhotra, A.; Lin, F.; Bozkurt, A.; Muth, J. F.; Zhu, Y. A Wearable Hydration Sensor with Conformal Nanowire Electrodes. *Adv. Healthcare Mater.* **2017**, *6*, 1601159.
(341) Zhong, Y.; Zhang, F.; Wang, M.; Gardner, C. J.; Kim, G.; Liu, Y.; Leng, J.; Jin, S.; Chen, R. Reversible Humidity Sensitive Clothing for Personal Thermoregulation. *Sci. Rep.* **2017**, *7*, 44208.
(342) Chi, H.; Liu, Y. J.; Wang, F.; He, C. Highly Sensitive and Fast Response Colorimetric Humidity Sensors Based on Graphene Oxides Film. *ACS Appl. Mater. Interfaces* **2015**, *7*, 19882−19886.
(343) Zhang, D.; Tong, J.; Xia, B. Humidity-Sensing Properties of Chemically Reduced Graphene Oxide/Polymer Nanocomposite Film

DOI: 10.1021/acsami.7b07063
ACS Appl. Mater. Interfaces 2017, 9, 34544−34586

Sensor Based on Layer-by-Layer Nano Self-Assembly. *Sens. Actuators, B* **2014**, *197*, 66−72.
(344) Guo, L.; Jiang, H.-B.; Shao, R.-Q.; Zhang, Y.-L.; Xie, S.-Y.; Wang, J.-N.; Li, X.-B.; Jiang, F.; Chen, Q.-D.; Zhang, T.; Sun, H.-B. Two-Beam-Laser Interference Mediated Reduction, Patterning and Nanostructuring of Graphene Oxide for the Production of a Flexible Humidity Sensing Device. *Carbon* **2012**, *50*, 1667−1673.
(345) Su, P.-G.; Shiu, W.-L.; Tsai, M.-S. Flexible Humidity Sensor Based on Au Nanoparticles/Graphene Oxide/Thiolated Silica Sol−Gel Film. *Sens. Actuators, B* **2015**, *216*, 467−475.
(346) Su, P.-G.; Lu, Z.-M. Flexibility and Electrical and Humidity-Sensing Properties of Diamine-Functionalized Graphene Oxide Films. *Sens. Actuators, B* **2015**, *211*, 157−163.
(347) Xuan, W.; He, X.; Chen, J.; Wang, W.; Wang, X.; Xu, Y.; Xu, Z.; Fu, Y. Q.; Luo, J. K. High Sensitivity Flexible Lamb-Wave Humidity Sensors with a Graphene Oxide Sensing Layer. *Nanoscale* **2015**, *7*, 7430−7436.
(348) Ma, R.; Tsukruk, V. V. Seriography-Guided Reduction of Graphene Oxide Biopapers for Wearable Sensory Electronics. *Adv. Funct. Mater.* **2017**, *27*, 1604802.
(349) Trung, T. Q.; Duy, L. T.; Ramasundaram, S.; Lee, N.-E. Transparent, Stretchable, and Rapid-Response Humidity Sensor for Body-Attachable Wearable Electronics. *Nano Res.* **2017**, *10*, 2021−2033.
(350) Naik, G.; Krishnaswamy, S. Room-Temperature Humidity Sensing Using Graphene Oxide Thin Films. *Graphene* **2016**, *5*, 1−13.
(351) Yu, H.-W.; Kim, H. K.; Kim, T.; Bae, K. M.; Seo, S. M.; Kim, J.-M.; Kang, T. J.; Kim, Y. H. Self-Powered Humidity Sensor Based on Graphene Oxide Composite Film Intercalated by Poly(sodium 4-styrenesulfonate). *ACS Appl. Mater. Interfaces* **2014**, *6*, 8320−8326.
(352) Yuan, Y.; Peng, B.; Chi, H.; Li, C.; Liu, R.; Liu, X. Layer-by-Layer Inkjet Printing SPS:PEDOT NP/RGO Composite Film for Flexible Humidity Sensors. *RSC Adv.* **2016**, *6*, 113298−113306.
(353) Tripathi, K. M.; Kim, T.; Losic, D.; Tung, T. T. Recent Advances in Engineered Graphene and Composites for Detection of Volatile Organic Compounds (VOCs) and Non-Invasive Diseases Diagnosis. *Carbon* **2016**, *110*, 97−129.
(354) Kybert, N. J.; Han, G. H.; Lerner, M. B.; Dattoli, E. N.; Esfandiar, A.; Johnson, A. T. C. Scalable Arrays of Chemical Vapor Sensors Based on DNA-Decorated Graphene. *Nano Res.* **2014**, *7*, 95−103.
(355) Gavgani, J. N.; Dehsari, H. S.; Hasani, A.; Mahyari, M.; Shalamzari, E. K.; Salehi, A.; Taromi, F. A. A Room Temperature Volatile Organic Compound Sensor with Enhanced Performance, Fast Response and Recovery Based on N-Doped Graphene Quantum Dots and Poly(3,4-ethylenedioxythiophene)-Poly(styrenesulfonate) Nanocomposite. *RSC Adv.* **2015**, *5*, 57559−57567.
(356) Ge, S.; Zheng, H.; Sun, Y.; Jin, Z.; Shan, J.; Wang, C.; Wu, H.; Li, M.; Meng, F. Ag/SnO_2/Graphene Ternary Nanocomposites and Their Sensing Properties to Volatile Organic Compounds. *J. Alloys Compd.* **2016**, *659*, 127−131.
(357) Gautam, M.; Jayatissa, A. H. Detection of Organic Vapors by Graphene Films Functionalized with Metallic Nanoparticles. *J. Appl. Phys.* **2012**, *112*, 114326.
(358) Meng, F.-L.; Li, H.-H.; Kong, L.-T.; Liu, J.-Y.; Jin, Z.; Li, W.; Jia, Y.; Liu, J.-H.; Huang, X.-J. Parts Per Billion-Level Detection of Benzene Using SnO_2/Graphene Nanocomposite Composed of Sub-6nm SnO_2 Nanoparticles. *Anal. Chim. Acta* **2012**, *736*, 100−107.
(359) Wang, C.; Zhu, J.; Liang, S.; Bi, H.; Han, Q.; Liu, X.; Wang, X. Reduced Graphene Oxide Decorated with CuO−ZnO Heterojunctions: Towards High Selective Gas-Sensing Property to Acetone. *J. Mater. Chem. A* **2014**, *2*, 18635−18643.
(360) Parmar, M.; Balamurugan, C.; Lee, D.-W. PANI and Graphene/PANI Nanocomposite Films—Comparative Toluene Gas Sensing Behavior. *Sensors* **2013**, *13*, 16611−16624.
(361) Singkammo, S.; Wisitsoraat, A.; Sriprachuabwong, C.; Tuantranont, A.; Phanichphant, S.; Liewhiran, C. Electrolytically Exfoliated Graphene-Loaded Flame-Made Ni-Doped SnO_2 Composite Film for Acetone Sensing. *ACS Appl. Mater. Interfaces* **2015**, *7*, 3077−3092.
(362) Konwer, S.; Guha, A. K.; Dolui, S. K. Graphene Oxide-Filled Conducting Polyaniline Composites as Methanol-Sensing Materials. *J. Mater. Sci.* **2013**, *48*, 1729−1739.
(363) Liu, S.; Chen, Z.; Zhang, N.; Tang, Z.-R.; Xu, Y.-J. An Efficient Self-Assembly of CdS Nanowires−Reduced Graphene Oxide Nanocomposites for Selective Reduction of Nitro Organics under Visible Light Irradiation. *J. Phys. Chem. C* **2013**, *117*, 8251−8261.
(364) Konwer, S.; Begum, A.; Bordoloi, S.; Boruah, R. Expanded Graphene-Oxide Encapsulated Polyaniline Composites as Sensing Material for Volatile Organic Compounds. *J. Polym. Res.* **2017**, *24*, 37.
(365) Teradal, N. L.; Marx, S.; Morag, A.; Jelinek, R. Porous Graphene Oxide Chemi-Capacitor Vapor Sensor Array. *J. Mater. Chem. C* **2017**, *5*, 1128−1135.
(366) Mannoor, M. S.; Tao, H.; Clayton, J. D.; Sengupta, A.; Kaplan, D. L.; Naik, R. R.; Verma, N.; Omenetto, F. G.; McAlpine, M. C. Graphene-Based Wireless Bacteria Detection on Tooth Enamel. *Nat. Commun.* **2012**, *3*, 763.
(367) Broza, Y. Y.; Haick, H. Nanomaterial-Based Sensors for Detection of Disease by Volatile Organic Compounds. *Nanomedicine* **2013**, *8*, 785−806.
(368) Nag, S.; Duarte, L.; Bertrand, E.; Celton, V.; Castro, M.; Choudhary, V.; Guegan, P.; Feller, J.-F. Ultrasensitive QRS Made by Supramolecular Assembly of Functionalized Cyclodextrins and Graphene for the Detection of Lung Cancer VOC Biomarkers. *J. Mater. Chem. B* **2014**, *2*, 6571−6579.
(369) Tung, T. T.; Castro, M.; Kim, T. Y.; Suh, K. S.; Feller, J.-F. Graphene Quantum Resistive Sensing Skin for the Detection of Alteration Biomarkers. *J. Mater. Chem.* **2012**, *22*, 21754−21766.
(370) Wang, B.; Chang, Y.-H.; Zhi, L.-J. High Yield Production of Graphene and Its Improved Property in Detecting Heavy Metal Ions. *New Carbon Mater.* **2011**, *26*, 31−35.
(371) Zhang, T.; Cheng, Z.; Wang, Y.; Li, Z.; Wang, C.; Li, Y.; Fang, Y. Self-Assembled 1-Octadecanethiol Monolayers on Graphene for Mercury Detection. *Nano Lett.* **2010**, *10*, 4738−4741.
(372) Wang, X.; Sun, X.; Hu, P. A.; Zhang, J.; Wang, L.; Feng, W.; Lei, S.; Yang, B.; Cao, W. Colorimetric Sensor Based on Self-Assembled Polydiacetylene/Graphene-Stacked Composite Film for Vapor-Phase Volatile Organic Compounds. *Adv. Funct. Mater.* **2013**, *23*, 6044−6050.
(373) Zou, J.; Liu, Z.; Guo, Y.; Dong, C. Electrochemical Sensor for the Facile Detection of Trace Amounts of Bisphenol a Based on Cyclodextrin-Functionalized Graphene/Platinum Nanoparticles. *Anal. Methods* **2017**, *9*, 134−140.
(374) Huang, Q.; Zeng, D.; Li, H.; Xie, C. Room Temperature Formaldehyde Sensors with Enhanced Performance, Fast Response and Recovery Based on Zinc Oxide Quantum Dots/Graphene Nanocomposites. *Nanoscale* **2012**, *4*, 5651−5658.
(375) Ye, Z.; Tai, H.; Xie, T.; Yuan, Z.; Liu, C.; Jiang, Y. Room Temperature Formaldehyde Sensor with Enhanced Performance Based on Reduced Graphene Oxide/Titanium Dioxide. *Sens. Actuators, B* **2016**, *223*, 149−156.
(376) Zhang, T.; Qin, L.; Kang, S.-Z.; Li, G.; Li, X. Novel Reduced Graphene Oxide/Ag Nanoparticle Composite Film with Sensitive Detection Activity Towards Trace Formaldehyde. *Sens. Actuators, B* **2017**, *242*, 1129−1132.
(377) Tian, F.; Li, H.; Li, M.; Li, C.; Lei, Y.; Yang, B. Synthesis of One-Dimensional Poly(3,4-ethylenedioxythiophene)-Graphene Composites for the Simultaneous Detection of Hydroquinone, Catechol, Resorcinol, and Nitrite. *Synth. Met.* **2017**, *226*, 148−156.
(378) Sayago, I.; Matatagui, D.; Fernández, M. J.; Fontecha, J. L.; Jurewicz, I.; Garriga, R.; Muñoz, E. Graphene Oxide as Sensitive Layer in Love-Wave Surface Acoustic Wave Sensors for the Detection of Chemical Warfare Agent Simulants. *Talanta* **2016**, *148*, 393−400.
(379) Hu, N.; Wang, Y.; Chai, J.; Gao, R.; Yang, Z.; Kong, E. S.-W.; Zhang, Y. Gas Sensor Based on P-Phenylenediamine Reduced Graphene Oxide. *Sens. Actuators, B* **2012**, *163*, 107−114.
(380) Facure, M. H. M.; Mercante, L. A.; Mattoso, L. H. C.; Correa, D. S. Detection of Trace Levels of Organophosphate Pesticides Using an Electronic Tongue Based on Graphene Hybrid Nanocomposites. *Talanta* **2017**, *167*, 59−66.

DOI: 10.1021/acsami.7b07063
ACS Appl. Mater. Interfaces 2017, 9, 34544−34586

(381) Xuan, X.; Park, J. Y. In *IEEE 30th International Conference on Micro Electro Mechanical Systems (MEMS)*, January 22−26, Las Vegas, NV, 2017; IEEE: New York, NY, 2017; pp 636−639.
(382) Yuan, K.; Guo-Wang, P.; Hu, T.; Shi, L.; Zeng, R.; Forster, M.; Pichler, T.; Chen, Y.; Scherf, U. Nanofibrous and Graphene-Templated Conjugated Microporous Polymer Materials for Flexible Chemosensors and Supercapacitors. *Chem. Mater.* **2015**, *27*, 7403−7411.
(383) An, J. H.; Park, S. J.; Kwon, O. S.; Bae, J.; Jang, J. High-Performance Flexible Graphene Aptasensor for Mercury Detection in Mussels. *ACS Nano* **2013**, *7*, 10563−10571.
(384) Su, B.; Shao, H.; Li, N.; Chen, X.; Cai, Z.; Chen, X. A Sensitive Bisphenol a Voltammetric Sensor Relying on AuPd Nanoparticles/Graphene Composites Modified Glassy Carbon Electrode. *Talanta* **2017**, *166*, 126−132.
(385) Qiao, J.; Chang, J.; Wang, H.; Sun, T.; Dong, C. Determination of Formaldehyde with a Platinum−Palladium−Graphene Nanocomposite Glassy Carbon Electrode. *Anal. Lett.* **2017**, *50*, 80−90.
(386) Asadian, E.; Shahrokhian, S.; Zad, A. I.; Ghorbani-Bidkorbeh, F. Glassy Carbon Electrode Modified with 3D Graphene−Carbon Nanotube Network for Sensitive Electrochemical Determination of Methotrexate. *Sens. Actuators, B* **2017**, *239*, 617−627.
(387) Sakthinathan, S.; Kubendhiran, S.; Chen, S.-M.; Govindasamy, M.; Al-Hemaid, F. M. A.; Ajmal Ali, M.; Tamizhdurai, P.; Sivasanker, S. Metallated Porphyrin Noncovalent Interaction with Reduced Graphene Oxide-Modified Electrode for Amperometric Detection of Environmental Pollutant Hydrazine. *Appl. Organomet. Chem.* **2017**, *31*, e3703.
(388) Kubendhiran, S.; Sakthinathan, S.; Chen, S. M.; Tamizhdurai, P.; Shanthi, K.; Karuppiah, C. Green Reduction of Reduced Graphene Oxide with Nickel Tetraphenyl Porphyrin Nanocomposite Modified Electrode for Enhanced Electrochemical Determination of Environmentally Pollutant Nitrobenzene. *J. Colloid Interface Sci.* **2017**, *497*, 207−216.
(389) Velmurugan, M.; Karikalan, N.; Chen, S.-M.; Dai, Z.-C. Studies on the Influence of β-Cyclodextrin on Graphene Oxide and Its Synergistic Activity to the Electrochemical Detection of Nitrobenzene. *J. Colloid Interface Sci.* **2017**, *490*, 365−371.
(390) Sha, R.; Puttapati, S. K.; Srikanth, V. V.; Badhulika, S. Ultra-Sensitive Phenol Sensor Based on Overcoming Surface Fouling of Reduced Graphene Oxide-Zinc Oxide Composite Electrode. *J. Electroanal. Chem.* **2017**, *785*, 26−32.
(391) Guo, D.; Cai, P.; Sun, J.; He, W.; Wu, X.; Zhang, T.; Wang, X.; Zhang, X. Reduced-Graphene-Oxide/Metal-Oxide p-n Heterojunction Aerogels as Efficient 3D Sensing Frameworks for Phenol Detection. *Carbon* **2016**, *99*, 571−578.
(392) Wiench, P.; Grzyb, B.; González, Z.; Menéndez, R.; Handke, B.; Gryglewicz, G. pH Robust Electrochemical Detection of 4-Nitrophenol on a Reduced Graphene Oxide Modified Glassy Carbon Electrode. *J. Electroanal. Chem.* **2017**, *787*, 80−87.
(393) Peleyeju, M. G.; Idris, A. O.; Umukoro, E. H.; Babalola, J. O.; Arotiba, O. A. Electrochemical Detection of 2,4-Dichlorophenol on a Ternary Composite Electrode of Diamond, Graphene, and Polyaniline. *ChemElectroChem* **2017**, *4*, 1074−1080.
(394) Liang, Y.; Yu, L.; Yang, R.; Li, X.; Qu, L.; Li, J. High Sensitive and Selective Graphene Oxide/Molecularly Imprinted Polymer Electrochemical Sensor for 2,4-Dichlorophenol in Water. *Sens. Actuators, B* **2017**, *240*, 1330−1335.
(395) Kaur, M.; Mehta, S. K.; Kansal, S. K. Nitrogen Doped Graphene Quantum Dots: Efficient Fluorescent Chemosensor for the Selective and Sensitive Detection of 2,4,6-Trinitrophenol. *Sens. Actuators, B* **2017**, *245*, 938−945.
(396) Zhang, K.; Hu, R.; Fan, G.; Li, G. Graphene Oxide/Chitosan Nanocomposite Coated Quartz Crystal Microbalance Sensor for Detection of Amine Vapors. *Sens. Actuators, B* **2017**, *243*, 721−730.
(397) Zhang, S.; Zhang, D.; Zhang, X.; Shang, D.; Xue, Z.; Shan, D.; Lu, X. Ultratrace Naked-Eye Colorimetric Detection of Hg^{2+} in Wastewater and Serum Utilizing Mercury-Stimulated Peroxidase Mimetic Activity of Reduced Graphene Oxide-PEI-Pd Nanohybrids. *Anal. Chem.* **2017**, *89*, 3538−3544.
(398) Borthakur, P.; Darabdhara, G.; Das, M. R.; Boukherroub, R.; Szunerits, S. Solvothermal Synthesis of CoS/Reduced Porous Graphene Oxide Nanocomposite for Selective Colorimetric Detection of Hg(II) Ion in Aqueous Medium. *Sens. Actuators, B* **2017**, *244*, 684−692.
(399) Magerusan, L.; Socaci, C.; Coros, M.; Pogacean, F.; Rosu, M. C.; Gergely, S.; Pruneanu, S.; Leostean, C.; Pana, I. O. Electrochemical Platform Based on Nitrogen-Doped Graphene/Chitosan Nanocomposite for Selective Pb^{2+} Detection. *Nanotechnology* **2017**, *28*, 114001.
(400) Xuan, W.; Ruiyi, L.; Saiying, F.; Zaijun, L.; Guangli, W.; Zhiguo, G.; Junkang, L. D-Penicillamine-Functionalized Graphene Quantum Dots for Fluorescent Detection of Fe^{3+} in Iron Supplement Oral Liquids. *Sens. Actuators, B* **2017**, *243*, 211−220.
(401) Zhu, Y.; Pan, D.; Hu, X.; Han, H.; Lin, M.; Wang, C. An Electrochemical Sensor Based on Reduced Graphene Oxide/Gold Nanoparticles Modified Electrode for Determination of Iron in Coastal Waters. *Sens. Actuators, B* **2017**, *243*, 1−7.
(402) Wen, Y.; Wen, W.; Zhang, X.; Wang, S. Highly Sensitive Amperometric Biosensor Based on Electrochemically-Reduced Graphene Oxide-Chitosan/Hemoglobin Nanocomposite for Nitromethane Determination. *Biosens. Bioelectron.* **2016**, *79*, 894−900.
(403) Wu, Z.; Chen, X.; Zhu, S.; Zhou, Z.; Yao, Y.; Quan, W.; Liu, B. Room Temperature Methane Sensor Based on Graphene Nanosheets/Polyaniline Nanocomposite Thin Film. *IEEE Sens. J.* **2013**, *13*, 777−782.
(404) Furue, R.; Koveke, E. P.; Sugimoto, S.; Shudo, Y.; Hayami, S.; Ohira, S.-I.; Toda, K. Arsine Gas Sensor Based on Gold-Modified Reduced Graphene Oxide. *Sens. Actuators, B* **2017**, *240*, 657−663.
(405) Fan, L.; Hu, Y.; Wang, X.; Zhang, L.; Li, F.; Han, D.; Li, Z.; Zhang, Q.; Wang, Z.; Niu, L. Fluorescence Resonance Energy Transfer Quenching at the Surface of Graphene Quantum Dots for Ultrasensitive Detection of TNT. *Talanta* **2012**, *101*, 192−197.
(406) Zhang, L.; Li, C.; Liu, A.; Shi, G. Electrosynthesis of Graphene Oxide/Polypyrene Composite Films and Their Applications for Sensing Organic Vapors. *J. Mater. Chem.* **2012**, *22*, 8438−8443.
(407) Uddin, A. S. M. I.; Phan, D.-T.; Chung, G.-S. Low Temperature Acetylene Gas Sensor Based on Ag Nanoparticles-Loaded ZnO-Reduced Graphene Oxide Hybrid. *Sens. Actuators, B* **2015**, *207*, 362−369.
(408) Zhang, Z.; Fu, X.; Li, K.; Liu, R.; Peng, D.; He, L.; Wang, M.; Zhang, H.; Zhou, L. One-Step Fabrication of Electrochemical Biosensor Based on DNA-Modified Three-Dimensional Reduced Graphene Oxide and Chitosan Nanocomposite for Highly Sensitive Detection of Hg (II). *Sens. Actuators, B* **2016**, *225*, 453−462.
(409) Palanisamy, S.; Thangavelu, K.; Chen, S.-M.; Velusamy, V.; Chang, M.-H.; Chen, T.-W.; Al-Hemaid, F. M. A.; Ali, M. A.; Ramaraj, S. K. Synthesis and Characterization of Polypyrrole Decorated Graphene/β-Cyclodextrin Composite for Low Level Electrochemical Detection of Mercury(II) in Water. *Sens. Actuators, B* **2017**, *243*, 888−894.
(410) Bian, S.; Shen, C.; Qian, Y.; Liu, J.; Xi, F.; Dong, X. Facile Synthesis of Sulfur-Doped Graphene Quantum Dots as Fluorescent Sensing Probes for Ag^{+} Ions Detection. *Sens. Actuators, B* **2017**, *242*, 231−237.
(411) Ensafi, A. A.; Noroozi, R.; Zandi-Atashbar, N.; Rezaei, B. Cerium(IV) Oxide Decorated on Reduced Graphene Oxide, a Selective and Sensitive Electrochemical Sensor for Fenitrothion Determination. *Sens. Actuators, B* **2017**, *245*, 980−987.
(412) Chen, C.; Zhao, D.; Hu, T.; Sun, J.; Yang, X. Highly Fluorescent Nitrogen and Sulfur Co-Doped Graphene Quantum Dots for an Inner Filter Effect-Based Cyanide Sensor. *Sens. Actuators, B* **2017**, *241*, 779−788.
(413) Pandey, A.; Gurbuz, Y.; Ozguz, V.; Niazi, J. H.; Qureshi, A. Graphene-Interfaced Electrical Biosensor for Label-Free and Sensitive Detection of Foodborne Pathogenic *E. Coli* O157:H7. *Biosens. Bioelectron.* **2017**, *91*, 225−231.
(414) Er, E.; Çelikkan, H.; Erk, N. A Novel Electrochemical Nano-Platform Based on Graphene/Platinum Nanoparticles/Nafion Composites for the Electrochemical Sensing of Metoprolol. *Sens. Actuators, B* **2017**, *238*, 779−787.
(415) Kirby, R.; Cho, E. J.; Gehrke, B.; Bayer, T.; Park, Y. S.; Neikirk, D. P.; McDevitt, J. T.; Ellington, A. D. Aptamer-Based Sensor Arrays for the

DOI: 10.1021/acsami.7b07063
ACS Appl. Mater. Interfaces 2017, 9, 34544−34586

Detection and Quantitation of Proteins. *Anal. Chem.* **2004**, *76*, 4066−4075.
(416) Zheng, G.; Patolsky, F.; Cui, Y.; Wang, W. U.; Lieber, C. M. Multiplexed Electrical Detection of Cancer Markers with Nanowire Sensor Arrays. *Nat. Biotechnol.* **2005**, *23*, 1294−1301.
(417) Bajaj, A.; Miranda, O. R.; Kim, I. B.; Phillips, R. L.; Jerry, D. J.; Bunz, U. H.; Rotello, V. M. Detection and Differentiation of Normal, Cancerous, and Metastatic Cells Using Nanoparticle-Polymer Sensor Arrays. *Proc. Natl. Acad. Sci. U. S. A.* **2009**, *106*, 10912−10916.
(418) Sekitani, T.; Yokota, T.; Zschieschang, U.; Klauk, H.; Bauer, S.; Takeuchi, K.; Takamiya, M.; Sakurai, T.; Someya, T. Organic Nonvolatile Memory Transistors for Flexible Sensor Arrays. *Science* **2009**, *326*, 1516−1519.
(419) Askim, J. R.; Mahmoudi, M.; Suslick, K. S. Optical Sensor Arrays for Chemical Sensing: The Optoelectronic Nose. *Chem. Soc. Rev.* **2013**, *42*, 8649−8682.
(420) Rock, F.; Barsan, N.; Weimar, U. Electronic Nose: Current Status and Future Trends. *Chem. Rev.* **2008**, *108*, 705−725.
(421) Pei, H.; Li, J.; Lv, M.; Wang, J.; Gao, J.; Lu, J.; Li, Y.; Huang, Q.; Hu, J.; Fan, C. A Graphene-Based Sensor Array for High-Precision and Adaptive Target Identification with Ensemble Aptamers. *J. Am. Chem. Soc.* **2012**, *134*, 13843−13849.
(422) Chou, S. S.; De, M.; Luo, J.; Rotello, V. M.; Huang, J.; Dravid, V. P. Nanoscale Graphene Oxide (nGO) as Artificial Receptors: Implications for Biomolecular Interactions and Sensing. *J. Am. Chem. Soc.* **2012**, *134*, 16725−16733.
(423) Alizadeh, T.; Soltani, L. H. Reduced Graphene Oxide-Based Gas Sensor Array for Pattern Recognition of DMMP Vapor. *Sens. Actuators, B* **2016**, *234*, 361−370.
(424) Xu, S.; Lu, X.; Yao, C.; Huang, F.; Jiang, H.; Hua, W.; Na, N.; Liu, H.; Ouyang, J. A Visual Sensor Array for Pattern Recognition Analysis of Proteins Using Novel Blue-Emitting Fluorescent Gold Nanoclusters. *Anal. Chem.* **2014**, *86*, 11634−11639.
(425) Lu, Y.; Liu, Y.; Zhang, S.; Wang, S.; Zhang, S.; Zhang, X. Aptamer-Based Plasmonic Sensor Array for Discrimination of Proteins and Cells with the Naked Eye. *Anal. Chem.* **2013**, *85*, 6571−6574.
(426) Sun, S.; Jiang, K.; Qian, S.; Wang, Y.; Lin, H. Applying Carbon Dots-Metal Ions Ensembles as a Multichannel Fluorescent Sensor Array: Detection and Discrimination of Phosphate Anions. *Anal. Chem.* **2017**, *89*, 5542−5548.
(427) Wu, Y.; Liu, X.; Wu, Q.; Yi, J.; Zhang, G. Differentiation and Determination of Metal Ions Using Fluorescent Sensor Array Based on Carbon Nanodots. *Sens. Actuators, B* **2017**, *246*, 680−685.
(428) Qu, J.; Ge, Y.; Zu, B.; Li, Y.; Dou, X. Transition-Metal-Doped p-Type ZnO Nanoparticle-Based Sensory Array for Instant Discrimination of Explosive Vapors. *Small* **2016**, *12*, 1369−1377.
(429) Matatagui, D.; Kolokoltsev, O. V.; Qureshi, N.; Mejía-Uriarte, E. V.; Ordoñez-Romero, C. L.; Vázquez-Olmos, A.; Saniger, J. M. Magnonic Sensor Array Based on Magnetic Nanoparticles to Detect, Discriminate and Classify Toxic Gases. *Sens. Actuators, B* **2017**, *240*, 497−502.
(430) Meyyappan, M. Carbon Nanotube-Based Chemical Sensors. *Small* **2016**, *12*, 2118−2129.
(431) Chang, H.; Wu, X.; Wu, C.; Chen, Y.; Jiang, H.; Wang, X. Catalytic Oxidation and Determination of β-NADH Using Self-Assembly Hybrid of Gold Nanoparticles and Graphene. *Analyst* **2011**, *136*, 2735−2740.
(432) Yan, Y.; Liu, Q.; Du, X.; Qian, J.; Mao, H.; Wang, K. Visible Light Photoelectrochemical Sensor for Ultrasensitive Determination of Dopamine Based on Synergistic Effect of Graphene Quantum Dots and TiO_2 Nanoparticles. *Anal. Chim. Acta* **2015**, *853*, 258−264.
(433) Hou, S.; Kasner, M. L.; Su, S.; Patel, K.; Cuellari, R. Highly Sensitive and Selective Dopamine Biosensor Fabricated with Silanized Graphene. *J. Phys. Chem. C* **2010**, *114*, 14915−14921.
(434) Wu, P.; Shao, Q.; Hu, Y.; Jin, J.; Yin, Y.; Zhang, H.; Cai, C. Direct Electrochemistry of Glucose Oxidase Assembled on Graphene and Application to Glucose Detection. *Electrochim. Acta* **2010**, *55*, 8606−8614.
(435) Luo, J.; Jiang, S.; Zhang, H.; Jiang, J.; Liu, X. A Novel Non-Enzymatic Glucose Sensor Based on Cu Nanoparticle Modified Graphene Sheets Electrode. *Anal. Chim. Acta* **2012**, *709*, 47−53.
(436) Kim, J.; Park, S.-Y.; Kim, S.; Lee, D. H.; Kim, J. H.; Kim, J. M.; Kang, H.; Han, J.-S.; Park, J. W.; Lee, H.; Choi, S.-H. Precise and Selective Sensing of DNA-DNA Hybridization by Graphene/Si-Nanowires Diode-Type Biosensors. *Sci. Rep.* **2016**, *6*, 31984.
(437) Esfandiar, A.; Irajizad, A.; Akhavan, O.; Ghasemi, S.; Gholami, M. R. Pd−WO_3/Reduced Graphene Oxide Hierarchical Nanostructures as Efficient Hydrogen Gas Sensors. *Int. J. Hydrogen Energy* **2014**, *39*, 8169−8179.
(438) Zou, Y.; Wang, Q.; Xiang, C.; Tang, C.; Chu, H.; Qiu, S.; Yan, E.; Xu, F.; Sun, L. Doping Composite of Polyaniline and Reduced Graphene Oxide with Palladium Nanoparticles for Room-Temperature Hydrogen-Gas Sensing. *Int. J. Hydrogen Energy* **2016**, *41*, 5396−5404.
(439) Wang, C.; Zhu, J.; Liang, S.; Bi, H.; Han, Q.; Liu, X.; Wang, X. Reduced Graphene Oxide Decorated with CuO−ZnO Hetero-Junctions: Towards High Selective Gas-Sensing Property to Acetone. *J. Mater. Chem. A* **2014**, *2*, 18635−18643.
(440) Wen, Y.; Peng, C.; Li, D.; Zhuo, L.; He, S.; Wang, L.; Huang, Q.; Xu, Q.-H.; Fan, C. Metal Ion-Modulated Graphene-DNAzyme Interactions: Design of a Nanoprobe for Fluorescent Detection of Lead(II) Ions with High Sensitivity, Selectivity and Tunable Dynamic Range. *Chem. Commun.* **2011**, *47*, 6278−6280.
(441) Zhao, X.-H.; Kong, R.-M.; Zhang, X.-B.; Meng, H.-M.; Liu, W.-N.; Tan, W.; Shen, G.-L.; Yu, R.-Q. Graphene−DNAzyme Based Biosensor for Amplified Fluorescence "Turn-on" Detection of Pb^{2+} with a High Selectivity. *Anal. Chem.* **2011**, *83*, 5062−5066.
(442) Li, M.; Zhou, X.; Guo, S.; Wu, N. Detection of Lead (II) with a "Turn-on" Fluorescent Biosensor Based on Energy Transfer from CdSe/ZnS Quantum Dots to Graphene Oxide. *Biosens. Bioelectron.* **2013**, *43*, 69−74.
(443) Zhao, Z.-Q.; Chen, X.; Yang, Q.; Liu, J.-H.; Huang, X.-J. Beyond the Selective Adsorption of Polypyrrole-Reduced Graphene Oxide Nanocomposite toward Hg^{2+}: Ultra-Sensitive and-Selective Sensing Pb^{2+} by Stripping Voltammetry. *Electrochem. Commun.* **2012**, *23*, 21−24.
(444) Wei, W.; Xu, C.; Ren, J.; Xu, B.; Qu, X. Sensing Metal Ions with Ion Selectivity of a Crown Ether and Fluorescence Resonance Energy Transfer between Carbon Dots and Graphene. *Chem. Commun.* **2012**, *48*, 1284−1286.
(445) Sadak, O.; Sundramoorthy, A. K.; Gunasekaran, S. Highly Selective Colorimetric and Electrochemical Sensing of Iron(III) Using Nile Red Functionalized Graphene Film. *Biosens. Bioelectron.* **2017**, *89*, 430−436.
(446) Mao, S.; Cui, S.; Lu, G.; Yu, K.; Wen, Z.; Chen, J. Tuning Gas-Sensing Properties of Reduced Graphene Oxide Using Tin Oxide Nanocrystals. *J. Mater. Chem.* **2012**, *22*, 11009−11013.
(447) Wei, Y.; Gao, C.; Meng, F.-L.; Li, H.-H.; Wang, L.; Liu, J.-H.; Huang, X.-J. SnO_2/Reduced Graphene Oxide Nanocomposite for the Simultaneous Electrochemical Detection of Cadmium(II), Lead(II), Copper(II), and Mercury(II): An Interesting Favorable Mutual Interference. *J. Phys. Chem. C* **2012**, *116*, 1034−1041.
(448) Zhang, D.; Liu, J.; Jiang, C.; Liu, A.; Xia, B. Quantitative Detection of Formaldehyde and Ammonia Gas Via Metal Oxide-Modified Graphene-Based Sensor Array Combining with Neural Network Model. *Sens. Actuators, B* **2017**, *240*, 55−65.
(449) Zhu, M.; Li, X.; Chung, S.; Zhao, L.; Li, X.; Zang, X.; Wang, K.; Wei, J.; Zhong, M.; Zhou, K.; Xie, D.; Zhu, H. Photo-Induced Selective Gas Detection Based on Reduced Graphene Oxide/Si Schottky Diode. *Carbon* **2015**, *84*, 138−145.
(450) Yuan, W.; Huang, L.; Zhou, Q.; Shi, G. Ultrasensitive and Selective Nitrogen Dioxide Sensor Based on Self-Assembled Graphene/Polymer Composite Nanofibers. *ACS Appl. Mater. Interfaces* **2014**, *6*, 17003−17008.
(451) Li, X.; Zhao, Y.; Wang, X.; Wang, J.; Gaskov, A. M.; Akbar, S. A. Reduced Graphene Oxide (rGO) Decorated TiO_2 Microspheres for Selective Room-Temperature Gas Sensors. *Sens. Actuators, B* **2016**, *230*, 330−336.

DOI: 10.1021/acsami.7b07063
ACS Appl. Mater. Interfaces 2017, 9, 34544−34586

(452) Panda, D.; Nandi, A.; Datta, S. K.; Saha, H.; Majumdar, S. Selective Detection of Carbon Monoxide (CO) Gas by Reduced Graphene Oxide (rGO) at Room Temperature. *RSC Adv.* **2016**, *6*, 47337−47348.
(453) Yu, C.; Guo, Y.; Liu, H.; Yan, N.; Xu, Z.; Yu, G.; Fang, Y.; Liu, Y. Ultrasensitive and Selective Sensing of Heavy Metal Ions with Modified Graphene. *Chem. Commun.* **2013**, *49*, 6492−6494.
(454) Kumar, S.; Bhanjana, G.; Dilbaghi, N.; Kumar, R.; Umar, A. Fabrication and Characterization of Highly Sensitive and Selective Arsenic Sensor Based on Ultra-Thin Graphene Oxide Nanosheets. *Sens. Actuators, B* **2016**, *227*, 29−34.
(455) Soni, M.; Arora, T.; Khosla, R.; Kumar, P.; Soni, A.; Sharma, S. K. Integration of Highly Sensitive Oxygenated Graphene with Aluminum Micro-Interdigitated Electrode Array Based Molecular Sensor for Detection of Aqueous Fluoride Anions. *IEEE Sens. J.* **2016**, *16*, 1524−1531.
(456) Wang, Y.; Lu, J.; Tang, L.; Chang, H.; Li, J. Graphene Oxide Amplified Electrogenerated Chemiluminescence of Quantum Dots and Its Selective Sensing for Glutathione from Thiol-Containing Compounds. *Anal. Chem.* **2009**, *81*, 9710−9715.
(457) Dinesh, B.; Veeramani, V.; Chen, S.-M.; Saraswathi, R. *In Situ* Electrochemical Synthesis of Reduced Graphene Oxide-Cobalt Oxide Nanocomposite Modified Electrode for Selective Sensing of Depression Biomarker in the Presence of Ascorbic Acid and Dopamine. *J. Electroanal. Chem.* **2017**, *786*, 169−176.
(458) Tao, Y.; Auguste, D. T. Array-Based Identification of Triple-Negative Breast Cancer Cells Using Fluorescent Nanodot-Graphene Oxide Complexes. *Biosens. Bioelectron.* **2016**, *81*, 431−437.
(459) Gao, Z.; Kang, H.; Naylor, C. H.; Streller, F.; Ducos, P.; Serrano, M. D.; Ping, J.; Zauberman, J.; Carpick, R. W.; Wang, Y.-J.; et al. Scalable Production of Sensor Arrays Based on High-Mobility Hybrid Graphene Field Effect Transistors. *ACS Appl. Mater. Interfaces* **2016**, *8*, 27546−27552.
(460) Gao, L.; Ju, L.; Cui, H. Chemiluminescent and Fluorescent Dual-Signal Graphene Quantum Dots and Their Application in Pesticide Sensing Arrays. *J. Mater. Chem. C* **2017**, *5*, 7753−7758.
(461) Mohamed, M. A.; Atty, S. A.; Salama, N. N.; Banks, C. E. Highly Selective Sensing Platform Utilizing Graphene Oxide and Multiwalled Carbon Nanotubes for the Sensitive Determination of Tramadol in the Presence of Co-Formulated Drugs. *Electroanalysis* **2017**, *29*, 1038−1048.
(462) Elçin, S.; Yola, M. L.; Eren, T.; Girgin, B.; Atar, N. Highly Selective and Sensitive Voltammetric Sensor Based on Ruthenium Nanoparticle Anchored Calix[4]amidocrown-5 Functionalized Reduced Graphene Oxide: Simultaneous Determination of Quercetin, Morin and Rutin in Grape Wine. *Electroanalysis* **2016**, *28*, 611−619.
(463) Fu, C.; Li, M.; Li, H.; Li, C.; Qu, C.; Yang, B. Fabrication of Graphene/Titanium Carbide Nanorod Arrays for Chemical Sensor Application. *Mater. Sci. Eng., C* **2017**, *72*, 425−432.
(464) Adachi, N.; Yoshinari, M.; Suzuki, E.; Okada, M. Oligo(*p*-phenylene ethynylene) with Cyanoacrylate Terminal Groups and Graphene Composite as Fluorescent Chemical Sensor for Cysteine. *J. Fluoresc.* **2017**, *27*, 1449−1456.
(465) Bi, H.; Yin, K.; Xie, X.; Ji, J.; Wan, S.; Sun, L.; Terrones, M.; Dresselhaus, M. S. Ultrahigh Humidity Sensitivity of Graphene Oxide. *Sci. Rep.* **2013**, *3*, 2714.
(466) Zhou, Y.; Jiang, Y.; Xie, T.; Tai, H.; Xie, G. A Novel Sensing Mechanism for Resistive Gas Sensors Based on Layered Reduced Graphene Oxide Thin Films at Room Temperature. *Sens. Actuators, B* **2014**, *203*, 135−142.
(467) Sun, J.; Muruganathan, M.; Mizuta, H. Room Temperature Detection of Individual Molecular Physisorption Using Suspended Bilayer Graphene. *Sci. Adv.* **2016**, *2*, e1501518.
(468) Muruganathan, M.; Sun, J.; Imamura, T.; Mizuta, H. Electrically Tunable van der Waals Interaction in Graphene-Molecule Complex. *Nano Lett.* **2015**, *15*, 8176−8180.
(469) Takeuchi, K.; Yamamoto, S.; Hamamoto, Y.; Shiozawa, Y.; Tashima, K.; Fukidome, H.; Koitaya, T.; Mukai, K.; Yoshimoto, S.; Suemitsu, M.; et al. Adsorption of CO_2 on Graphene: A Combined TPD, XPS, and vdW-DF Study. *J. Phys. Chem. C* **2017**, *121*, 2807−2814.
(470) Wang, S.; Chen, Z.; Umar, A.; Wang, Y.; Tian, T.; Shang, Y.; Fan, Y.; Qi, Q.; Xu, D. Supramolecularly Modified Graphene for Ultrafast Responsive and Highly Stable Humidity Sensor. *J. Phys. Chem. C* **2015**, *119*, 28640−28647.
(471) Alizadeh, T.; Hamedsoltani, L. Managing of Gas Sensing Characteristic of a Reduced Graphene Oxide Based Gas Sensor by the Change in Synthesis Condition: A New Approach for Electronic Nose Design. *Mater. Chem. Phys.* **2016**, *183*, 181−190.
(472) Choi, T.; Hwang, B.-U.; Kim, B.-Y.; Trung, T. Q.; Nam, Y. H.; Kim, D.-N.; Eom, K.; Lee, N.-E. Stretchable, Transparent and Stretch-Unresponsive Capacitive Touch Sensor Array with Selectively Patterned Silver Nanowires/Reduced Graphene Oxide Electrodes. *ACS Appl. Mater. Interfaces* **2017**, *9*, 18022−18030.
(473) Du, D.; Li, P.; Ouyang, J. Graphene Coated Nonwoven Fabrics as Wearable Sensors. *J. Mater. Chem. C* **2016**, *4*, 3224−3230.
(474) Lee, S. W.; Park, J. J.; Park, B. H.; Mun, S. C.; Park, Y. T.; Liao, K.; Seo, T. S.; Hyun, W. J.; Park, O. O. Enhanced Sensitivity of Patterned Graphene Strain Sensors Used for Monitoring Subtle Human Body Motions. *ACS Appl. Mater. Interfaces* **2017**, *9*, 11176−11183.
(475) Yun, J.; Lim, Y.; Jang, G. N.; Kim, D.; Lee, S.-J.; Park, H.; Hong, S. Y.; Lee, G.; Zi, G.; Ha, J. S. Stretchable Patterned Graphene Gas Sensor Driven by Integrated Micro-Supercapacitor Array. *Nano Energy* **2016**, *19*, 401−414.
(476) Yun, Y. J.; Hong, W. G.; Kim, D. Y.; Kim, H. J.; Jun, Y.; Lee, H.-K. E-Textile Gas Sensors Composed of Molybdenum Disulfide and Reduced Graphene Oxide for High Response and Reliability. *Sens. Actuators, B* **2017**, *248*, 829−835.
(477) Kim, H. W.; Kwon, Y. J.; Mirzaei, A.; Kang, S. Y.; Choi, M. S.; Bang, J. H.; Kim, S. S. Synthesis of Zinc Oxide Semiconductors-Graphene Nanocomposites by Microwave Irradiation for Application to Gas Sensors. *Sens. Actuators, B* **2017**, *249*, 590−601.
(478) Zhao, S.; Li, J.; Cao, D.; Zhang, G.; Li, J.; Li, K.; Yang, Y.; Wang, W.; Jin, Y.; Sun, R.; Wong, C. P. Recent Advancements in Flexible and Stretchable Electrodes for Electromechanical Sensors: Strategies, Materials, and Features. *ACS Appl. Mater. Interfaces* **2017**, *9*, 12147−12164.
(479) Potyrailo, R. A. Multivariable Sensors for Ubiquitous Monitoring of Gases in the Era of Internet of Things and Industrial Internet. *Chem. Rev.* **2016**, *116*, 11877−11923.
(480) Swan, M. 2012. Sensor Mania! The Internet of Things, Wearable Computing, Objective Metrics, and the Quantified Self 2.0. *J. Sensor Actuator Networks* **2012**, *1*, 217−253.

DOI: 10.1021/acsami.7b07063
ACS Appl. Mater. Interfaces 2017, 9, 34544−34586